Off-target identification for a multitarget kinase inhibitor by Chemical Proteomics

Dissertation
zur Erlangung des akademischen Grades des
Doktors der Naturwissenschaften (Dr. rer. nat.)

vorgelegt von
Diplom-Biochemiker Enrico Mißner
aus Berlin

eingereicht im Fachbereich Biologie, Chemie, Pharmazie
der Freien Universität Berlin

März, 2009

1. Gutachter: Prof. Dr. Peter Donner

2. Gutachter: Prof. Dr. Petra Knaus

Disputation am: 07. Juli 2009

This work has been performed from January 2006 until December 2008 at the Bayer Schering Pharma AG (Berlin). The PhD thesis was supervised by Prof. Peter Donner and Prof. Petra Knaus. Parts of this thesis were already published or presented:

Publications:

Off-target decoding of a multitarget kinase inhibitor by Chemical Proteomics, **Missner, E.**, Bahr, I., Badock, V., Luecking, U., Siemeister G. and Donner, P., *ChemBioChem 2009, vol. 10, no. 7, page 1163-1174*

Oral Presentations:

An off-target decoding approach for a small-molecule multitarget CDK inhibitor by Chemical Proteomics, Free University, Berlin, September 10, 2008

Beyond kinase panels – profiling a novel multi-target protein kinase inhibitor by targeted proteomics, 14th European Pharmaceutical Proteomics Laboratories, Berlin, Germany, April 26, 2007

Unveiling potential off-targets: Profile of binding proteins of a novel multi-target protein kinase inhibitor by inhibitor affinity chromatography (IAC) using different strategies of immobilization, Workshop on Chemical Genomics, Helmholtz Centre for Infection Research, March 6, 2007, Braunschweig, Germany

Poster Presentations:

An off-target decoding approach for a multitarget CDK inhibitor by Chemical Proteomics, Bayer Schering Pharma AG, Young Scientists Poster Session, Berlin, GER, October 29, 2008

Investigation of the interaction between a multitarget CDK inhibitor and the human pyridoxal kinase (PDXK) by Chemical Proteomics, 56th American Society for Mass Spectrometry (ASMS) Conference, Denver , CO, USA, June 5, 2008

Unveiling potential off-targets: Profile of binding proteins of a novel multi-target protein kinase inhibitor by inhibitor affinity chromatography (IAC) using different strategies of immobilization, Workshop on Chemical Genomics, Helmholtz Centre for Infection Research, Braunschweig, Germany, March 6, 2007

Table of Contents

Summary

An unbiased Chemical Proteomics approach for the identification of non-protein kinase off-targets of the multitarget protein kinase inhibitor C1 is presented. Two different compound immobilization routes were applied in order to identify off-targets interacting with distinct compound moieties. Furthermore, a soluble mimic of the immobilized compound was employed to confirm an appropriate compound immobilization with regard to protein kinase capturing. After having captured several protein kinases by using C1-matrix, 27 kinases were selected for a biochemical selectivity screen. A strong enzyme inhibition was found for the CDKs, demonstrating a high inhibitory potency, as well as for several other kinases from different kinase families indicating a poor selectivity of that compound. Besides this, several kinases which were captured by the C1-matrix showed only a low inhibition in the selectivity studies. Thus, an affinity capturing by the C1-matrix in the setup used for this study is not necessarily correlated with a high affinity binding but depends on both, affinity and expression level. In addition, a protein extract might differ from the physiological conditions with regard to the physico-chemical behavior of the proteins. Moreover, an indirect capturing of proteins via their association to other target proteins and protein complexes might occur. The low inhibitiory potency of C1 toward some kinases initially identified by the affinity pull-down and the identification of cyclins which are known to form complexes with CDKs support this assumption. This underlines the essential need for additional methods such as quantitative biochemical binding studies whenever reasonable in order to (de-)validate the results from affinity pull-down experiments. Furthermore, the mimic was applied to assess the functional effects of the linker on target binding. For this purpose, the mimic was screened in the same panel of kinases which was used for the selectivity studies of C1. The comparison of the selectivity patterns of compound and mimic revealed individual effects of the linker on distinct targets. Predominantly, the linker caused a reduction of inhibitory potential, very likely due to steric effects. However, some kinases showed an increased inhibition by the mimic compared to C1, presumably due to additional interaction options provided by the linker. Thus, a mimic helps to improve the data interpretation of Chemical Proteomics experiments, but it does not allow a general prediction of functional effects of the linker on target binding.

Within this Chemical Proteomics approach, the human pyridoxal kinase (PDXK) was identified as being captured by C1-matrix. Interestingly, PDXK is described to bind to the CDK2 inhibitor (R)-roscovitine, as well. PDXK is a non-protein kinase, responsible for the

phosphorylation of vitamin B6, a cofactor for numerous enzymes such as aminotransferases and decarboxylases. The PDXK/ C1 interaction was shown to occur at the substrate binding site rather than at the ATP site. However, subsequent quantitative binding studies including several C1 analogs revealed a very limited inhibition of PDXK activity. It was concluded that effects in pharmacological applications caused by a PDXK/ C1 interaction seem unlikely.

By employing an alternative immobilization route of C1, the carbonic anhydrase 2 (CA2) was found among others to be captured by the C1a-matrix. Since the ubiquitous CA2 is inhibited by C1 in the submicromolar range (IC_{50}), as demonstrated by subsequent activity assays, unwanted pharmacological effects or a trapping of the compound due to this interaction have to be taken into consideration. However, these results indicate that a modification at the sulfonamide group prevents CA2 from binding, most likely due to steric hindrance. To summarize, the utilization of different compound immobilization routes as a valuable method for an unbiased off-target profiling by Chemical Proteomics was introduced. By successfully applying this methodology, several off-targets interacting with distinct compound moieties were identified. The strategy of different compound immobilization routes can be employed for the target identification for hit compounds originating from phenotypic screens in cell-based assays or animal studies, as well. Thus, the utilization of different immobilization routes may become a useful tool for future off-target and target identification strategies.

Zusammenfassung

Ziel dieser Arbeit war die Identifizierung unbekannter sekundärer Zielproteine, so genannter off-targets, des multitarget Proteinkinase-Inhibitors C1 mit Hilfe eines ergebnisoffenen Chemical Proteomics-Ansatzes. Um off-targets zu finden, die an unterschiedliche Substanzmotive binden, wurde die Methodik der unterschiedlichen Immobilisierungsstrategien eingeführt. Darüber hinaus wurde ein so genanntes Mimik, d.h. eine lösliche Nachahmung der immobilisierten Substanz, verwendet, um die prinzipielle Eignung der gewählten Inhibitor-Kupplung hinsichtlich einer Anreicherung von Proteinkinasen zu zeigen und potentielle Linkereffekte zu untersuchen. Nachdem eine Reihe von Proteinkinasen angereichert und identifiziert werden konnten, wurden 27 davon für eine biochemische Selektivitätsstudie mit rekombinant hergestellten Enzymen ausgewählt. Zum einen wurde eine starke Inhibierung der Enzymaktivität der getesteten CDKs gefunden, womit das große inhibitorische Potential der Substanz gezeigt wurde. Zum anderen wurden auch bei einer Reihe weiterer Kinasen verschiedener Proteinkinase-Familien eine starke Abnahme der Enzymaktivität in Gegenwart des Inhibitors gefunden. Dies offenbarte die begrenzte Selektivität des Kinase-Inhibitors. Des Weiteren trat bei einigen Kinasen eine nur geringe Aktivitätsabnahme auf. Es wurde geschlussfolgert, dass die Anreicherung eines Proteins in dem für diese Arbeit verwendetem Chemical Proteomics-Ansatz nicht zwangsläufig mit einer hohen Affinität korreliert. Vielmehr scheint die Anreicherung von Proteinen in Abhängigkeit von der jeweiligen Affinität und Expressionsstärke zu erfolgen. Darüber hinaus könnte die Präparation eines geeigneten Proteinextraktes eine Veränderung des physiko-chemische Verhaltens der Proteine induziert haben. Auch eine indirekte Anreicherung von Proteinen über deren Assoziation mit anderen Zielproteinen und Proteinkomplexen kann nicht ausgeschlossen werden. Diese Annahme wird durch die Identifizierung von Cyclinen, von denen bekannt ist, dass sie feste Proteinkomplexe mit verschiedenen CDKs eingehen, untermauert. Diese Ergebnisse führten zu der Erkenntnis, dass weiterführende quantitative biochemische Bindungsstudien zur Validierung der Resultate aus Proteomics-Versuchen essentiell sind. Im Rahmen weiterer Untersuchungen wurde ein Mimik des gekuppelten Inhibitors verwendet, um funktionelle Effekte des Linkers auf das Binden der Zielproteine zu untersuchen. Dazu wurde das Mimik der gleichen Selektivitätsstudie wie zuvor die Substanz C1 unterzogen. Der Vergleich der beiden Selektivitätsmuster zeigte in der Mehrheit eine Abnahme der inhibitorischen Wirkung der Substanz infolge der Einführung des Linkers, vermutlich aufgrund von sterisch Effekten. Allerdings konnte vereinzelt auch ein Gewinn des inhibitorischen Potentials beobachtet

werden. Hervorgerufen durch die funktionellen Gruppen des Linkers, traten bei den betroffenen Kinasen vermutlich zusätzliche Wechselwirkungen und einhergehend damit höhere Bindungsaffinitäten auf. Es wurde geschlussfolgert, dass ein Mimik hilfreich bei Interpretation der Daten aus Chemical Proteomics-Ansätzen ist, allerdings nicht die generelle Vorhersage von funktionalen Effekten des Linkers auf das Binden von Zielproteinen erlaubt.

Im Rahmen dieser Arbeit wurde die humane Pyridoxalkinase (PDXK) als potentielles off-target des Inhibitors C1 identifiziert. Interessanterweise ist in der Literatur ein Binden dieses Enzyms an den CDK-Inhibitor (R)-roscovitine beschrieben. PDXK ist eine Nicht-Proteinkinase, die für die Phosphorylierung von Vitamin B6 verantwortlich ist. Dieses Vitamin ist ein essentieller Cofaktor für zahlreiche Aminotransferasen und Decarboxylasen. Es konnte gezeigt werden, dass die PDXK/ C1-Interaktion an der Substrat-Bindungsstelle auftritt und nicht, wie ursprünglich vermutet, über die ATP-Bindungsstelle vermittelt wird. In anschließenden Bindungsstudien wurde jedoch auch bei hohen Inhibitorkonzentrationen (50 µM) eine nur sehr begrenzte Enzym-Inhibition gemessen. Effekte in pharmakologischen Anwendungen des Inhibitors C1 aufgrund einer Wechselwirkung mit der Pyridoxalkinase erscheinen daher sehr unwahrscheinlich.

Im Rahmen einer zweiten Immobilisierungsstrategie wurde eine alternative Inhibitor-Matrix generiert. Diese führte zur Identifizierung weiterer potentieller off-targets, darunter der Carboanhydrase 2 (CA2). In anschließende Enzym-Aktivitätsassays konnte eine starke Bindungsaffinität (IC_{50}) im submikromolaren Bereich gezeigt werden. Daher müssen ungewollte pharmakologische Effekte oder zumindest das „Wegfangen“ des Inhibitors aufgrund dieser starken Wechselwirkung der Substanz mit der ubiquitär exprimierten CA2 in Betracht gezogen werden. Es konnte jedoch gezeigt werden, dass durch eine Modifikation des Sulfonamidmotivs diese ungewollte Wechselwirkung, vermutlich aufgrund von sterischen Effekten, vollständig unterbunden werden kann.

Zusammenfassend konnte in dieser Arbeit gezeigt werden, dass die Verwendung unterschiedlicher Immobilisierungsstrategien eine wertvolle Methodik darstellt, um neue und unbekannte off-targets von potentiellen Wirkstoffkandidaten zu identifizieren. Durch die erfolgreiche Anwendung dieser Methodik auf den Proteinkinase-Inhibitor C1 wurden verschiedene off-targets identifiziert, die mit unterschiedlichen Substanzmotiven wechselwirken. Die Methodik unterschiedlicher Immobilisierungsstrategien erscheint ebenfalls geeignet, um Zielproteine von Substanzen zu identifizieren, die in phänotypischen Screens in zell-basierten Assays oder Tierstudien gefunden wurden und deren Wirkmechanismen noch unbekannt sind.

1. Introduction

1.1. Protein kinases play a key role in many cellular processes and represent suitable drug targets

The 518 human protein kinases constitute about 1.7 % of all human genes (Manning, G. et al. 2002b) and are representing one of the largest families of genes in eukaryotes (Manning, G. et al. 2002a). On the basis of their structural relatedness, the members of that family are grouped into about 20 subfamilies. In 1963, the phosphorylation of proteins was identified as a regulatory mechanism for the control of the glycogen metabolism (Cohen, P. et al. 2001). Since than, the awareness of protein phosphorylation mediated by protein kinases as a mechanism of utmost importance for the regulation of protein function has grown remarkably (Cohen, P. et al. 2001). Protein kinases have turned out to have a key role in many cellular processes like metabolism, transcription, cell cycle progression, cytoskeletal rearrangement and cell movement, apoptosis, and differentiation. Additionally, protein kinases are significantly involved in intercellular communication during development, in physiological responses and in homeostasis, and in the functioning of the nervous and immune systems (Manning, G. et al. 2002b). Accordingly, a variety of studies shows that protein kinases are suitable pharmaceutical target proteins, whose activity can be modified by a drug in order to treat the diseases which are caused by their dysregulation. Dysregulated kinase activities caused by upregulation, constitutional activation or inactivation were shown to cause various severe pathological conditions (Cohen, P. 2002), e.g. cancer (Boehm, J. S. et al. 2007; Carpten, J. D. et al. 2007; Davies, H. et al. 2002; Engelman, J. A. et al. 2007; Soda, M. et al. 2007; Strebhardt, K. et al. 2006; Tse, A. N. et al. 2007), central nervous system disorders (Hayashi, M. L. et al. 2007; Smith, W. W. et al. 2006), autoimmune diseases (Whartenby, K. A. et al. 2005), post-transplant immunosuppression (Changelian, P. S. et al. 2003), osteoporosis (Buckbinder, L. et al. 2007) and metabolic disorders (Solinas, G. et al. 2007).

In particular, proliferative diseases such as cancer have stimulated considerable efforts in order to develop therapies against uncontrolled cell proliferation and tumor growth (Weinmann, H. et al. 2005). Since cyclin-dependent protein kinases (CDKs) have essential roles during the correct initiation and co-ordination of the cell division cycle phases, the manipulation of CDK activity is considered as one of potential therapy approaches for the treatment of cancer and non-cancer indications (Meijer, L. et al. 1999).

1.2. The cell cycle

The eukaryotic cell division cycle consists of four highly regulated and co-ordinated sequential phases during which the genome is replicated and segregated, giving two genetically identical daughter cells. The G1-phase is characterized by cell growth and the response to extracellular stimuli. The DNA replication occurs during the S-phase resulting in a tetraploid DNA content (4N). The entry into the M-phase (mitosis) is prepared during the G2-phase and in the mitosis, the duplicated DNA gets segregated (division of the cell nucleus). Subsequently, the cell divides and the DNA is distributed to the two genetically identical daughter cells, each containing a diploid amount of DNA (2N). A reversible exit, which may occur after the M-phase, is termed G0-phase or quiescence, whereas the irreversible exit from the cell cycle is known as senescence or terminal differentiation.

1.3. Cell cycle co-ordination by cyclin-dependent kinase/ cyclin complexes

The co-ordinated progression through the cell cycle of eukaryotic cells is highly regulated by the activity of cyclin-dependent kinases (CDKs), a family of Ser/ Thr protein kinases. At certain times during the cell cycle, they non-covalently form specific 1:1 complexes with different cyclins (Cyc), the regulatory subunits of the resulting CDK holoenzymes (CDK/ Cyc) (Morgan, D. O. 1997). The entry and the progression through the restriction point in G1 require a combination of CDK4,6/ CycD and CDK2/ CycE activity (Massague, J. 2004; Woo, R. A. et al. 2003). Once this restriction point has been passed, the cell no longer requires growth factors and proliferative signaling molecules in order to initiate DNA synthesis and complete one cell cycle (Hitomi, M. et al. 2006). A key substrate of CDK4,6/ CycD and CDK2/ CycE is the tumor suppressor gene product retino blastoma (Rb). In its functional state it acts as a transcriptional corepressor. Besides other mechanisms, unphosphorylated Rb binds E2F-type transcription factors and forms histone deacetylase (HDAC)-containing transcription repressor complexes (Lipinski, M. M. et al. 1999). A hyperphosphorylation of Rb by CDKs causes a release of bound E2F, resulting in the transcription of the respective E2F target genes involved in DNA synthesis, and in cell cycle progression (Zhu, L. 2005). Additionally, Rb phosphorylation disrupts Rb-HDAC repressor complexes leading to further gene activation (Zhang, H. S. et al. 2000), the transition through the G1-restriction point and the entry into the S-phase. CDK2/ CycE and CDK2/ CycA are responsible for the progression through the S-phase and its finalization (Senderowicz, A. M.

et al. 2000). As soon as the cell has entered the S-phase, CDK2/ CycA phosphorylates and thereby inactivates E2F. After the replication of the DNA has been completed, the CDK1/ CycB complex co-ordinates the passage through the G2- and the M-phase (Nilsson, I. et al. 2000) (Figure 1).

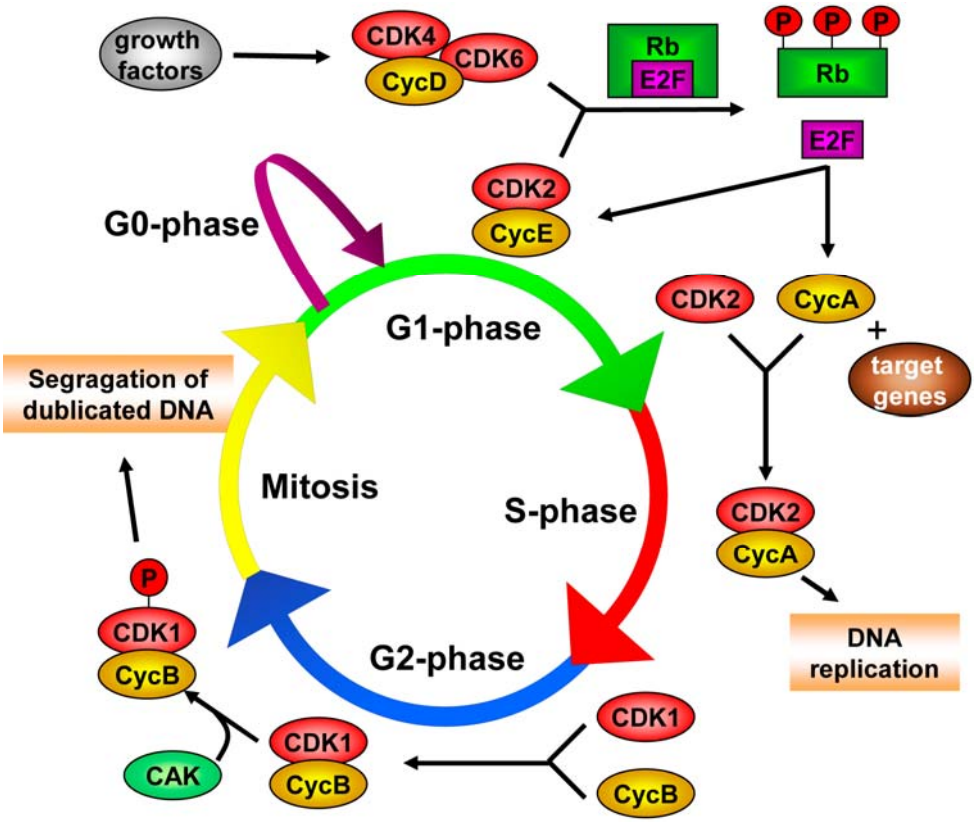

Figure 1. Co-ordination of the eukaryotic cell cycle by CDK/ cyclin complexes. The co-ordinated progression through the cell cycle of eukaryotic cells is highly regulated by the activity of 1:1 complexes of cyclin-dependent kinases (CDKs) with different cyclins (Cyc). In response to extracellular stimuli by growth factors, the CDK4,6/ CycD complex is activated and phosphorylates the tumor suppressor gene product retino blastoma (Rb) in the G1-phase. Unphosphorylated Rb binds E2F-type transcription factors which are released upon the hyperphosphorylation of Rb. Subsequently, the released E2F induces the transcription of target genes involved in DNA synthesis, and in cell cycle progression, resulting in the entry into the S-phase. CDK2/ CycE phosphorylates Rb in the late G1-phase and thereby enhances this process. Afterwards, CDK2/ CycE and CDK2/ CycA are responsible for the progression through the S-phase and its finalization. After the replication of the DNA has been completed, the CDK1/ CycB complex is activated by the phosphorylation by CDK activating kinases (CAKs). Upon activation, CDK1/ CycB co-ordinates the passage through the G2- and the M-phase.

1.4. Cell cycle regulation and checkpoint control

The paramount importance of the cell cycle is reflected in its high degree of regulation. Indeed, the activity of CDKs is tightly controlled by several control mechanisms including cyclin synthesis and degradation, association of CDK/ Cyc complexes, phosphorylation and dephosphorylation of regulatory Thr and Tyr residues of CDKs, and association of CDKs with natural inhibitor proteins. Whereas the protein levels of CDKs are rather constant in proliferating cells, the levels of cyclins vary through the cell cycle (Morgan, D. O. 1997). For instance, CycD expression peaks in the early G1-phase due to growth factor stimuli whereas the expression of CycE is induced by E2F transcription factors once the cell has passed the G1-restriction point. Cyclin downregulation is regulated by the N-terminal destruction-box (D-box) of unbound cyclins and an ubiquitin-mediated proteolysis (King, R. W. et al. 1996). In addition, CDK activity is regulated by their phosphorylation state. By phosphorylating regulatory Thr residues, CDK activating kinases (CAKs) can induce CDK activity (Kaldis, P. 1999). In contrast, the kinase family Wee1/ Myt1 is described to mediate inactivating phosphorylations of Thr/ Tyr residues (Booher, R. N. et al. 1997; Fattaey, A. et al. 1997; Lundgren, K. et al. 1991), though, dephosphorylation by cdc25 phosphatase reconstitutes CDK activity (Nilsson, I. et al. 2000). Furthermore, the activity of CDK/ Cyc complexes is regulated by a group of natural CDK inhibitor proteins (CKIs) belonging to the CIP/ KIP family (p21, p27, and p57) and the INK family (p15, p16, p18, and p19), respectively (Harper, J. W. et al. 1996). By binding to certain CDKs via their N-terminus, they prevent ATP binding to the catalytic domain of the respective CDKs (Pavletich, N. P. 1999). In addition to the network of CDK activity, the correct progression of cell cycle events is monitored by a checkpoint control system. The G1 checkpoint senses if the cell is appropriate nourished, if it is correctly interacting with other cells or the substratum, and if DNA is intact. Thereby, the G1 checkpoint ensures, that the DNA synthesis does not start until all requirements are fulfilled (Massague, J. 2004). At the G2/ M checkpoint, the correct DNA replication and assembly of the mitotic spindle is checked. Errors are repaired or the cell cycle is aborted and apoptosis is induced to prevent passing these errors to daughter cells (Smits, V. A. et al. 2001).

1.5. CDKs – Targets for intervention in the cell cycle

Corresponding to the mechanisms illustrated above, the vast majority of human cancers have abnormalities in some component of the Rb pathway because of hyperactivation of CDKs. This abnormal activity results from an overexpression of cyclins and CDKs, respectively, or Rb gene mutations, or a decrease in natural CDK inhibitor proteins (CKIs) (Senderowicz, A. M. et al. 2000). For instance, the loss of the p27KIP1 protein confers a poor prognosis for patients with breast, prostate, lung, colon, or gastric carcinoma (Tsihlias, J. et al. 1999). Furthermore, the loss of the p16INK4a protein predicts a poor outcome in patients with non-small-cell lung cancer or melanoma (Tsihlias, J. et al. 1999). For this reason, a mechanism-based therapy using pharmacologic CDK inhibitors is described in the literature as a promising approach in order to treat neoplasms by the induction of cell cycle arrest, apoptosis, cell differentiation or sensitization to standard chemotherapies (Senderowicz, A. M. et al. 2000). For therapeutic interventions, direct and indirect strategies are proposed to modulate CDK activity. Indirect CDK modulators could target the expression level and synthesis of the CDK/ Cyc complexes or the CKIs. Alternatively, they could modulate the phosphorylation state of CDKs by targeting CAKs or affecting cdc25 and Wee1/ Myt1. Furthermore, the manipulation of the proteolytic machinery which regulates the degradation of CDK/ Cyc complexes or their regulators is discussed (Senderowicz, A. M. et al. 2000). In contrast, ATP competitive small molecule CDK inhibitors provide the opportunity for a rational drug design in order to directly target the ATP binding site of CDKs. Figure 2 shows several CDK inhibitors against various cancer indications which are currently in advanced preclinical testing or in clinical trials (Malumbres, M. et al. 2008; Popowycz, F. et al. 2009; Sharma, P. S. et al. 2008).

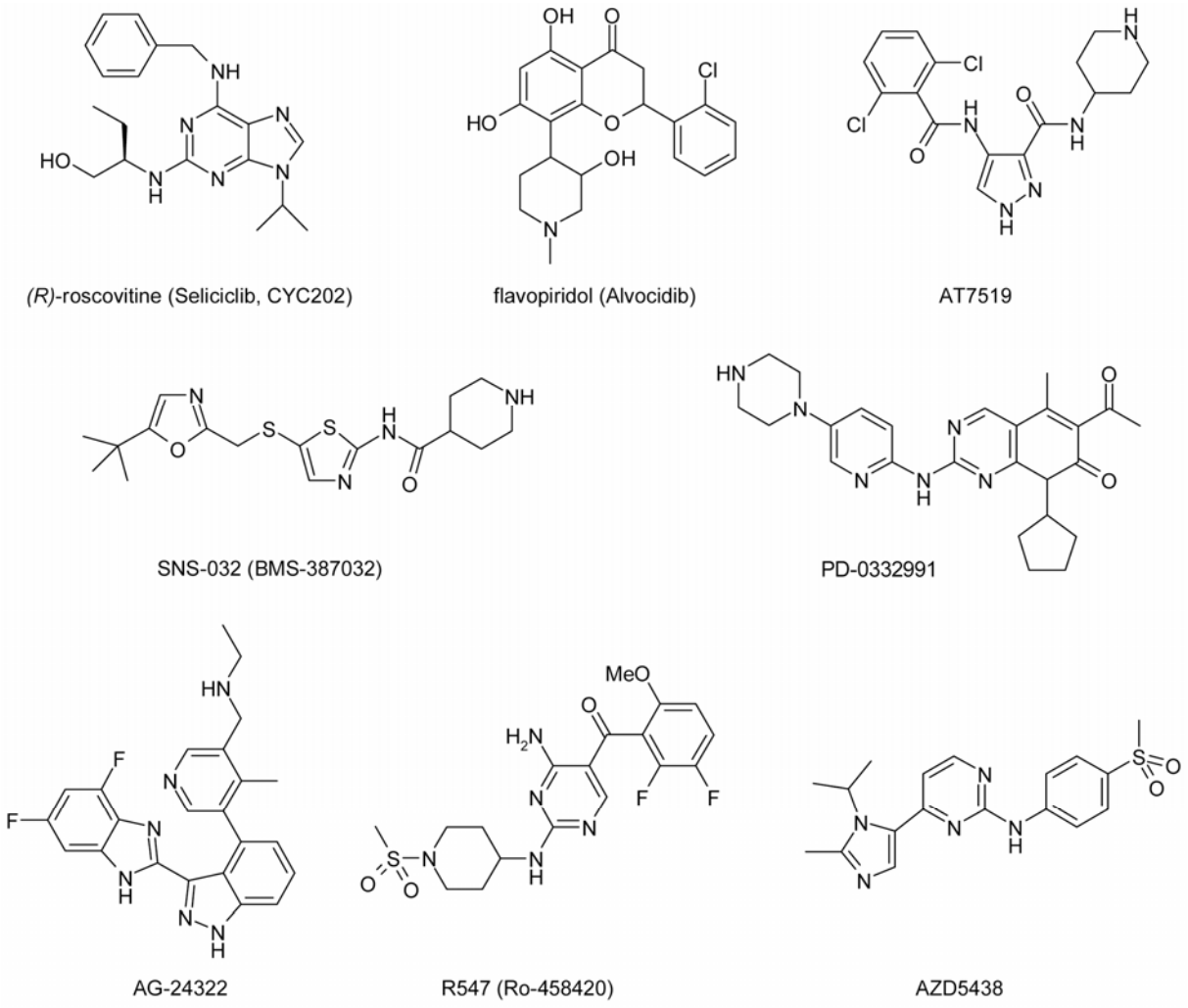

Figure 2. Several CDK inhibitors in preclinical testing or clinical trials.

1.6. ATP competitive small molecule protein kinase inhibitors

Since all protein kinases employ the nucleotide ATP for the phosphorylation reaction, the ATP binding pocket was originally thought not to be an appropriate target for drug discovery (Toledo, L. M. et al. 1999). First, due to the high degree of conservation of the ATP-binding pocket within the protein kinase family, selectivity is a significant challenge for drug development. Moreover, the high intracellular ATP concentration of up to 5 mM and K_m values in the micromolar range for most of the protein kinases in order to ensure ATP saturation, ATP competitive inhibitors need to have an inhibitory potential in the low nanomolar range for an efficient *in vivo* competition (Lawrence, D. S. et al. 1998). Finally, a multitude of ATP-dependent enzymes exists, representing an immense potential of toxicity for indiscriminant ATP mimetic compounds (Morin, M. J. 2000). Nevertheless, the approval of the first selective tyrosine-kinase inhibitor imatinib (Gleevec, Novartis, Figure 3) (Capdeville, R. et al. 2002) has demonstrated that protein kinases represent an attractive target

class. Its success has extremely encouraged pharma industry to generate a multitude of kinase inhibitors, showing that imatinib is not unique (Baselga, J. 2006; Collins, I. et al. 2006). Besides G-protein coupled receptors, protein kinases have now become the most important drug target class (Cohen, P. 2002; Goldstein, D. M. et al. 2008). The increasing availability of x-ray structures of protein kinases in complex with selective, ATP-site directed compounds has helped to elucidate the inhibitory mechanisms. It was shown that selective compounds occupy both conserved and non-conserved residues within the ATP binding site (Cherry, M. et al. 2004; Fischer, P. M. 2004; Toledo, L. M. et al. 1999). These non-conserved amino acid residues are not involved in the ATP binding but can be unique for a subset of protein kinases and therefore provide opportunities for specific interactions and the chemical optimization of inhibitors.

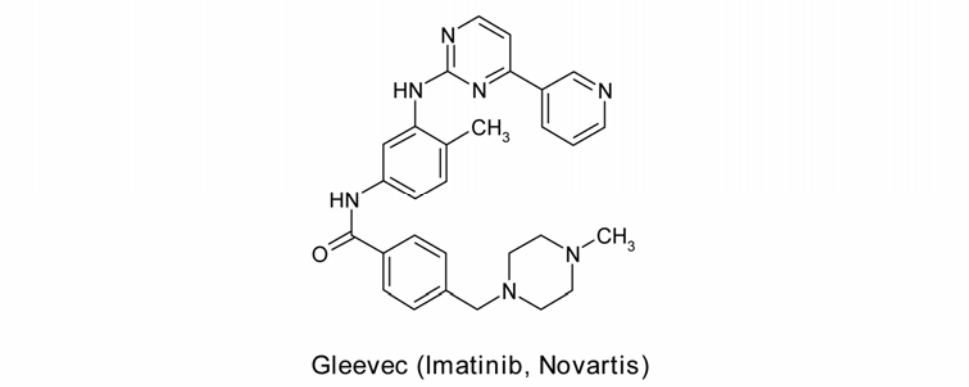

Figure 3. Gleevec (imatinib, a 2-phenylaminopyrimidine, Novartis) is an ATP-competitive drug which is used for the treatment of chronic myelogenous leukemia (CML), gastrointestinal stromal tumors (GISTs) and other types of cancer. The hematological stem cell disorder CML arises from a reciprocal translocation between chromosome 9 and 22, giving the Philadelphia chromosome. The molecular consequence is a fusion gene of *c-Abl* (Abelson tyrosine kinase) and *Brc* (breakpoint cluster region). The resulting gene product is the constitutively active Brc-Abl tyrosine kinase, which leads to an excessive proliferation of myeloid cells in the bone marrow. Imatinib decreases the kinase activity by occupying the ATP site of Brc-Abl. Further known targets of Imatinib are c-Kit and PDGF-R. Imatinib was the first selective tyrosine-kinase inhibitor to be approved by the FDA and triggered a variety of pharmaceutical drug development programs aimed at identifying selective kinase inhibitors for various indications.

1.7. Current rational drug discovery strategies might miss unknown off-targets

The majority of current rational drug discovery strategies are based on a target-centric process. Several technologies, e.g. northern array-based platforms, are used for the identification of targets and target classes. Once a target had been identified, it is functional validated by RNA interference (RNAi, used especially for target overexpression or

knockdown), transgenic animals, and model organisms (Benson, J. D. et al. 2006). Subsequently, for lead generation, libraries of compounds are screened against the recombinant, isolated, purified target protein or functional protein domain in order to identify hits. Hits are compounds which are capable of inhibiting the enzymatic activity of the selected target with weak or moderate potency and often poor selectivity. During the lead optimization process, these initially identified hits are further profiled and optimized with regard to their potency. The compound selectivity is addressed by counterscreens in protein kinase assay panels resulting in a small number of lead compounds. In theory, a further improvement of pharmacological properties leads to a candidate structure which is preclinical profiled in animal models and finally tested in clinical trials (Figure 4) (Morwick, T. et al. 2006; Pevarello, P. et al. 2004; Wittman, M. et al. 2005). In practice, however, results from biochemical screening data do not necessarily correlate with the observed effects in cells, animals or in human. Discrepancies may be explained by additional, unknown drug effects. Besides the desired on-target kinase inhibition, the compounds might affect multiple unknown off-targets, which either contribute to the biological effect of the kinase inhibitor or which counteract or lead to detrimental side-effects. Indeed, it has been estimated that another 1500 human proteins besides protein kinases may exist utilizing ATP (Valsasina, B. et al. 2004), e.g. ATPases such as heat shock proteins (HSP) and kinesins, GTPases, sulfotransferases and others (Chene, P. 2003). Thus, due to a high degree of structural conservation of the ATP binding site, toward which most inhibitors are directed, multiple targets and off-target effects contributing to the biological activity have been reported for several drugs (Bantscheff, M. et al. 2007; Budillon, A. et al. 2005; Hall, S. E. 2006; Morphy, R. et al. 2004; Verweij, J. et al. 2007). In order to obtain deeper insights into the target space of a compound, additional strategies for a more global compound profiling have been developed, such as Chemical Proteomics (Daub, H. 2005; Drewes G. et al. 2007; Katayama, H. et al. 2007; Knockaert, M. et al. 2002), active-site labeling probes (Cravatt, B. F. et al. 2008; Sadaghiani, A. M. et al. 2007), compound-immobilized surface plasmon resonance (SPR) technologies (Boozer, C. et al. 2006) and small molecule microarrays (Uttamchandani, M. et al. 2005).

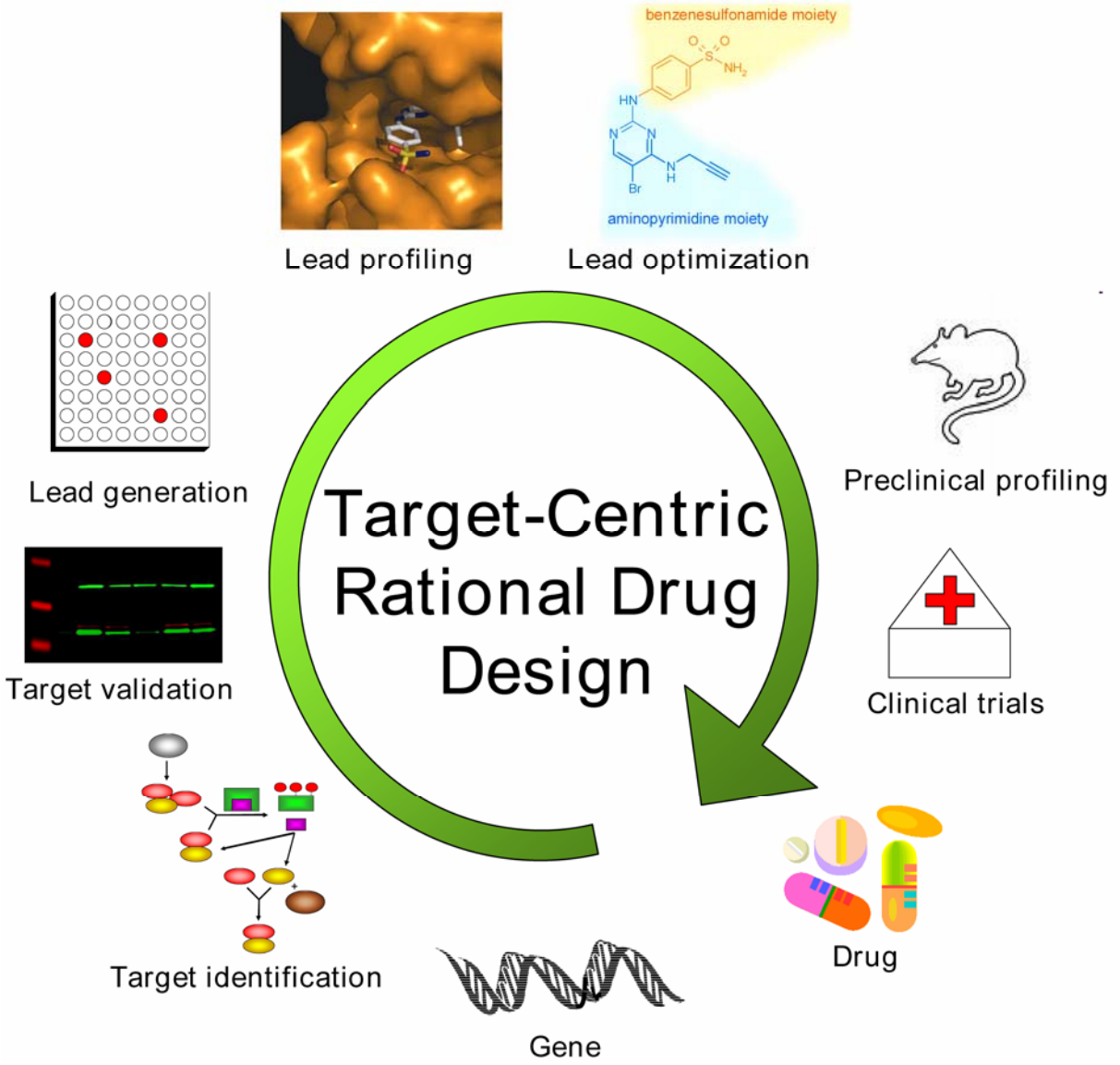

Figure 4. The scheme illustrates the process of a target-based rational drug design. Suitable targets are identified and validated by employing several technology platforms before lead discovery starts to screen libraries of compounds against the recombinant, isolated, purified target protein or functional target domain in order to find a hit compound. Once an appropriate hit structure had been identified, such techniques as x-ray crystallography and NMR spectroscopy are used to obtain three-dimensional information about the target/ compound complex. Based on these information, the compound potency is increased during the lead generation and optimization process by generating suitable derivatives of the compound. In addition, the selectivity of a compound is addressed by counterscreens in enzyme assay panels. A further improvement of pharmacological properties can lead to a candidate structure which is preclinical profiled in animal models and finally tested in clinical trials before approval. However, unknown off-target effects might occur, which either contribute to the biological effect of the drug or lead to detrimental side-effects, potentially resulting in the project exit.

1.8. Chemical Proteomics is a valuable tool for additional compound characterization

Chemical proteomics is a direct and unbiased approach in order to obtain protein-binding profiles of compounds of interest. Compared to biochemical screening assays using recombinant proteins, a Chemical Proteomics approach provides the opportunity to profile a compound against any proteome of interest containing fully three-dimensional folded proteins, including all of their post-translational modifications. For this purpose, a small-molecule ligand is modified by introducing a suitable reactive group, e.g. a primary amine, or a linker enabling the immobilization to a solid support, referred to as matrix. Crystallographic data of the target/ compound complex or computational modeling studies can provide valuable information for the selection of an appropriate coupling region which would not interfere with the known binding orientation of the compound in the ATP pocket. Afterwards, an inhibitor affinity chromatography (IAC) is carried out. To this end, the compound matrix is incubated with a protein extract which can be cell, tissue, or tumor extracts for the affinity capturing of potential drug targets. An extensive washing procedure using 1 M salt and several washing steps are crucial parameter in order to reduce non-specific interaction of high abundant proteins with the matrix or the linker. If non-specific binders are not removed, they not only might produce artefacts but may also bind and saturate the compound matrix, thereby impairing the capturing of high-affinity, low abundant binders. Subsequently, the captured proteins are eluted either specifically using free compound or non-specifically by denaturation. Due to the often very limited solubility of compounds in aqueous buffers, reducing their capability of a complete elution, a combination of free inhibitor and ATP was introduced for a specific and more comprehensive elution (Godl, K. et al. 2003). Moreover, a sequential elution was suggested to provide additional information of the strength of interactions (Lolli, G. et al. 2003). Finally, eluted proteins are identified by mass spectrometry or immunodetection. (Figure 5.)

The concept of a serial affinity chromatography was introduced in order to confirm a specific enrichment of a potential target protein (Yamamoto, K. et al. 2006). To this end, the protein extract is incubated with the compound matrix. Subsequently, the flow-through is mixed with the same amount of fresh compound matrix. Specific binders are essentially captured by the first affinity matrix whereas the amounts of non-specifically bound proteins are similar for both matrices. Using this method, the protein target of FK506 (FKBP12), benzenesulfonamide (carbonic anhydrase 2) and methotrexate (dihydrofolate reductase) were identified in proof-of-concept experiments (Yamamoto, K. et al. 2006). In parallel to

capturing experiments using compound matrix, a control matrix can be employed for pull-down experiments. By comparing the resultant protein patterns, non-specific binders as well as biologically irrelevant interactions can be identified. If available, an inactive compound can be used to prepare the control matrix, as suggested by (Knockaert M et al. 2000). Alternatively, control experiments can be carried out by using blocked and thereby inactivated matrices as demonstrated in the literature (Godl, K. et al. 2003).

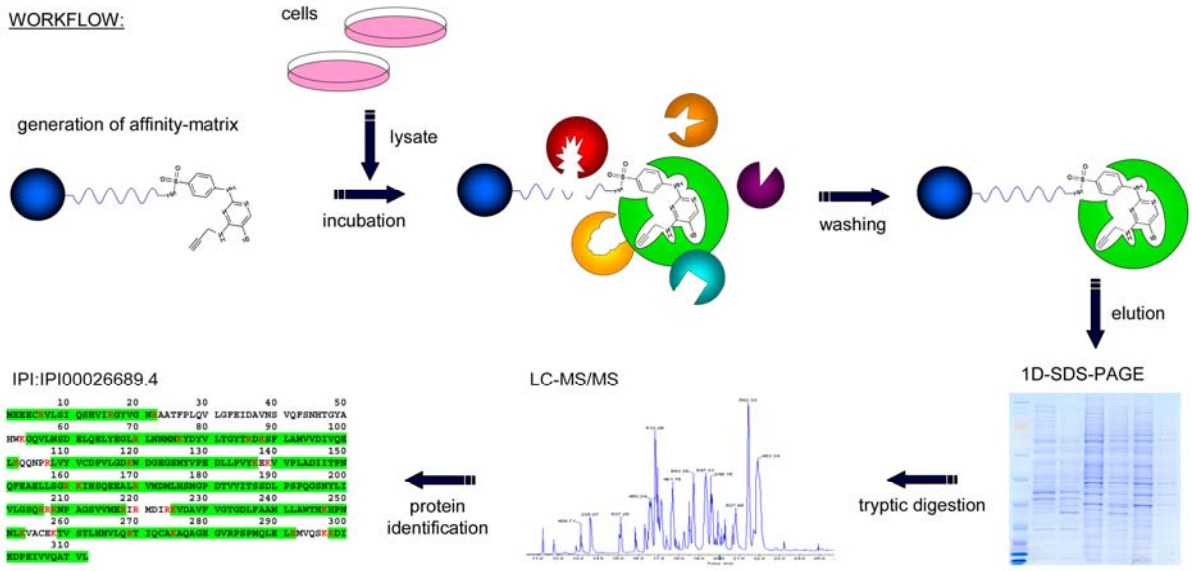

Figure 5. Protein/ compound interaction profiling by Chemical Proteomics. Linkable compound analogs provided with a suitable linker are synthesized and covalently immobilized to a solid support. It has to be made sure that the linker does not interfere with the activity of the compound. The resulting compound affinity matrix is employed for affinity capturing of interacting protein targets from cell, tissue or tumor lysate. After extensive washing, bound proteins are eluted specifically using free compound (often, compound solubility is limited) or non-specifically by denaturation (or sequentially by applying both) and subsequently analyzed by 1D-SDS-PAGE, LC-MS/MS, and bioinformatical data processing. Non-specifically bound proteins can be identified in parallel experiments where a control matrix (e.g. an immobilized inactive compound analog or blocked Sepharose^{TM}) is used for pull-down experiments.

Several studies illustrate that Chemical Proteomics has been successfully implemented for the characterization of kinase inhibitors and other drug candidates. For instance, the FK506-binding protein and mammalian histone deacetylase 1 were identified by employing Chemical Proteomics (Harding, M. W. et al. 1989; Taunton, J. et al. 1996). Fukuda et al. identified leptomycin B as a specific inhibitor of the nuclear export signal-dependent protein, CRM1 (Fukuda, M. et al. 1997). Godl et al. demonstrated the enrichment of several previously unknown high-affinity kinase targets of the anti-inflammatory drug SB203580 and of the

angiogenesis inhibitor SU6668 by the respective compound matrices (Godl, K. et al. 2003; Godl, K. et al. 2005). Several other examples exist, revealing further targets of ATP-mimetic compounds by inhibitor affinity chromatography (Brehmer, D. et al. 2004; Brehmer, D. et al. 2005; Knockaert M et al. 2000; Knockaert, M. et al. 2002; Liu, Y. et al. 2005; Wissing, J. et al. 2004).

The Kinobeads approach is an advanced technology which quantitatively measures the competition of a free compound with an affinity matrix consisting of several immobilized tool compounds selected to capture a large portion of the expressed kinome and other purine binding proteins (Bantscheff, M. et al. 2007; Kruse, U. et al. 2008). Imatinib, dasatinib and bosutinib (Capdeville, R. et al. 2002; Hantschel, O. et al. 2004; Weisberg, E. et al. 2007) were successfully reprofiled by the Kinobeads technology (Bantscheff, M. et al. 2007). Known targets of the drugs were confirmed and new targets identified, demonstrating the capability of Chemical Proteomics to provide valuable information for drug discovery. However, by profiling compounds against a subset of proteins captured by tool compounds, the unbiased character in regard to potential off-targets, a particular advantage of Chemical Proteomics, gets lost to some extent . In fact, an unbiased off-target characterization during lead optimization processes is highly desirable in order to gain deeper insights into the biological activity and the off-target profile of a drug, respectively. Emphasizing this, the investigation of the off-target profile of *(R)*-roscovitine (Seliciclib, Cyclacel Pharmaceuticals, Figure 6) by affinity chromatography with the drug immobilized on a Sepharose^{TM} matrix (Bach, S. et al. 2005; Bettayeb, K. et al. 2008), revealed an unexpected off-target. *(R)*-roscovitine is an ATP-competitive small molecule CDK inhibitor which is currently in phase 2 clinical trials for various cancer indications (de la, Motte S. et al. 2004; McClue, S. J. et al. 2002). In addition to its expected targets extracellular signal-regulated kinase 1 (ERK1), ERK2, and cyclin-dependent kinases (CDKs), the previously unknown off-target pyridoxal kinase (PDXK) was identified. It has been suggested that the unexpected binding activity of *(R)*-roscovitine to PDXK explains some of the biological effects of the drug or dilutes its on-target effects by reducing the amount of free *(R)*-roscovitine which is available for the desired target interaction.

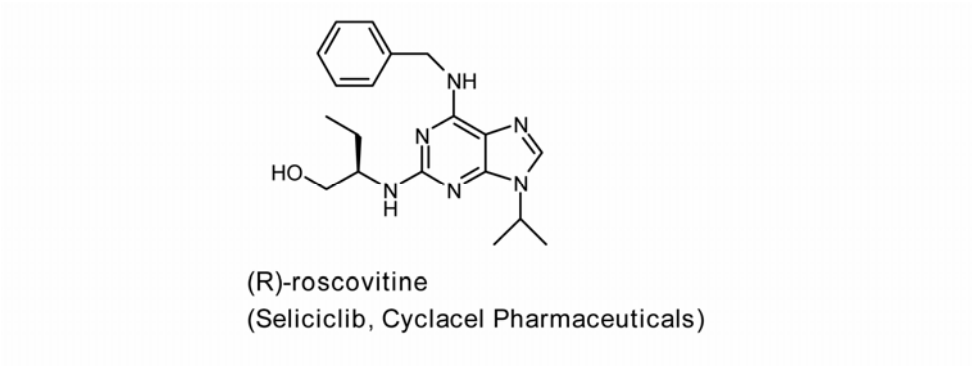

Figure 6. Structure of the purine class CDK inhibitor *(R)*-roscovitine (Seliciclib, Cyclacel Pharmaceuticals). The off-target profile of this ATP-competitive inhibitor was investigated by inhibitor affinity chromatography by others and the previously unknown off-target pyridoxal kinase (PDXK) was identified.

1.9. Compound C1

The research compound C1 (Figure 7) was generated in an in-house drug discovery program aimed at identifying and optimizing a small molecule multitarget CDK inhibitor in order to investigate its suitability for the treatment of cancer. The ATP-competitive compound was previously shown to have high potency against CDK2 and macrocyclic derivatives were described as multitarget CDK and VEGF-R inhibitors with potent antiproliferative activities towards various human tumor cells and in a human tumor xenograft model (Luecking, U. et al. 2007). The inhibitor C1 chemically belongs to the group of diaminopyrimidines and contains an aminopyrimidine and a benzenesulfonamide moiety with the sulfonamide group in the *para* position. Collaborative efforts of high-throughput screening, medicinal chemistry, and structural biology compiled broad knowledge about the structure-activity relationship with regard to CDK2 binding. For instance, the aminopyrimidine moiety was shown to bind to the hinge region of CDK2 by two hydrogen bonds and the sulfonamide group is known to form two hydrogen bonds to the main chain and side chain of Asp-86 and one water-mediated hydrogen bond to the carbonyl group of Ile-10 (Luecking, U. et al. 2007). However, little is known about the off-target profile of that compound, particularly with regard to potential non-protein kinase interactions.

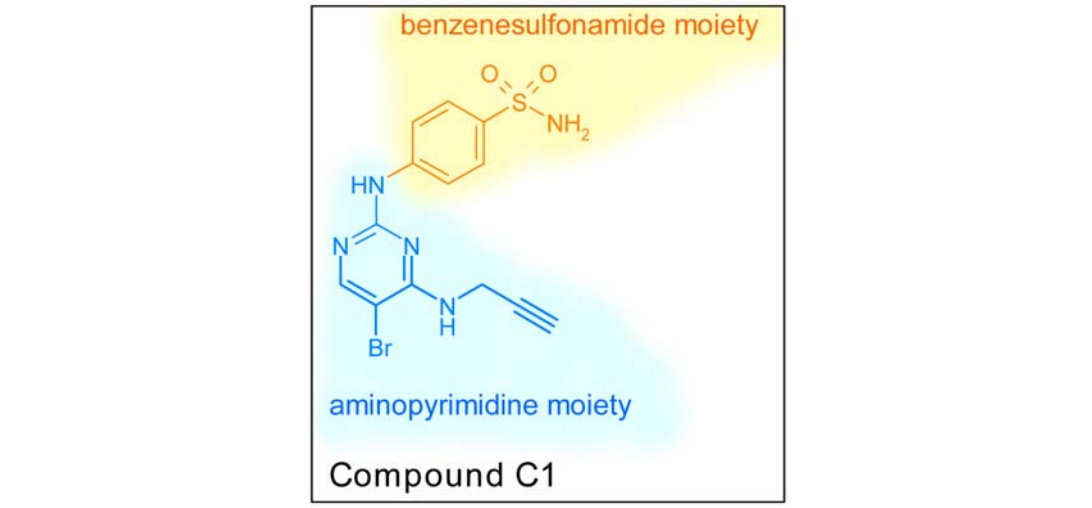

Figure 7. Structure of the compound C1. The pyrimidine class compound contains an aminopyrimidine and a benzenesulfonamide moiety with the sulfonamide group in the *para* position. The ATP-competitive inhibitor was identified in a drug discovery program aimed at generating a small molecule multitarget CDK inhibitor. Previous studies demonstrated that its inhibitory potential toward CDK2 activity is in the low nanomolar range.

2. Aim of this thesis

Cyclin-dependent kinases are described in the literature as promising targets for small molecule kinase inhibitors in order to treat cancer by the induction of cell cycle arrest, apoptosis, cell differentiation or sensitization to standard chemotherapies. Thus, pharma industry has generated several ATP-competitive CDK inhibitors some of which are currently tested in clinical trials. In contrast, the in-house generated multitarget CDK inhibitor C1 is still object of ongoing optimization processes, although, its high inhibitory potential against CDK2 activity has already been shown and some knowledge of its structure-activity relationship with regard to the desired target binding has been obtained, yet (Luecking, U. et al. 2007). However, the available technologies reveal little about the non-protein kinase off-target profile of that compound. The objective of this work was therefore to introduce the Chemical Proteomics technology as a tool broadening the knowledge about the off-target profile of compound C1, particularly with respect to potential non-protein kinase interactions.

Based on a computational model of a compound/ target complex, the first goal was to identify appropriate compound immobilization routes in order to capture proteins interacting with distinct compound moieties. Furthermore, a compound derivative provided with a suitable linker and a functional group for the desired coupling reaction was synthesized within this work. Additional derivatives, including a soluble mimic and another linkable analog, were provided by colleagues. An additional goal was to employ the soluble mimic of the coupled inhibitor to confirm, that the immobilization of the compound would not interfere with its functionality and to analyze potential linker effects due to the immobilization. Moreover, it was necessary to introduce a suitable assay protocol for the Chemical Proteomics approach. This included washing and sample preparation procedures in order to comprehensively analyze the captured proteins over the entire molecular weight range by mass spectrometry.

Additionally, an essential aim of this thesis was the biochemical characterization of identified compound/ off-target interactions. This included the testing of the compound in a protein kinase assay panel as well as the recombinant expression and purification of a potential off-target protein for biochemical binding studies.

3. Materials and Methods

3.1. Reagents and antibodies:

Unless otherwise stated, all reagents were purchased from Sigma (Munich, Germany). Primary antibodies used were monoclonal mouse anti-CDK2 antibody (Santa Cruz Biotechnology, Inc., Heidelberg, Germany), polyclonal rabbit anti-PDXK (Abcam plc**,** Cambridge, UK), and polyclonal rabbit anti-CA2 (Chemicon/ Millipore, Billerica, MA, USA). IRDye® 800CW conjugated donkey anti-mouse antibody and IRDye® 700DX donkey anti-rabbit antibody (both from Rockland Immunochemicals, Inc., Gilbertsville, PA, USA) were used as the corresponding fluorescently-labeled secondary antibodies. All antibodies were diluted as recommended by the manufacturer.

3.2. Chemical Proteomics

3.2.1. Computational modeling

Based on previously published co-crystallization experiments of CDK2 in complex with various C1 analogs (Luecking, U. et al. 2007), C1 was modeled into the ATP binding pocket of CDK2 using Discovery Studio 2.1 (Accelrys, Cambridge, UK). The solvent accessible surface was calculated using Pymol (DeLano Scientific LLC, Palo Alto, CA, USA). This work was done by Dr. Martina Schaefer (Bayer Schering Pharma AG, Structural Biology).

3.2.2. Synthetic procedures

Figure 8 shows the synthesis of compound C1-SL, which was performed within this thesis. Analogous to this synthetic procedure, compound C1 and its analogs C1-LL (mimic), and C1a (Figure 9) were generated in-house by Dr. Ulrich Luecking (Bayer Schering Pharma AG, Medicinal Chemistry Berlin). The correct compound identity was confirmed by ^{1}H-NMR and MS.

*4-Amino-benzenesulfonyl fluoride (**B**)*: 4-Nitro-benzenesulfonyl fluoride **A** (5 g, 24.4 mmol) (Acros, Geel, Belgium) in 125 mL ethanol was hydrogenated for 2 h at room temperature under normal pressure using Raney nickel. Subsequently, the suspension was filtered and 4-Amino-benzenesulfonyl fluoride (**B**) was recrystallized from diisopropyl ether/ hexane (1:1, v/v). 3.8 g (21.7 mmol, 89 % yield) of the product (**B**) was obtained.

*(5-Bromo-2-chloro-pyrimidin-4-yl)-prop-2-ynyl-amine (**E**):* Prop-2-ynylamine (**D**) (1.5 mL, 21.9 mmol) and triethylamine (3 mL, 21.9 mmol) were added to a stirred solution of 5-Bromo-2,4-dichloro-pyrimidine **C** (5 g, 21.9 mmol) in 100 mL acetonitrile at RT. After 4 h, the reaction was stopped by the addition of citric acid (20 %) and extracted with ethyl acetate (2x). The organic phase was dried (Na_2SO_4) and concentrated in vacuo. 5.3 g (21.5 mmol, 98 % yield) of the product (5-Bromo-2-chloro-pyrimidin-4-yl)-prop-2-ynyl-amine (**E**) was obtained.

*4-(5-Bromo-4-prop-2-ynylamino-pyrimidin-2-ylamino)-benzenesulfonyl fluoride (**F**):* (5-Bromo-2-chloro-pyrimidin-4-yl)-prop-2-ynyl-amine (**E**) (3.1 g, 12.7 mmol) and HCl (6.4 mL, 4 M in dioxane) were added to a stirred solution of 4-Amino-benzenesulfonyl fluoride (**B**) (3.3 g, 19.1 mmol) in 44.6 mL 2-butanol. Subsequently, the reaction mixture was stirred under reflux for 22 h at 60 °C. After cooling, the precipitate formed was drained via a suction pump, washed with water and diisopropyl ether, and dried in vacuo. 4.9 g (11.6 mmol, 91 % yield) of the product 4-(5-Bromo-4-prop-2-ynylamino-pyrimidin-2-ylamino)-benzenesulfonyl fluoride (**F**) was obtained in form of the hydrochloride.

*{2-[4-(5-Bromo-4-prop-2-ynylamino-pyrimidin-2-yl-amino)-benzenesulfonyl amino]-ethyl}-carbamic acid tert-butyl ester (**H**):* (2-Amino-ethyl)-carbamic acid tert-butyl ester **G** (1.14 g, 7.1 mmol) in 5 mL 2-butanol, 4-Dimethylaminopyridine (DMAP) (175 mg, 1.4 mmol) and triethylamine (1.31 mL, 9.4 mmol) were added to a stirred solution of 4-(5-Bromo-4-prop-2-ynylamino-pyrimidin-2-ylamino)-benzenesulfonyl fluoride hydrochloride (**F**) (2 g, 4.7 mmol) in 20 mL 2-butanol. After the addition, the reaction mixture was stirred under reflux for 140 h at 80 °C. After cooling, the precipitate formed was drained via a suction pump, washed with cold ethanol, and dried in vacuo. 1.94 g (3.7 mmol, 79 % yield) of the product {2-[4-(5-Bromo-4-prop-2-ynylamino-pyrimidin-2-yl-amino)-benzenesulfonyl amino]-ethyl}-carbamic acid tert-butyl ester (**H**) was obtained.

*N-(2-Amino-ethyl)-4-(5-bromo-4-prop-2-ynyl-amino-pyrimidin-2-ylamino)-benzenesulfonamide (**C1-SL, J**):* 4.2 mL trifluoroacetic acid (TFA) (4 °C) were added to a stirred solution of {2-[4-(5-Bromo-4-prop-2-ynylamino-pyrimidin-2-yl-amino)-benzene-sulfonyl amino]-ethyl}-carbamic acid tert-butyl ester (**H**) (1.92 g, 3.7 mmol) in 30 mL acetonitrile. After the addition, the reaction mixture was stirred under reflux for 24 h at room temperature. Subsequently, the temperature was increased to 50 °C for one hour. The reaction

mixture was made basic by the addition of $NaHCO_3$ (saturated) and extracted with ethyl acetate (2x). The combined organic phases were dried (Na_2SO_4), filtered, and concentrated in vacuo. The resulting mixture of educt and product was separated by semi-preparative HPLC. A C18 column (XBridge, Waters, Eschborn, Germany) with 3.5 µm particle size, 4.6 mm ID and 10 cm length and a 15 min linear gradient of 1 to 99 % acetonitrile in water, containing 0.1 % TFA were used to separate the samples. 0.89 g (2.1 mmol, 57 % yield) of the product N-(2-Amino-ethyl)-4-(5-bromo-4-prop-2-ynyl-amino-pyrimidin-2-ylamino)-benzenesulfon-amide (**C1-SL**, **J**) was obtained.

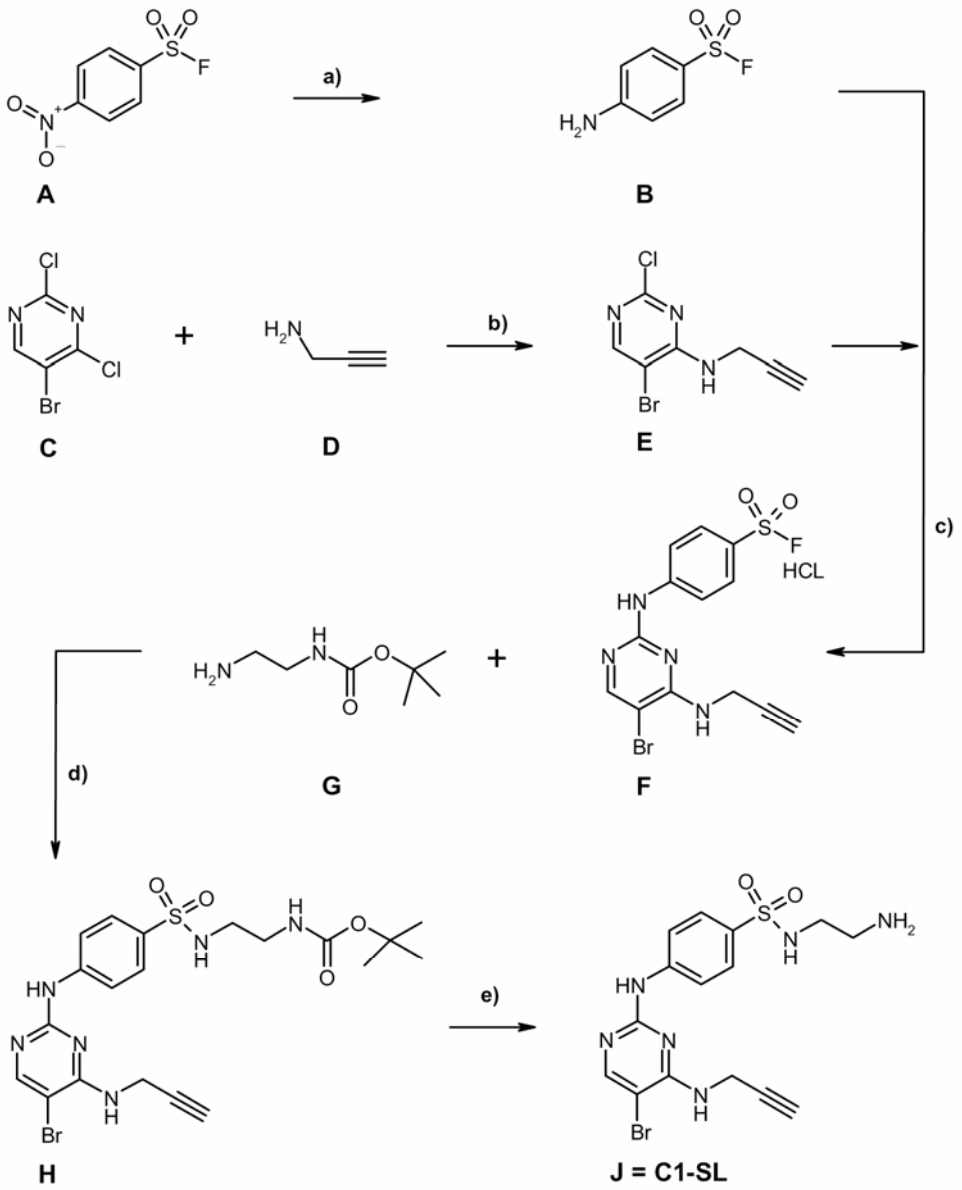

Figure 8. Synthesis of C1-SL: a) Raney-nickel, EtOH, RT, 89 %; b) NEt_3 , MeCN, RT, 98 %; c) 2-butanol, HCl (4 M in dioxane), reflux, 60 °C → RT, then water and diisopropyl ether, 91 %; d) 2-butanol, DMAP, NEt_3, reflux, 80 °C → 4 °C, then cold EtOH, 79%; e) MeCN, TFA, reflux, RT → 50 °C; then $NaHCO_3$, ethyl acetate, HPLC, 57 %.

3.2.3. Generation of inhibitor matrices via immobilization routes 1 & 2 and control matrix

In order to perform alternative immobilization routes of compound C1, the analogs C1-SL (for route 1) and C1a (for route 2) were generated (as described above) and coupled to epoxy-activated Sepharose™ 6B (GE Healthcare Bio-Sciences AB, Uppsala, Sweden), similarly as described (Brehmer, D. et al. 2004; Godl, K. et al. 2003) (Figure 9). For this purpose, drained Sepharose™ beads were resuspended in 2 volumes of 20 mM C1-SL or C1a dissolved in coupling buffer (50 % dimethylformamide/ 0.1 M Na_2CO_3 pH 11) and incubated overnight at room temperature in the dark. After three washes with coupling buffer, remaining reactive groups were blocked with 1 M ethanolamine, pH 11. Subsequently, washing steps were performed according to the manufacturer's instructions. Control matrix was prepared by directly blocking epoxy-activated Sepharose™ 6B with 1 M ethanolamine, pH 11 and equal treatment as described above. The matrices were stored at 4 °C in the dark.

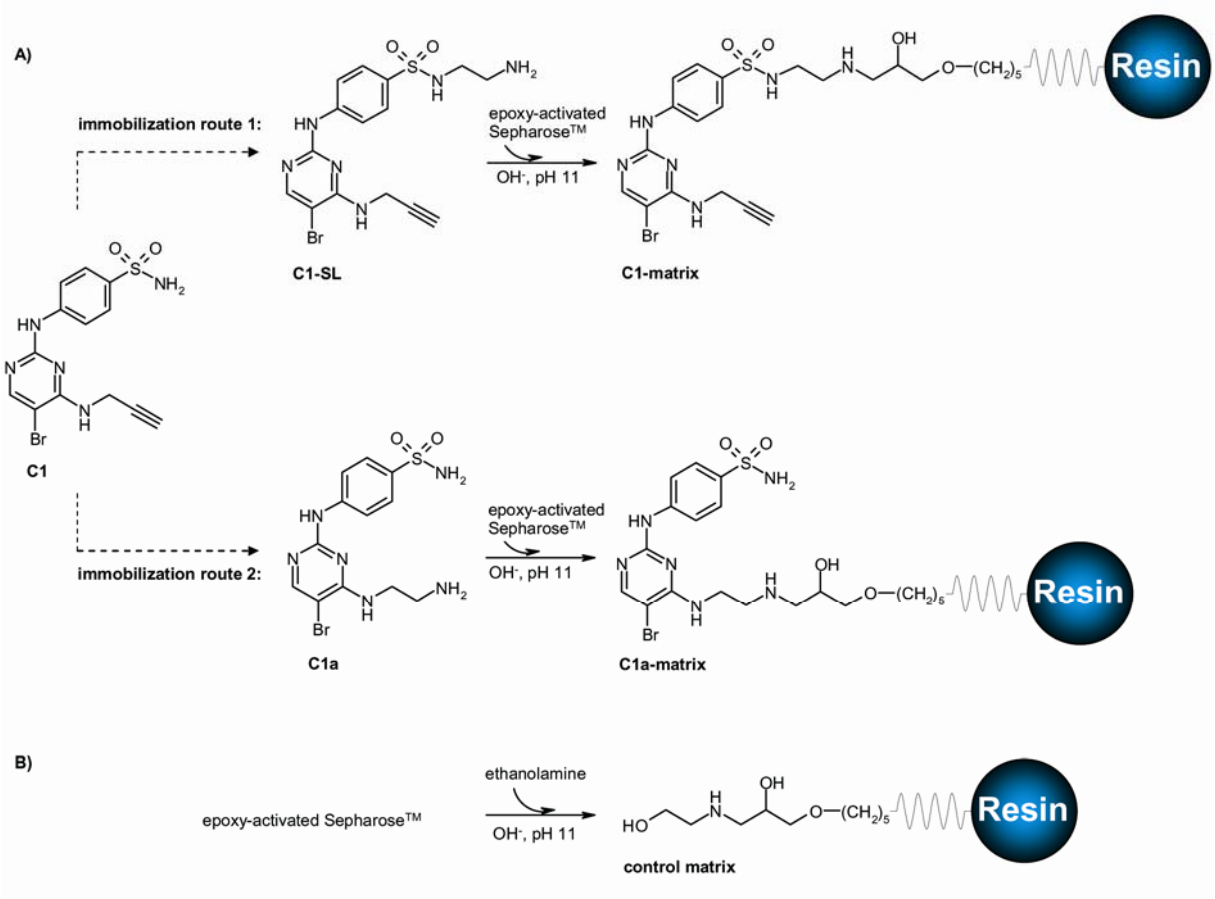

Figure 9. A) For immobilization route 1 of compound C1, the "short linker"-analog C1-SL was generated and coupled to epoxy-activated Sepharose™ beads in a one step reaction, resulting in the C1-matrix. For the generation of an alternative inhibitor matrix, the C1 analog C1a was coupled to epoxy-activated Sepharose™ beads at the 4-position according to the immobilization route 2, resulting in the C1a-matrix. B) Control matrix was prepared by directly blocking epoxy-activated Sepharose™ 6B with ethanolamine.

3.2.4. Calculation of the coupling rate and the compound density exemplified for C1-matrix

For the calculation of the coupling rate of compound C1-SL to epoxy-activated Sepharose™ 6B, the absorbance of C1-SL solution was determined photometrically at 280 nm before and after incubation with the Sepharose™ beads against a blank (solvent without compound). C1-SL solution incubated with blocked Sepharose™ (control matrix) was used as a reference. A SpectraMax 190 spectrophotometer (Molecular Devices, Sunnyvale, CA, USA) and UV-Vis transparent 96-well microtitre plates (BD Biosciences Europe, Erembodegem, Belgium) were employed for the measurements. A C1-SL calibration curve was used to calculate the respective compound concentrations.

3.2.5. Immobilization of pyridoxal

Coupling of pyridoxal to EAH–Sepharose™ 4B (GE Healthcare Bio-Sciences AB) was adapted from the protocol described (Cash, C. D. et al. 1980). The beads (50 mL) were pretreated as recommended by the manufacturer and added to 350 mL of a 120 mM pyridoxal hydrochloride solution, pH 7. After incubating overnight at room temperature in the dark, sodium borohydride (20 mg/ mL) was added dropwise until all traces of yellow color had disappeared. Meanwhile, 7 % acetic acid was used to keep the pH below 9 (Figure 10). Subsequently, the matrix was allowed to reach room temperature and the pH was adjusted to pH 6 with 7 % acetic acid in order to destroy residual sodium borohydride. After washing the pyridoxal matrix with 250 mL of 3 M potassium chloride solution and 250 mL CV of water, the matrix was stored at 4 °C in the dark.

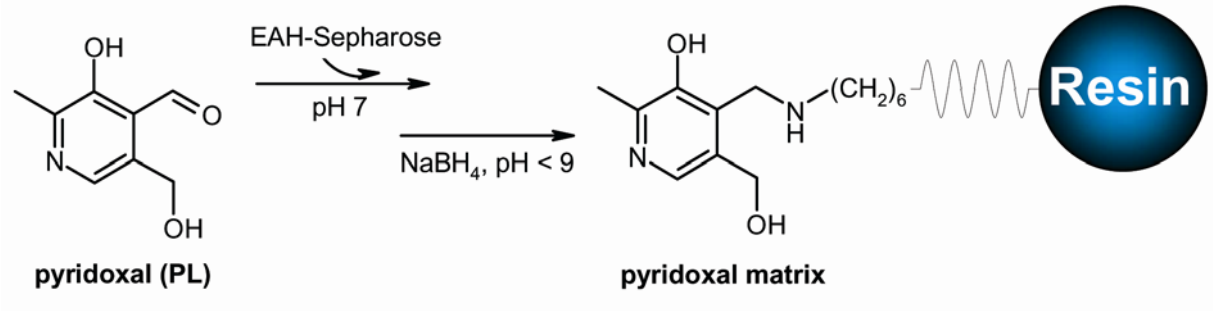

Figure 10. The substrate of PDXK, pyridoxal, was coupled to EAH–Sepharose™ in a two-step reaction. The resulting pyridoxal matrix was employed for the purification of recombinant PDXK and for the characterization of the PDXK/ C1 interaction.

3.2.6. Cells, cell culture, and cell lysis

NCl-H460 cells (human large cell lung carcinoma cell line, HTB-177, ATCC/ LGC Standards GmbH, Wesel, Germany) were cultured in DMEM/ Ham's F12 (1:1) (Biochrom, Berlin, Germany) supplemented with 10 % FBS. Frozen HeLa cells (human cervix carcinoma cell line, CilBiotech, Mons, Belgium) and H460 cells were lysed in lysis buffer containing 50 mM Tris/ HCl, pH 8.0, 150 mM NaCl, 10 % glycerol, 0.5 % NP-40, 1 mM EGTA, 1 mM EDTA, 5 mM DTT, 1 mM orthovanadate and Complete protease inhibitor cocktail (Roche Diagnostics GmbH, Mannheim, Germany). For affinity chromatography experiments, lysates were precleared by centrifugation (30 min, 50000 g, 4 °C, Optima ™ L-90K Ultracentrifuge, Beckmann Coulter, Krefeld, Germany) and the protein concentration was determined using the Bradford method.

3.2.7. Determination of protein concentration using the Bradford method

Protein concentrations were determined using the Bradford method (Bradford, M. M. 1976) which is based on a colorimetrical measuring of the reduction potential of proteins by a redox reaction. For this purpose, a BSA calibration curve was prepared. A BSA stock solution (2 mg/ mL, albumin standard, Pierce Biotechnology, Rockford, IL, USA) was diluted in PBS resulting in standards of increasing BSA concentration covering a range of 20 µg/ mL to 2000 µg/ mL. 25 µL of each concentration standard were added in triplicates to 200 µL of a mixture of BCA™ Protein Assay Reagent A und B (50:1, reagent A:B, v/v, Pierce Biotechnology), mixed and incubated for 30 min at 37 °C. Samples of interest were treated equally. Afterwards, the absorption was measured at 595 nm using a SpectraMax 190 spectrophotometer (Molecular Devices, Sunnyvale, CA, USA). The resulting calibration curve was used to determine the protein concentration of the respective samples.

3.2.8. Inhibitor affinity chromatography (IAC)

Inhibitor affinity chromatography experiments were performed similarly as described (Brehmer, D. et al. 2004; Godl, K. et al. 2003). HeLa and H460 cell extracts corresponding to 9 mg of total protein (approx. 200 µL) were adjusted to 1 M NaCl. Optionally, 10 mM pyridoxine in low-salt washing buffer (see below) was spiked into the sample. Cell extracts were incubated with 25 µL of drained affinity matrix (C1-, C1a-, pyridoxal matrix) or 50 µL of control matrix for 3 h at 4 °C in Micro Bio-Spin Chromatography Columns (Biorad, Hercules, CA, USA). Subsequently, the flow-through was discarded whereas the beads were kept for the washing procedure. After three washing steps with 450 µL of high-salt washing buffer (1 M NaCl, 50 mM Tris/ HCl, pH 8.0, 10 % glycerol, 1 mM EGTA, 1 mM EDTA) and

three steps with 450 µL of low-salt washing buffer (150 mM NaCl, otherwise the same composition as the high-salt washing buffer) the beads were (sequentially) eluted by 200 µL each of several elution buffers (depending on the question addressed) for 20 min at 4 °C, or by 22.5 µL of LDS-SB elution buffer for 10 min at 90 °C. ATP buffer: 10 mM ATP, 20 mM $MgCl_2$ in low-salt washing buffer; compound buffer: saturated compound solution in low-salt washing buffer; pyridoxine buffer: 10 mM pyridoxine in low-salt washing buffer; LDS-SB: 2x LDS-sample buffer, 1x sample reducing agent (both from Invitrogen, Karlsruhe, Germany). The volume of the elution fractions (with exception of LDS-SB elution fraction which was directly loaded on SDS-PAGE (Laemmli, U. K. 1970) was reduced to 100 µL in a Speed Vac® Plus SC110A concentrator (GMI**,** Ramsey**,** MN, USA) before precipitation of proteins using the 2-D Clean-Up Kit (GE Healthcare Bio-Sciences AB). Precipitated proteins were dissolved in 20 µL LDS-SB and after reduction (1x sample reducing agent, 90 °C, 10 min) and alkylation (by 50 mM iodoacetamide, 30 min, room temperature, in the dark) separated by 1-D SDS-PAGE. Proteins were either transferred to a nitrocellulose membrane and immunoblotted with the indicated antibodies or stained with Coomassie and prepared for analysis by mass spectrometry.

3.2.9. Serial inhibitor affinity chromatography

Cell extracts were treated as described above. The flow-through, however, was not discarded, but mixed with fresh affinity or control matrix and incubated for 3 h at 4 °C. After washing and elution steps as described for inhibitor affinity chromatography, samples were separated by SDS-PAGE and immunoblotted using an anti-PDXK antibody.

3.2.10. SDS-PAGE

SDS or LDS (sodium or lithium dodecyl sulfate) is used to denatured proteins and apply a negative charge to each protein in proportion to its mass. Subsequently, a voltage is applied to separate denatured proteins according to their size and charge in a polyacrylamide gel (Laemmli, U. K. 1970). The NuPage-XCell SureLock^{TM} Mini-Cell-System (Invitrogen GmbH, Karlsruhe, Germany) was used for the separation of protein mixtures. Protein samples were incubated in NuPAGE® LDS-sample buffer containing NuPAGE® sample reducing agent for 10 min at 95 °C. Subsequently, samples and the SeeBlue® Plus 2 pre-stained marker were loaded on NuPAGE® Novex 4-12% Bis-Tris pre-cast gels and separated at 200 V for 45 min using 1x NuPAGE® MOPS buffer (all reagents from Invitrogen GmbH).

3.2.11. Coomassie staining

The dyes Coomassie Brilliant Blue R250 and G250 (both SERVA Electrophoresis GmbH, Heidelberg, Germany) were used for non-specifically staining protein bands in polyacrylamide protein gels. For this purpose, the protein gels were incubated for approx. 30 min in Coomassie staining solution (0.12 % (w/v) Coomassie Brilliant Blue R250, 0.12 % (w/v) Coomassie Brilliant Blue G250, 10 % (v/v) acetic acid, 50 % (v/v) ethanol, water) and destained in destaining solution (10 % (v/v) acetic acid, water) at room temperature.

3.2.12. LC-coupled mass spectrometry

Lanes from Coomassie stained SDS-PAGEs were sliced across the separation range and subjected to in-gel tryptic digestion similarly as described (Shevchenko, A. et al. 2006). ESI-based LC-MS/MS analyses were carried out using an Eksigent NanoLC 2D system (Eksigent, Dublin, CA, USA). A C18 capillary column (NanoSeparations, Nieuwkoop, Netherlands) with 5 µm biosphere material, 75 µm ID and 15 cm length was used at a flow rate of 250 nL/ min. A C18 Zorbax 300 SB column (Agilent, Technologies Deutschland GmbH, Böblingen, Germany) with 5 µm pore material, 300 µm ID and 5 mm length was used as a trap column. The samples were separated by a 35 min linear gradient of 2 to 35 % acetonitrile in water, containing 0.1 % formic acid. The HPLC was coupled to a quadrupole/ time-of-flight mass spectrometer (QSTAR XL) using a nanoelectrospray source (both from Applied Biosystems/ MDS Sciex, Concord, Canada). The electrospray voltage was set to 2.0 kV. The data acquisition mode was set to one full MS scan (m/z range 350 to 1100) followed by three MS/MS events using information-dependent acquisition (the three most intense ions from a given MS scan were subjected to CID). The peptide masses, which were selected for CID, were excluded from reanalysis for 30 s.

For the mass determination of intact proteins, a 4000 Å PLRP-S column (Michrom Bioresources, Inc., Auburn, AC, USA) with 8 µm pore material, 75 µm ID and 15 cm length was used at a flow rate of 300 nL/ min. A CapTrap Protein column (Michrom Bioresources) with 200 µm ID and 2 mm length was used as a trap column. The samples were separated by a 25 min linear gradient of 4,8 to 50 % acetonitrile in water, containing 0.1 % formic acid. The HPLC was coupled to a quadrupole/ time-of-flight mass spectrometer (QSTAR XL) using a nanoelectrospray source (both from Applied Biosystems/ MDS Sciex).

3.2.13. Data processing

The raw files from the QSTAR XL were converted to Mascot generic format-files by Mascot Daemon (version 2.2). MS/MS spectra were searched using Mascot™ 2.0 software (Matrix Science Ltd., London, UK) against an in-house curated version of the human IPI (International Protein Index) protein database combined with a decoy version of this database (Elias, J. E. et al. 2005), which was created by a script supplied by Matrix Science. The search was performed with tryptic cleavage specificity with one missed cleavage site, a mass tolerance of 100 ppm for the precursor ions and 0.5 Da for the fragment ions, methionine oxidation and cysteine carbamidomethylation as variable modifications. Protein identifications were accepted when at least two peptides with a Mascot ion score of ≥ 25 for each peptide were found. The false discovery rate (FDR) for peptides was < 5 % in each case. The protein redundancy in the dataset was eliminated by the ProteinScape software (Version 1.3 SR2, Protagen/ Bruker Daltonik GmbH, Bremen, Germany) (Bluggel, M. et al. 2004). In order to further reduce dataset complexity by combining several splicing variants for one protein, and because gene IDs are more stable, BioXM software (version 2.5, BioMax Informatics AG, Martinsried, Germany) was used to replace IPI numbers by gene IDs as provided by the Entrez gene database. Resulting lists of gene IDs and gene products were used for further data analyses.

3.2.14. Western Blot

The iBlot™ Dry Blotting System (Invitrogen) was used for Western blotting. A gel matrix technology enables the system to generate a high voltage field strength and high protein currents to increase the transfer speed. Proteins were transferred subsequent to SDS-PAGE separation from polyacrylamide gels onto nitrocellulose membranes in 6 min at 20 V.

3.2.15. Immunodetection of proteins

The membranes were blocked in Odyssey® Blocking Buffer (LI-COR Biosciences GmbH, Bad Homburg, Germany) for 1 h at room temperature and incubated overnight at 4 °C with the specified primary antibodies diluted in Odyssey® Blocking Buffer. Afterwards, the membranes were washed with PBS/ 0.1 % (v/v) Tween-20 for 10 min (3x) and incubated with the corresponding fluorescently-labeled secondary antibodies diluted in Odyssey® Blocking Buffer for 1 h at room temperature. After three washing steps in PBS/ 0.1 % (v/v) Tween-20 for 10 min and one in PBS for 5 min, the membranes were scanned using an Odyssey® Infrared Imaging System (LI-COR) and the appropriate IR channel.

3.3. PDXK expression & purification

3.3.1. PDXK expression vector

The recombinant vector pET11a-PDXK kindly provided by Kastner et al. (Kastner, U. et al. 2007). The coding sequence of the splice isoform 1 of PDXK had been introduced into a NdeI and BamHI restriction site (w/o tag, Figure 11). The vector was analyzed by digestion with specific restriction endonucleases and agarose gel electrophoresis.

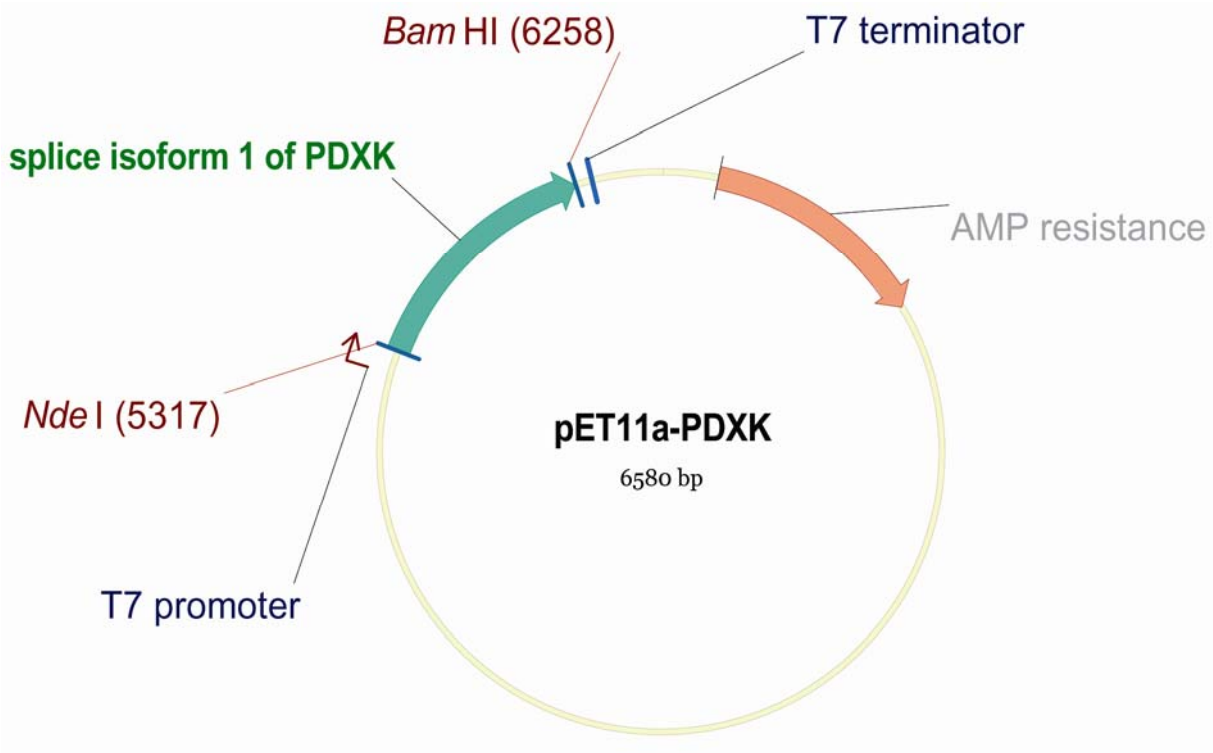

Figure 11. The recombinant vector pET11a-PDXK for expression of the splice isoform 1 of the human pyridoxal kinase (PDXK) in *E. coli.*

3.3.2. Restriction digest

Double restriction digest was carried out as recommended by the manufacturer (New England Biolabs homepage, "Double digest Finder", www.neb.com). 10 units of BamH1 and 20 units of NdeI were added to NEBuffer 3 supplemented with BSA (all from New England Biolabs GmbH, Frankfurt am Main, Germany) and applied to 1 µg of DNA in a final volume of 30 µL for 75 min at 37 °C. Digested DNA was analyzed by agarose gel electrophoresis.

3.3.3. Agarose gel electrophoresis

For the analysis of the restriction digest, the DNA was separated according to their size in an agarose gel. For this purpose, SYBR® Safe DNA gel stain *10,000X concentrate in DMSO (5 µL, Invitrogen GmbH) was added to a solution of agarose NA (1 % (w/v), GE Healthcare Bio-Sciences AB) in 1xTAE buffer (40 mM Tris/ HCl, 1 mM EDTA, pH 8.3, Invitrogen GmbH). The samples were dissolved in Blue Juice^{TM} sample buffer (65 % (w/v) sucrose, 10 mM Tris/ HCl (pH 7.5), 10 mM EDTA, and 0.3 % (w/v) bromophenol blue, Invitrogen GmbH), loaded on the gel and separated at 130 V for 75 min. 1xTAE was used as running buffer, a 1kb DNA ladder and a 100bp DNA ladder were used as markers (all from Invitrogen GmbH).

3.3.4. Transformation

50 ng plasmid DNA (pET11a-PDXK) were added to thawed BL21 (DE3) competent cells (50 µL, Novagen/ EMD Chemicals Inc., Darmstadt, Germany). The cells were incubated on ice for 30 min and at 42 °C for 30 s. Subsequent to another incubation on ice for 1 min, 250 µL S.O.C. medium (Invitrogen) were added and the cells were incubated for 1 h at 37 °C with shaking (200 rpm). Afterwards, the cells were plated on agar plates containing ampicillin and incubated overnight.

3.3.5. Plasmid DNA isolation and sequencing

Subsequent to transformation, one clone was grown in Luria–Bertani medium containing ampicillin (200 µg/ mL) for 8 h at 37 °C with shaking (180 rpm). In order to prepare a cell stock solutions, 100 µL of cell culture were mixed with 900 µL of 10 % (v/v) glycerol and frozen at -80 °C. The remaining culture was used for plasmid DNA preparation employing a QIAprep Spin Miniprep Kit (QIAGEN, Hilden, Germany). Subsequently, the plasmid DNA was sequenced over its entire length (AGOWA GmbH, Berlin, Germany) to ensure that no mutations had been introduced and that the DNA sequence was correct. The respective sequencing primers (Table 1) were provided by AGOWA GmbH. The Vector NTI v10.0.1 Software (Invitrogen) was used to analyze the obtained dataset.

Table 1. Primers for sequencing of the recombinant vector pET11a-PDXK.

Primers	**Sequence 5'–3'**
T7prom	TAATACGACTCACTATAGGG
T7term	GCTAGTTATTGCTCAGCGG

3.3.6. Determination of DNA and protein concentration by NanoDrop

The NanoDrop SD-1000 Spectrophotometer (NanoDrop Technologies, Wilmington, DE, USA) was used to determine DNA and protein (purified) concentrations. DNA absorbance was measured at 260 nm and protein absorbance at 280 nm. The molecular weight and the molar extinction coefficient of the PDXK are listed in Table 2.

Table 2. The molecular weight and the molar extinction coefficient of the human pyridoxal kinase (PDXK).

Protein	**Molecular Weight [kDa]**	**Molar Ext. Coeff. [cm^{-1} mM^{-1}][a]**
native PDXK	35.1	29,9
[a] calculated by the GPMAW v6.21 (Lighthouse data, Odense M, DK)		

3.3.7. PDXK expression

The recombinant *E.coli* strain BL21 (DE3)-pET11a-PDXK was grown in Luria–Bertani medium containing ampicillin (200 µg/ mL) overnight at 37 °C. The cells of this preculture were harvested, washed and grown in CIRCLEGROW® medium (Qbiogene, Heidelberg, Germany) supplemented with ampicillin at 37 °C until $OD_{600} = 1$. Isopropyl thio-β-D-galactoside (IPTG) was added to a final concentration of 0.03 mM, and the culture was incubated with shaking for 24 h at 37 °C. The cell pellet derived from 2 L of culture was frozen at -80 °C.

3.3.8. Purification of PDXK

For affinity purification of PDXK, its substrate pyridoxal was coupled to EAH–Sepharose™ (GE Healthcare Bio-Sciences AB) as described above. A preparative LC glass column (TAC 35x125 mm, Kronlab, Dislaken, Germany) was packed with the resulting pyridoxal matrix and equilibrated with column buffer (50 mM Tris⁄HCl, pH 7.4; 200 mM NaCl, 1 mM EDTA). The frozen bacterial cells derived from 2 L of culture were resuspended in ice cold column buffer before Microfluidizer (Microfluidics, Lampertheim, Germany) treatment for cell disruption. After sedimentation of the cell debris (45 min, 100000 g, 4 °C, Optima ™ L-90K Ultracentrifuge, Beckmann Coulter) the supernatant was adjusted to 100 mM KCl and loaded onto the pyridoxal column for affinity purification similar as described (Cash, C. D. et al. 1980) at 4 °C. To remove unbound proteins, the column was sequentially washed with washing buffer WB1 (2 mM potassium phosphate pH 7, 0.1 mM glutathione, 100 mM KCl), washing buffer WB2 (2 mM potassium phosphate pH 7, 0.1 mM glutathione, 400 mM KCl)

and again with washing buffer WB1. A pyridoxine elution buffer (2 mM potassium phosphate pH 7, 0.1 mM glutathione, 100 mM KCl, 10 mM pyridoxine) was applied for an isocratic elution of PDXK at a flowrate of 5 mL/ min. Since both, pyridoxine and the PDXK, absorb UV-light at 280 nm, capillary electrophoresis (LabChip® 90 System, Caliper, Ruesselsheim, Germany) (Lin, S. et al. 2003) was used to monitor the purification and identify the protein containing fractions. In order to determine whether the native state of the purified recombinant PDXK was a monomer or a higher oligomer and to sense the presence of aggregated proteins, an analytical size exclusion chromatography was performed at 4 °C using a Superdex^{TM} 200 5/ 150 GL column (GE Healthcare Bio-Sciences AB) equilibrated with SEC buffer (0.1 M potassium phosphate pH 6) at a flowrate of 0.3 mL/ min. Subsequently, a gel filtration standard (Bio-Rad Laboratories GmbH, Munich, Germany) was applied to the same column as a calibration standard for a molecular weight determination of the PDXK. Afterwards, a preparative size exclusion chromatography (SEC) was performed in order to separate PDXK from the pyridoxine. To this end, the respective protein pool was concentrated using Amicon Ultra-15 Centrifugal Filter Units (10 kDa cut-off, Millipore, Schwalbach, Germany) and loaded onto a HiLoad^{TM} 26/60 Superdex 75 column (GE Healthcare Bio-Sciences AB), which had been equilibrated with SEC buffer (0.1 M potassium phosphate pH 6). The same SEC buffer was used for elution at a flowrate of 1 mL/ min. An aliquot of the SEC buffer was kept for later isothermal titration calorimetry (ITC) experiments. Capillary electrophoresis (LabChip® 90 System, Caliper) was used to monitor the preparative size exclusion chromatography. The identity and the purity of the PDXK in the final pool fraction was confirmed by SDS-PAGE and LC-ESI-MS/MS analysis (as described above).

3.4. Enzymatic Assays

3.4.1. Pyridoxal kinase (PDXK)

The activity of recombinantly expressed and purified human PDXK (w/o tag) was assayed for the determination of the Michaelis constant K_m, as well as for IC_{50}-determination in the presence of test compounds covering a range of 1 nM - 50 µM, similarly as described (Kastner, U. et al. 2007). The assay determines phosphorylation of pyridoxal by PDXK by measuring pyridoxal 5'-phosphate at its absorption maximum of 388 nm (Figure 12). Test compounds dissolved in Me_2SO were pipetted into the wells of a UV-Vis transparent 96-well microtitre plate (BD Biosciences Europe, Erembodegem, Belgium) containing assay buffer

(250 µL 70 mM potassium phosphate pH 6.2, 0.1 mM $ZnCl_2$, 2.5 mM ATP, 2,5 µg/ mL PDXK). The enzymatic reaction was started by addition of substrate dissolved in water (final pyridoxal concentration was 0.5 mM). Absorbance was determined photometrically at 388 nm against a blank (same mixture of reagents but without enzyme) using a SpectraMax 190 spectrophotometer (Molecular Devices, Sunnyvale, CA, USA) at 37 °C. The initial linear formation rate of pyridoxal 5'-phosphate was used to calculate the PDXK activity, which is expressed as percentage of vehicle control (wells containing 2 % Me_2SO without test compounds), representing maximal activity. Curves were fitted to the averaged value of each triplicate using Sigma Plot 8.02 (Systat Software GmbH, Erkrath, Germany). 10 mM EDTA served as a negative control; 2 % Me_2SO was shown to have no effect on PDXK activity.

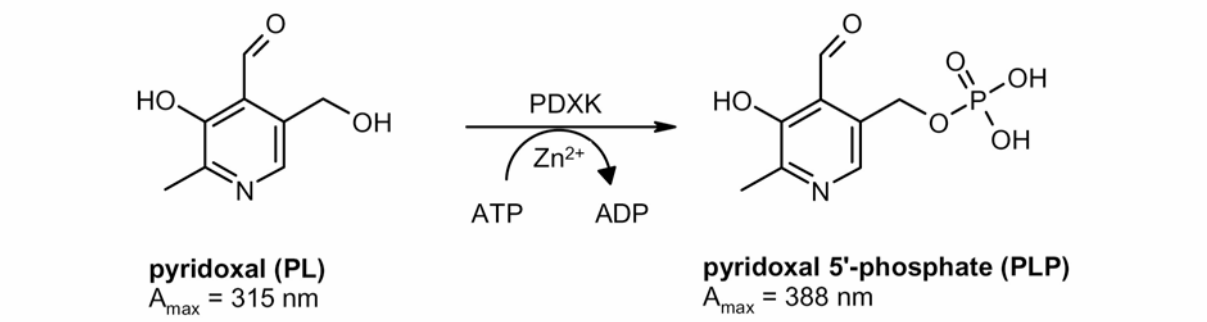

Figure 12. For K_m and IC_{50} determination, the PDXK activity was assayed by measuring the phosphorylation of pyridoxal by PDXK at different substrate concentrations or in the presence of test compounds. For this purpose, pyridoxal 5'-phosphate was measured at its peak absorption at 388 nm.

3.4.2. Cyclin-dependent kinase 2/ Cyclin E (CDK2/ CycE)

CDK2/ CycE-inhibitory activity of compounds was quantified employing a CDK2/ CycE HTRF® assay. Recombinant GST fusion proteins of human CDK2 and human CycE (ProQinase GmbH, Freiburg, Germany) were used to measure the phosphorylation of the biotinylated peptide biotin-Ttds-YISPLKSPYKISEG-amide (JERINI peptide technologies, Berlin, Germany). The CDK2/ CycE was incubated for 60 min at 22 °C in the presence of different concentrations of test compounds in 5 µL assay buffer [50 mM Tris/ HCl pH 8.0, 10 mM $MgCl_2$, 1.0 mM dithiothreitol, 0.1 mM sodium orthovanadate, 10 µM ATP, 0.75 µM substrate, 0.01 % (v/v) Nonidet-P40 (Sigma), 1 % (v/v) dimethylsulfoxide]. The concentration of CDK2/ CycE was adjusted depending on the activity of the enzyme lot and was chosen appropriately to measure the assay in the linear range. Typical concentrations were in the range of 1 ng/ mL. The reaction was stopped by addition of 5 µL of a solution of HTRF® detection reagents (0.2 µM streptavidine-XLent and 3.4 nM Phospho-(Ser) CDKs Substrate

Antibody (product #2324B, Cell Signaling Technology, Danvers, MA, USA) and 4 nM Prot-A-EuK (Protein A labeled with Europium Cryptate from Cis biointernational, France, product no. 61PRAKLB)) in an aqueous EDTA-solution (100 mM EDTA, 800 mM KF, 0.2 % (w/v) bovine serum albumin in 100 mM HEPES/ NaOH pH 7.0). The resulting mixture was incubated 1 h at 22 °C to allow the formation of the complex between the phosphorylated biotinylated peptide and the detection reagents. Afterwards, the amount of phosphorylated substrate was evaluated by measurement of the resonance energy transfer from the Prot-A-EuK to the streptavidine-XLent. For this purpose, the fluorescence emissions at 620 nm and 665 nm after excitation at 350 nm were measured in a HTRF® reader, e.g. a Rubystar (BMG Labtechnologies, Offenburg, Germany) or a Viewlux (Perkin-Elmer, Wiesbaden, Germany). The ratio of the emissions at 665 nm and 622 nm was taken as the measure for the amount of phosphorylated substrate. The data were normalized (enzyme reaction without inhibitor = 0 % inhibition, all other assay components but no enzyme = 100 % inhibition) and IC_{50} values were calculated by a 4 parameter fit using an in-house software.

3.4.3. Carbonic anhydrase 2 (CA2)

The inhibitory potential of compounds on human CA2 activity was determined (IC_{50}). The assay determines the hydrolysis of 4-nitrophenyl acetate by carbonic anhydrases (Pocker, Y. et al. 1967), by measuring 4-nitrophenolate anion at 400 nm (Figure 13). A Tecan Rainbow 96-well spectrophotometer (Tecan Group Ltd., Maennedorf, Switzerland) was used for measurement. Test compounds dissolved in Me_2SO covering a concentration range of 0.01 – 25 µM (final) were pipetted in triplicates into the wells of a 96-well microtitre ELISA plate. Wells containing solvent without test compound served as reference. Degassed assay buffer (10 mM Tris/ HCl pH 7.4, 80 mM NaCl) with 3 units/ well of CA2 was added. The enzymatic reaction was started by addition of substrate solution (1 mM 4-nitrophenyl acetate dissolved in water-free acetonitrile; final substrate concentration was 50 µM). The plate was incubated at room temperature for 60 min. Absorbance was determined photometrically at 400 nm against a blank (same mixture of reagents but without enzyme). The enzyme activity is expressed as percentage of vehicle control (2 % Me_2SO without test compounds), representing maximal activity.

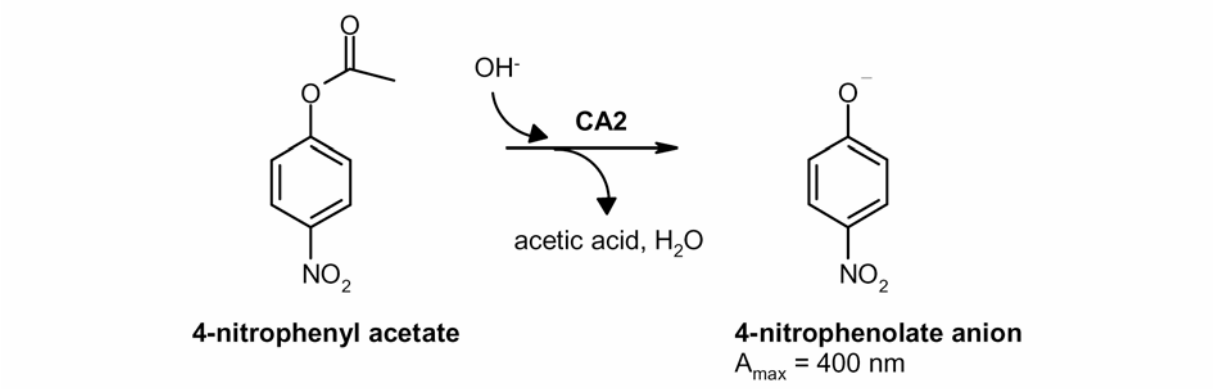

Figure 13. For IC_{50} determination, CA2 activity was assayed by measuring the hydrolysis of 4-nitrophenyl acetate by CA2 in the presence of test compounds. To this end, 4-nitrophenolate anion was measured at its absorption maximum of 400 nm.

3.4.4. Selectivity screen by KinaseProfiler™ Service

Inhibitory potential of C1 and the mimic (C1-LL) for selected kinases was screened by KinaseProfiler™ Service provided by Upstate/ Millipore (Dundee, UK) at 1 µM compound and 10 µM ATP. Detailed information and assay protocols are available under http://www.millipore.com.

3.5. Isothermal titration calorimetry for K_D determination

The ITC experiments were performed using a Microcal VP-ITC instrument (MicroCal, LLC, Northampton, MA, USA). The calorimeter was calibrated using standard electrical pulses as recommended by the manufacturer. The sample cell was loaded with purified PDXK (12.6 µM) in 0.1 M potassium phosphate (pH 6.0). The syringe was loaded with C1-SL (140 µM) in the same buffer. To ensure the same buffer conditions an aliquot of the size exclusion chromatography buffer for protein purification was used to prepare the compound solution. Titrations were performed at 25 °C with injection volumes of 12 µL and a spacing of 300 s. Raw data were collected, corrected for ligand heats of dilution, and integrated using the MicroCal Origin software supplied with the instrument.

4. Results

4.1. Two suitable compound immobilization routes derived from a computational model of a compound/ target complex

A computational model of the protein kinase inhibitor C1 in complex with its target protein CDK2 was derived from co-crystallization experiments of CDK2 in complex with various C1 analogs (Luecking, U. et al. 2007), (Figure 14 B). The model shows that the aminopyrimidine moiety is located deep within in the ATP binding pocket of the kinase, whereas the sulfonamide moiety is accessible from the solvent (Figure 14 C). Based on this computational model, two suitable immobilization strategies of compound C1 were derived in order to generate alternative compound affinity matrices for Chemical Proteomics approaches (Figure 15). For the immobilization route one, the sulfonamide group was identified as an appropriate site for the coupling of the compound. According to the computational model, the resulting compound affinity matrix was supposed to be suitable for the capturing of proteins interacting with the aminopyrimidine moiety of compound C1 (e.g. protein kinases). The immobilization route two via the side chain at the 4-position of the aminopyrimidine moiety, however, appeared suitable for the capturing of proteins interacting via the sulfonamide moiety of C1.

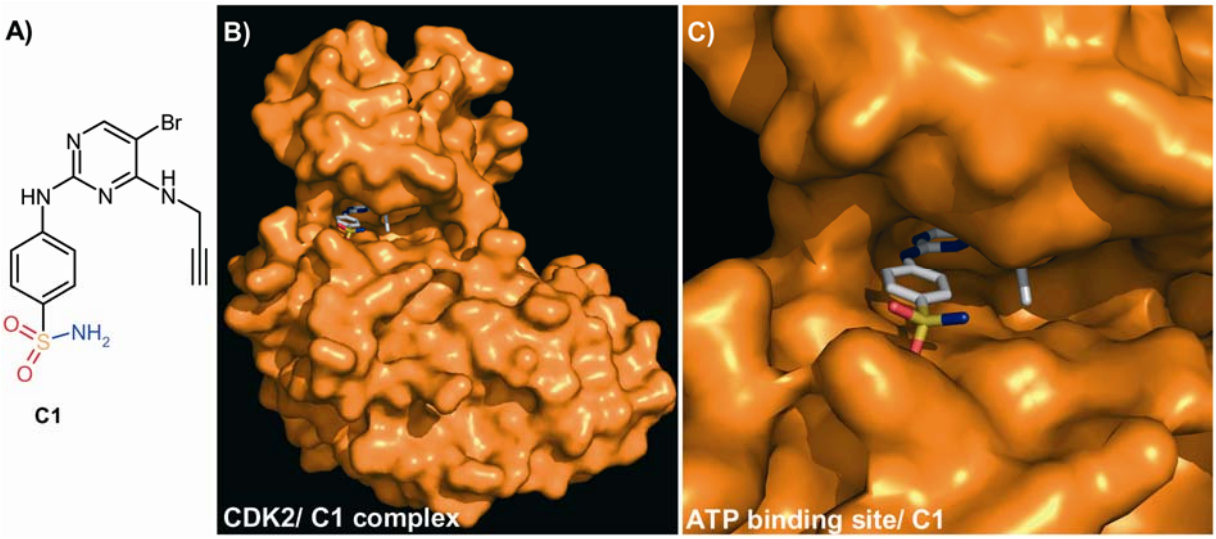

Figure 14. Computational model: A) Compound C1, the sulfonamide moiety is highlighted in colour. B) A general view of the target protein CDK2 in complex with its inhibitor C1. C) Detail view of the ATP binding site in complex with C1. The aminopyrimidine moiety is located deep within in the binding pocket, whereas the sulfonamide moiety (in colour) is accessible from the solvent. Two different immobilization routes, via the aminopyrimidine moiety and the sulfonamide moiety, respectively, were derived for Chemical Proteomics approaches in order to capture proteins interacting with both compound moieties. (The computational model was prepared by Dr. M. Schaefer, Bayer Schering Pharma AG Berlin, Germany.)

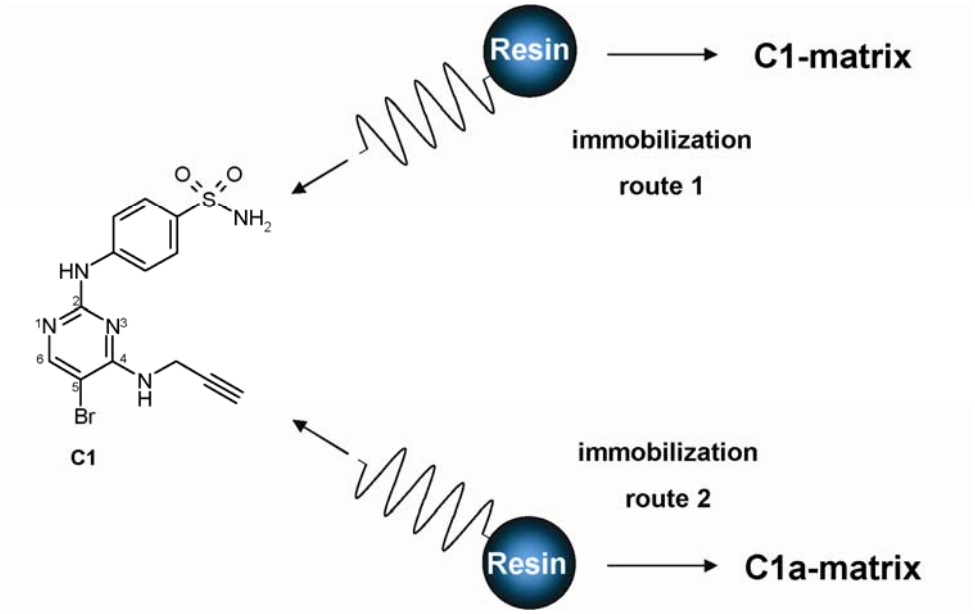

Figure 15. Based on the computational model (see above), the sulfonamide group of C1 was identified as an appropriate site for the immobilization route one in order to capture proteins interacting with the aminopyrimidine moiety (e.g. protein kinases). The immobilization route two via the side chain at the 4-position was supposed to be suitable for the capturing of proteins interacting via the sulfonamide moiety.

4.2. Compound immobilization routes and the mimic

Having identified the sulfonamide group of compound C1 as an appropriate site for a compound immobilization (route 1), a short linker was attached at this group. The resulting short linker analog C1-SL was immobilized to epoxy-activated Sepharose™ beads (Figure 16). The resulting C1-matrix was used for affinity purification of binding proteins in a Chemical Proteomics approach. Futhermore, a soluble mimic of the C1-matrix was synthesized to confirm that the immobilization via the sulfonamide does not interfere with the functionality of the compound and to analyze potential linker effects due to the compound immobilization. For this purpose, C1 was provided with a linker similar to the linking structure of the Sepharose™ matrix, giving the long linker analog C1-LL, referred to as mimic (Figure 16). In addition, the C1 analog C1a was generated and coupled via the 4-position of the aminopyrimidine moiety to epoxy-activated Sepharose™ beads (route 2) giving the C1a-matrix (Figure 16). This affinity matrix was used to capture proteins interacting via the sulfonamide moiety.

Finally, a control matrix was generated by blocking the functional groups of the epoxy-activated Sepharose™ beads with ethanolamine. The resulting inactivated resin was used in control experiments.

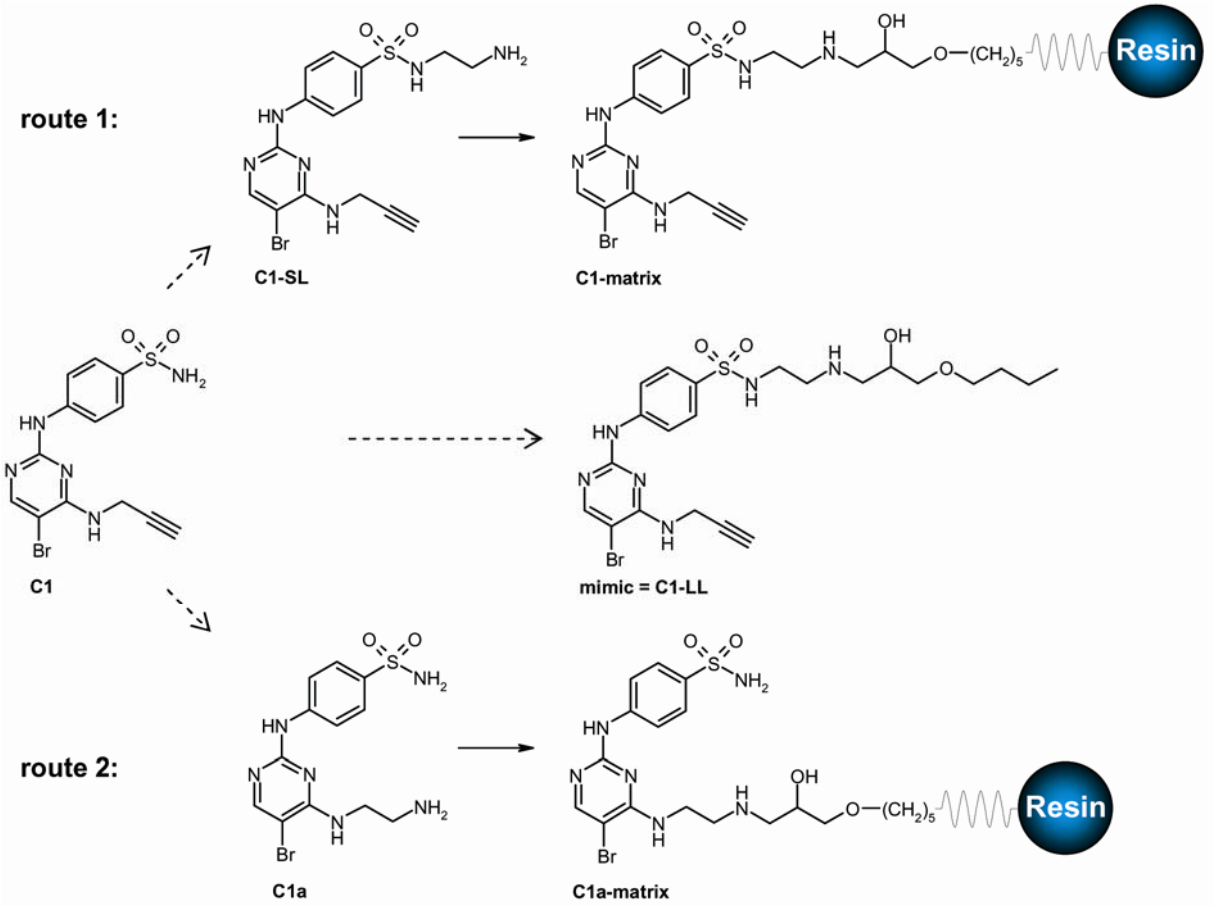

Figure 16. For the compound immobilization route 1, the short linker analog C1-SL was generated and coupled to a solid support (epoxy-activated Sepharose™ beads). Furthermore, a soluble mimic of the immobilized inhibitor, referred to as C1-LL (C1-"long-linker") or mimic, was generated to confirm a suitable compound immobilization with regard to target protein binding. Additionally, the mimic was used to analyze potential effects of the linker. For the second immobilization route, the C1 analog C1a was immobilized to epoxy-activated Sepharose™ beads at the 4-position resulting in the C1a-matrix.

4.3. Synthetic procedures

In order to immobilize compound C1 to epoxy-activated Sepharose™ beads via its sulfonamide moiety, the analog C1-SL was synthesized within this thesis as described in the Materials and Methods section. Analogous to this synthetic procedure, compound C1, C1a and C1-LL (mimic) were generated in-house by Dr. Ulrich Luecking (Bayer Schering Pharma AG, Medicinal Chemistry Berlin). The correct identities of the respective intermediates and final compounds were confirmed by ^{1}H-NMR and MS. The results are listed in Table 3.

Table 3. ^{1}H-NMR and MS data of intermediates and compounds according to the synthetic procedures described in the Materials and Methods section.

Compound	**^{1}H-NMR ([D6] DMSO)**	**MS**
*4-Amino-benzenesulfonyl fluoride (**B**)*	7.63 ppm (m, 2H), 6.68 ppm (m, 4H)	174 m/z (ESI-)
*(5-Bromo-2-chloro-pyrimidin-4-yl)-prop-2-ynyl-amine (**E**)*	8.28 ppm (s, 1H), 8.13 ppm (br, 1H), 4.07 ppm (br, 2H), 3.09 ppm (t, 1H)	246 m/z (ESI+)
*4-(5-Bromo-4-prop-2-ynylamino-pyrimidin-2-ylamino)-benzenesulfonyl fluoride (**F**)*	10.53 ppm (s, 1H), 8.25 ppm (s, 1H), 8.12 ppm (m, 2H), 8.06 ppm (t, 1H), 7.95 ppm (m, 2H), 4.14 ppm (d, 2H), 3.10 ppm (t, 1H)	385 m/z (ESI+)
*{2-[4-(5-Bromo-4-prop-2-ynylamino-pyrimidin-2-yl-amino)-benzenesulfonyl amino]-ethyl}-carbamic acid tert-butyl ester (**H**)*	9.78 ppm (s, 1H), 8.11 ppm (s, 1H), 7.96 ppm (m, 2H), 7.60 ppm (m, 2H), 7.54 ppm (t, 1H), 6.73 ppm (t, 1H), 4.11 ppm (d, 2H), 3.10 ppm (t, 1H), 2.91 ppm (q, 2H), 2.69 ppm (q, 2H), 1.30 ppm (s, 9H)	525 m/z (ESI+)
*N-(2-Amino-ethyl)-4-(5-bromo-4-prop-2-ynyl-amino-pyrimidin-2-ylamino)-benzenesulfonamide (**C1-SL, J**)*	9.87 (s, 1H), 8.13 (s, 1H), 7.98 (m, 2H), 7.74 (br, 2H), 7.61 (m, 4H), 4.11 (dd, 2H), 3.11 (tr, 1H), 2.83 (m, 4H)	425 m/z (ESI+)
compound C1	10.35 (s, 1H), 8.23 (br, 2H), 7.89 (m, 2H), 7.70 (m, 2H), 7.20 (br, 2H), 4.12 (m, 2H), 3.19 (br, 1H)	383 m/z (ESI+)
mimic (C1-LL)	9.86 (s, 1H), 8.43 (m, 2H), 8.12 (s, 1H), 7.99 (m, 2H), 7.61 (m, 4H), 4.11 (dd, 2H), 3.85 (m, 2H), 3.35 (m, 3H), 3.26 (m, 1H), 3.11 (tr, 1H), 2.98 (m, 4H), 2.81 (m, 1H), 1.43 (m, 2H), 1.27 (m, 2H), 0.83 (tr, 3H)	555 m/z (ESI+)
compound C1a	9.68 (s, 1H), 8.12 (s, 1H), 7.75 (m, 6H), 7.20 (tr, 1H), 7.13 (s, 2H), 3.61 (m, 2H), 3.08 (m, 2H)	387 m/z (CI+)

4.4. Structure-activity relationship observations

In order to perform different immobilization routes of C1, small modifications or linkers were introduced into the compound as described above. To analyze the impact of these modifications on the inhibitory potential towards the target protein CDK2, C1, C1-SL, C1-LL (mimic) and C1a were assayed in a CDK2 activity assay for IC_{50}-determination (The data were provided by an in-house screening facility; the results are summarized in Table 4). Since the inhibition (IC_{50}) found for C1-SL and the mimic (C1-LL) was in the same single-digit range as shown for C1, the corresponding compound matrix (C1-matrix) was anticipated to be suitable for the affinity enrichment of binders. In contrast, a modification at the side chain in

position 4 of the aminopyrimidine moiety of C1a caused a decrease in the inhibitory potential by approximately one order of magnitude compared to the inhibitory activity of C1 (summarized in table 4-4_1). However, the remaining high inhibitory activity of 18 nM (IC_{50}) was assumed to be suitable for the efficient affinity capturing of binders.

Table 4. Structure-activity relationship observations for C1-analogs.

compound	C1	C1-SL	mimic (C1-LL)	C1a
IC_{50} [nM] CDK2/CycE[a]	1	1	3	18

[a] HTRF® = *Homogeneous Time Resolved Fluorescence* Assay

4.5. Characterization of the C1-matrix

4.5.1. Calculation of the coupling rate and the compound density for C1-matrix

The C1-matrix was characterized with regard to its compound density and the compound coupling rate. For this purpose, the absorbance of a C1-SL coupling solution was determined photometrically at 280 nm before and after incubation with the Sepharose™ beads against a blank. C1-SL solution incubated with blocked Sepharose™ was used as a reference. Afterwards, a compound calibration curve (Figure 17) was used to calculate the amount of C1-SL which had been immobilized to the beads. Starting with a 20 mM C1-SL coupling solution, 3 µmol of C1-SL were coupled to approximately 1.1 mL of drained Sepharose™ beads, as described in detail in the calculation below. Thus, the final compound density was 2.7 µmol compound per milliliter drained Sepharose™. This corresponds to a coupling rate of approximately 7 – 14 %, assuming an active group density of 19 - 40 µmol/ mL drained Sepharose™, as specified by the manufacturer. The compound concentration on the bead surface could not be calculated, due to missing manufacturer's specifications regarding the respective active group concentration. However, it was assumed to be high with respect to the high compound density calculated above. Similar characteristics were assumed for the C1a-matrix.

Amount of coupled C1-SL($n_{C1\text{-}SL}$):

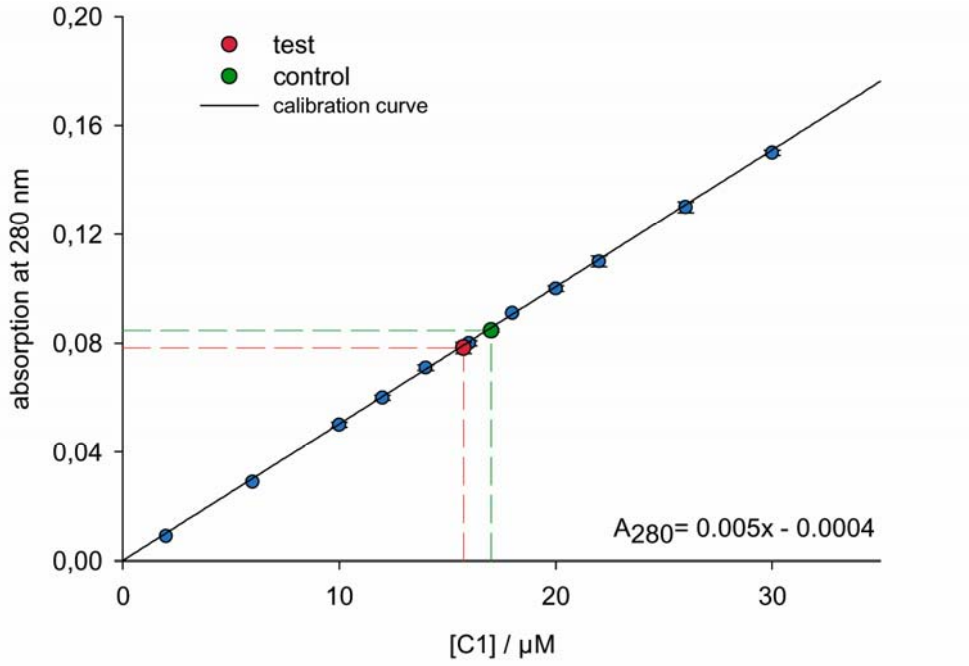

Figure 17. The absorbance at 280 nm of a C1-SL coupling solution (test) was determined photometrically before and after incubation with epoxy-activated Sepharose™ beads against a blank. C1-SL solution incubated with blocked Sepharose™ was used as a reference (control). ΔA_{280} and a compound calibration curve were used to calculate the amount of C1-SL which was immobilized to the Sepharose™ beads.

A_{Test}	= 0.078	(1:1000)
A_{Ctr}	= 0.085	(1:1000)
A_{280}	= 0.005 $c_{C1\text{-}SL}$ – 0.0004	(As indicated by the C1-SL calibration curve, Figure 17)
$c_{C1\text{-}SL}$	= (ΔA_{280} + 0.0004) x dilution factor / 0.005	
$c_{C1\text{-}SL}$	= 1.5 µmol/ mL	
$n_{C1\text{-}SL}$	= $c_{C1\text{-}SL}$ x $V_{C1\text{-}SL}$	($V_{C1\text{-}SL}$: 2 mL of a 20 mM C1-SL solution were applied.)
$n_{C1\text{-}SL}$	**= 3 µmol**	(n = amount of substance.)

3 µmol of compound C1-SL were coupled to approx. 1.1 mL of drained Sepharose™ beads.

Compound density ($d_{C1\text{-}SL}$):

$d_{C1\text{-}SL}$ = $n_{C1\text{-}SL}$/ $V_{Sepharose}$ ($V_{Sepharose}$: 0.3 g freeze-dried Sepharose™ powder gave approx. 1.1 mL final volume of medium, as specified by the manufacterer)

$d_{C1\text{-}SL}$ = 2.7 µmol/ mL

The compound density of C1-matrix was 2.7 µmol/ mL drained Sepharose™ beads.

Coupling rate ($r_{C1\text{-}SL}$):

$r_{C1\text{-}SL} = d_{C1\text{-}SL} / d_{active\ groups}$ ($d_{active\ groups}$: 19-40 µmol/ mL, as specified by the manufacterer)

$r_{C1\text{-}SL}$ = 7 – 14 %

The coupling rate of compound C1-SL to epoxy-activated Sepharose™ was approximately 7 – 14 %.

4.5.2. Proof-of-concept experiments

To demonstate the suitability of the C1-matrix for the affinity enrichment of target proteins, affinity capturing experiments were performed. To this end, HeLa cell extracts were incubated with C1-matrix and control matrix, respectively. Binding of the target protein CDK2 to the compound matrix was confirmed by immunodetection after elution (Figure 18, lane 1-3). No CDK2 enrichment resulted from using control matrix (lanes 4-6).

For the identification of a suitable elution buffer, the captured CDK2 was sequentially eluted by applying 10 mM ATP/ 10 mM $MgCl_2$/ low-salt washing buffer (detailed in experimental section), followed by a saturated C1-SL solution (approx. 150 µM) in low-salt washing buffer and finally LDS-sample buffer (lithium dodecyl sulfate-sample buffer, LDS-SB) and heat (Figure 18, lane 1-3). Neither ATP nor compound buffer were found to quantitatively elute CDK2 from the matrix. Thus, unless otherwise stated, denaturing conditions by boiling beads in LDS-SB were applied for subsequent experiments for a complete but non-specific elution of the captured proteins.

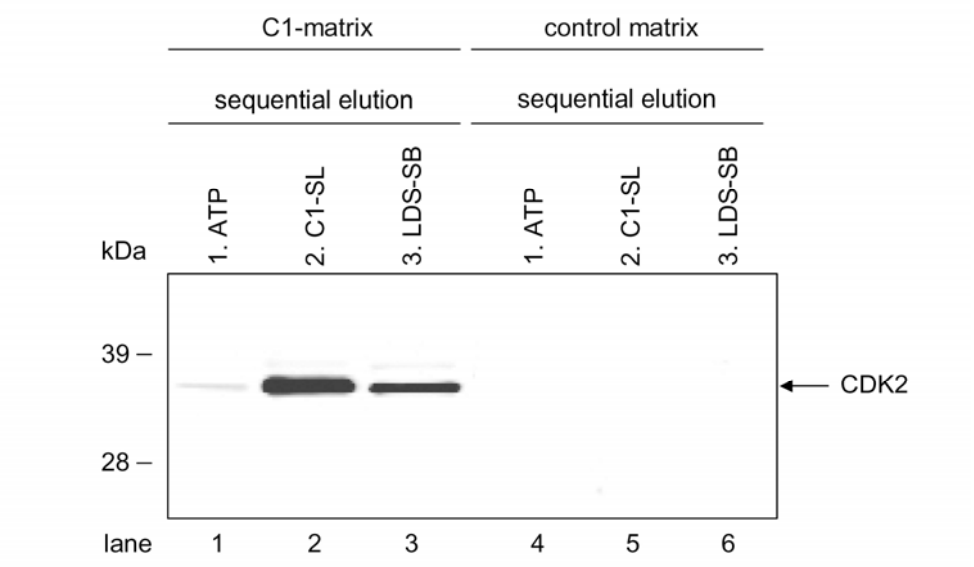

Figure 18. Proof-of-concept: HeLa cell extracts were incubated with compound matrix and control matrix, respectively. After several washing steps, captured proteins were eluted sequentially by 1.) 10 mM ATP/ 10 mM $MgCl_2$/ low-salt washing buffer; 2.) a saturated C1-SL solution in low-salt washing buffer; 3.) 2x LDS-SB/ heat. CDK2 binding to C1-matrix was demonstrated by immunodetection (lanes 1-3). No CDK2 enrichment resulted from using control matrix (lanes 4-6).

4.6. The protein binding profile of C1-matrix

Having demonstrated the suitability of C1-matrix for the capturing of CDK2 from HeLa cell extracts, LC-MS/MS analysis of eluted proteins was employed to obtain a protein binding profile for the C1-matrix (Figure 19). An initial LC-MS/MS-analysis of the entire separation range (approximately 10 kDa – 200 kDa) resulted in the identification of more than three hundred proteins, the majority of which were supposably non-specific binders. Thus, several measures were taken in order to improve the discrimination of non-specific interactions from the primary compound targets. First, a more stringent data processing procedure was used similar to the guidelines in publication of protein identification data described by (Carr, S. et al. 2004). For this purpose, the false discovery rate was adjusted to < 5 %, the threshold for a peptide match was set to a Mascot ion score ≥ 25 and proteins, identified by just one peptide ("one-hit-wonders") were removed from the list. Moreover, the redundancy of the data set was eliminated by replacing the protein IDs by the corresponding gene IDs in order to combine several splicing variants and protein IDs of one protein. Additionally, a biological replicate of the Chemical Proteomics approach was conducted and the overlap of binders identified in both experiments was kept for further data analysis. Finally, a control matrix was employed for negative affinity purification experiments. Non-specific protein binders as well as biological irrelevant interactions identified by using the control matrix were then, together

with keratins, subtracted from the positive list resulted from using the C1-matrix. As a result, approximately 90 proteins were identified fulfilling acceptance criteria described above. As proteins assumed to be specific binders more than 30 protein kinases, several oxidoreductases, ATP and GTP binding enzymes, and non-protein kinases were found. Additionally, associated proteins, which are known to interact with several of the identified protein kinases (cyclins), were detected. Furthermore, the list contained more than 30 proteins, which are presumably non-specific binders since isoforms or other subunits of the same proteins, or other members of the same protein families were found in control experiments, as well (e.g. members of the tyrosine 3/tryptophan 5-monooxygenase activation protein family, tubulin isoforms, exportin isoforms, importin isoforms, etc.). The results are summarized in Table 5**.** To obtain a comprehensive interaction profile for the C1-matrix, more cell lines will have to be screened.

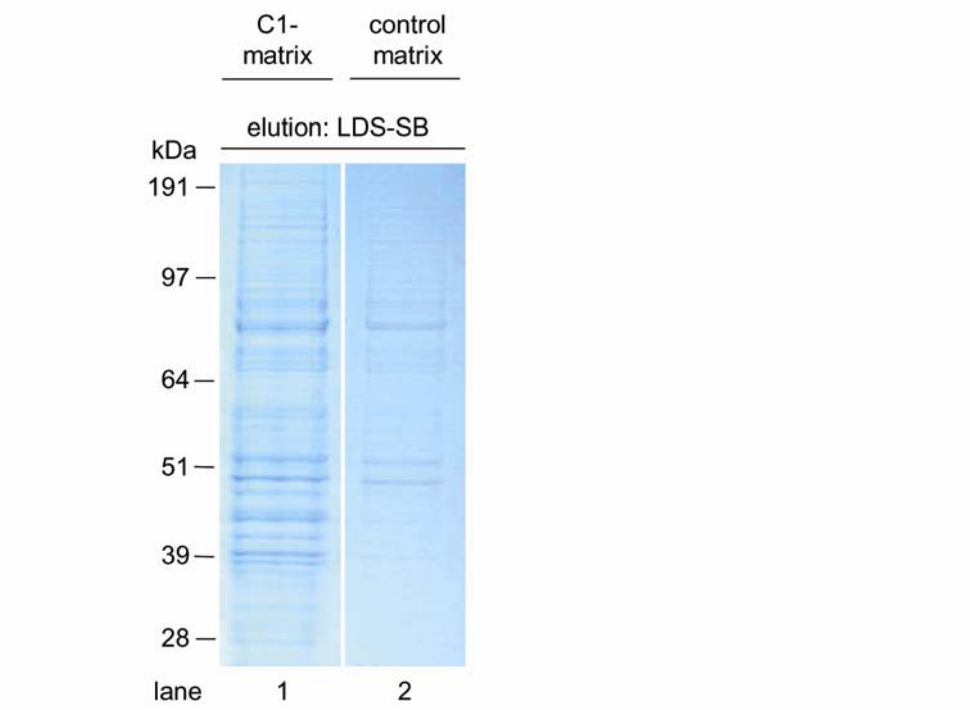

Figure 19. Affinity pull-down using C1-matrix: HeLa cell extracts were loaded on C1-matrix and control matrix, respectively. After extensive washing, bound proteins were eluted by boiling the beads in 2x LDS-SB and analyzed by SDS-PAGE, Coomassie staining and LC-MS/MS.

Table 5. Proteins identified by Chemical Proteomics using C1-matrix.	
Gene Product[a]	Gene[a]
protein kinases	
AMP-activated protein kinase alpha 2 catalytic subunit [Homo sapiens]	PRKAA2 [Homo sapiens]
AP2 associated kinase 1 [Homo sapiens]	AAK1 [Homo sapiens]
aurora kinase A [Homo sapiens];serine/threonine protein kinase 6 [Homo sapiens]	AURKA [Homo sapiens]

calcium/calmodulin-dependent protein kinase II delta isoform 3 [Homo sapiens]	CAMK2D [Homo sapiens]
calcium/calmodulin-dependent protein kinase II gamma isoform 6 [Homo sapiens]	CAMK2G [Homo sapiens]
CDC42-binding protein kinase beta [Homo sapiens]	CDC42BPB [Homo sapiens]
cell division cycle 2 protein isoform 1 [Homo sapiens]	CDK1 [Homo sapiens]
CHK1 checkpoint homolog [Homo sapiens]	CHEK1 [Homo sapiens]
conserved helix-loop-helix ubiquitous kinase [Homo sapiens]	CHUK [Homo sapiens]
cyclin-dependent kinase 2 isoform 1 [Homo sapiens]	CDK2 [Homo sapiens]
cyclin-dependent kinase 5 [Homo sapiens]	CDK5 [Homo sapiens]
cyclin-dependent kinase 7 [Homo sapiens]	CDK7 [Homo sapiens]
cyclin-dependent kinase 9 [Homo sapiens]	CDK9 [Homo sapiens]
fer (fps/fes related) tyrosine kinase (phosphoprotein NCP94) [Homo sapiens]	FER [Homo sapiens]
microtubule associated serine/threonine kinase-like [Homo sapiens]	MASTL [Homo sapiens]
mitogen-activated protein kinase 1 [Homo sapiens]	MAPK1 [Homo sapiens]
mitogen-activated protein kinase 3 isoform 2 [Homo sapiens]	MAPK3 [Homo sapiens]
mitogen-activated protein kinase 8 isoform 2 [Homo sapiens]	MAPK8 [Homo sapiens]
mitogen-activated protein kinase 9 isoform 1 [Homo sapiens]	MAPK9 [Homo sapiens]
mitogen-activated protein kinase kinase 1 [Homo sapiens]	MAP2K1 [Homo sapiens]
mitogen-activated protein kinase kinase 2 [Homo sapiens]	MAP2K2 [Homo sapiens]
mitogen-activated protein kinase kinase kinase 11 [Homo sapiens]	MAP3K11 [Homo sapiens]
MLK-related kinase isoform 1 [Homo sapiens]	ZAK [Homo sapiens]
p21-activated kinase 4 isoform 1 [Homo sapiens]	PAK4 [Homo sapiens]
PCTAIRE protein kinase 1 [Homo sapiens]	PCTK1 [Homo sapiens]
PCTAIRE protein kinase 2 [Homo sapiens]	PCTK2 [Homo sapiens]
protein kinase D2 [Homo sapiens]	PRKD2 [Homo sapiens]
protein kinase D3 [Homo sapiens]	PRKD3 [Homo sapiens]
protein kinase N2 [Homo sapiens]	PKN2 [Homo sapiens]
receptor (TNFRSF)-interacting serine-threonine kinase 1 [Homo sapiens]	RIPK1 [Homo sapiens]
receptor-interacting serine-threonine kinase 2 [Homo sapiens]	RIPK2 [Homo sapiens]
serine/threonine kinase 10 [Homo sapiens]	STK10 [Homo sapiens]
serine/threonine kinase 17a (apoptosis-inducing) [Homo sapiens]	STK17A [Homo sapiens]
serine/threonine kinase 17b (apoptosis-inducing) [Homo sapiens]	STK17B [Homo sapiens]
serine/threonine kinase 2 [Homo sapiens]	SLK [Homo sapiens]
serine/threonine kinase 3 (STE20 homolog, yeast) [Homo sapiens]	STK3 [Homo sapiens]
serine/threonine kinase 4 [Homo sapiens]	STK4 [Homo sapiens]
unc-51-like kinase 3 (C. elegans) [Homo sapiens]	ULK3 [Homo sapiens]
viral oncogene yes-1 homolog 1 [Homo sapiens]	YES1 [Homo sapiens]
non-protein kinases	
fructosamine-3-kinase-related protein [Homo sapiens]	FN3KRP [Homo sapiens]

pyridoxal kinase [Homo sapiens]	PDXK [Homo sapiens]
non-catalytical subunits of protein kinases	
AMP-activated protein kinase beta 2 non-catalytic subunit [Homo sapiens]	PRKAB2 [Homo sapiens]
oxidoreductases	
acyl-Coenzyme A dehydrogenase family, member 10 [Homo sapiens]	ACAD10 [Homo sapiens]
acyl-Coenzyme A dehydrogenase family, member 11 [Homo sapiens]; putative acyl-CoA dehydrogenase [Homo sapiens]	ACAD11 [Homo sapiens]
apoptosis-inducing factor (AIF)-like mitchondrion-associated inducer of death [Homo sapiens]	AMID [Homo sapiens]
biliverdin reductase B (flavin reductase (NADPH)) [Homo sapiens]	BLVRB [Homo sapiens]
NAD synthetase 1 [Homo sapiens]	NADSYN1 [Homo sapiens]
NAD(P)H dehydrogenase, quinone 2 [Homo sapiens]	NQO2 [Homo sapiens]
thioredoxin peroxidase [Homo sapiens]	PRDX4 [Homo sapiens]
associated proteins	
cyclin A [Homo sapiens]	CCNA2 [Homo sapiens]
cyclin B1 [Homo sapiens]	CCNB1 [Homo sapiens]
cyclin B2 [Homo sapiens]	CCNB2 [Homo sapiens]
cyclin T1 [Homo sapiens]	CCNT1 [Homo sapiens]
ATP-binding proteins	
ATP citrate lyase isoform 1 [Homo sapiens]	ACLY [Homo sapiens]
small GTP-binding proteins	
ADP-ribosylation factor-like 1 [Homo sapiens]	ARL1 [Homo sapiens]
cell division cycle 42 isoform 1 [Homo sapiens]	CDC42 [Homo sapiens]
keratins and proteins which were also identified in control experiments using blocked Sepharose^{TM} as affinity matrix	
acyl-Coenzyme A dehydrogenase, very long chain isoform 1 precursor [Homo sapiens]	ACADVL [Homo sapiens]
aldolase A [Homo sapiens]	ALDOA [Homo sapiens]
ATP synthase, H+ transporting, mitochondrial F0 complex, subunit d isoform b [Homo sapiens]	ATP5H [Homo sapiens]
ATP synthase, H+ transporting, mitochondrial F1 complex, alpha subunit precursor [Homo sapiens]	ATP5A1 [Homo sapiens]
ATP synthase, H+ transporting, mitochondrial F1 complex, beta subunit precursor [Homo sapiens]	ATP5B [Homo sapiens]
basic leucine zipper and W2 domains 1 [Homo sapiens]	BZW1 [Homo sapiens]
basic leucine zipper and W2 domains 1 [Homo sapiens]	LOC151579 [Homo sapiens]
beta actin [Homo sapiens]	ACTB [Homo sapiens]
calnexin precursor [Homo sapiens]	CANX [Homo sapiens]
carbamoyl-phosphate synthetase 1, mitochondrial [Homo sapiens]	CPS1 [Homo sapiens]
carbamoylphosphate synthetase 2/aspartate transcarbamylase/dihydroorotase [Homo sapiens]	CAD [Homo sapiens]
chaperonin containing TCP1, subunit 2 [Homo sapiens]	CCT2 [Homo sapiens]
chaperonin containing TCP1, subunit 4 (delta) [Homo sapiens]	CCT4 [Homo sapiens]
chaperonin containing TCP1, subunit 6A isoform b [Homo sapiens]	CCT6A [Homo sapiens]
chaperonin containing TCP1, subunit 7 isoform b [Homo sapiens]	CCT7 [Homo sapiens]

clathrin heavy chain 1 [Homo sapiens]	CLTC [Homo sapiens]
cytochrome b5 reductase isoform 1 [Homo sapiens]	CYB5R3 [Homo sapiens]
dynein, cytoplasmic 1, heavy chain 1 [Homo sapiens]	DNCH1 [Homo sapiens]
dynein, cytoplasmic 1, heavy chain 1 [Homo sapiens];dynein, cytoplasmic, heavy polypeptide 1 [Homo sapiens]	DYNC1H1 [Homo sapiens]
eukaryotic translation initiation factor 2, subunit 3 gamma, 52kDa [Homo sapiens]	EIF2S3 [Homo sapiens]
exportin 1 [Homo sapiens]	XPO1 [Homo sapiens]
GCN1 general control of amino-acid synthesis 1-like 1 [Homo sapiens]	GCN1L1 [Homo sapiens]
heat shock 60kDa protein 1 (chaperonin) [Homo sapiens]	SPG13 [Homo sapiens]
heat shock 60kDa protein 1 (chaperonin) [Homo sapiens];chaperonin [Homo sapiens]	HSPD1 [Homo sapiens]
heat shock 70kDa protein 5 (glucose-regulated protein, 78kDa) [Homo sapiens]	HSPA5 [Homo sapiens]
heat shock 70kDa protein 8 isoform 1 [Homo sapiens]	HSPA8 [Homo sapiens]
heat shock protein 90kDa alpha (cytosolic), class B member 1 [Homo sapiens]	HSPCB [Homo sapiens]
heat shock protein 90kDa alpha (cytosolic), class B member 1 [Homo sapiens] ;heat shock 90kDa protein 1, beta [Homo sapiens]	HSP90AB1 [Homo sapiens]
heat shock protein 90kDa beta (Grp94), member 1 [Homo sapiens];tumor rejection antigen (gp96) 1 [Homo sapiens]	HSP90B1 [Homo sapiens]
heme oxygenase (decyclizing) 2 [Homo sapiens]	HMOX2 [Homo sapiens]
hydroxyacyl dehydrogenase, subunit A [Homo sapiens]	HADHA [Homo sapiens]
importin 7 [Homo sapiens]	IPO7 [Homo sapiens]
IQ motif containing GTPase activating protein 1 [Homo sapiens]	IQGAP1 [Homo sapiens]
karyopherin beta 1 [Homo sapiens]	KPNB1 [Homo sapiens]
keratin 1 [Homo sapiens]	KRT1 [Homo sapiens]
keratin 10 [Homo sapiens]	KRT10 [Homo sapiens]
keratin 9 [Homo sapiens]	KRT9 [Homo sapiens]
lactate dehydrogenase A [Homo sapiens]	LDHA [Homo sapiens]
leucine rich repeat containing 59 [Homo sapiens];hypothetical protein LOC55379 [Homo sapiens]	LRRC59 [Homo sapiens]
leucine-rich PPR motif-containing protein [Homo sapiens]	LRPPRC [Homo sapiens]
mannose 6 phosphate receptor binding protein 1 [Homo sapiens]	M6PRBP1 [Homo sapiens]
Na+/K+ -ATPase alpha 1 subunit isoform a proprotein [Homo sapiens]	ATP1A1 [Homo sapiens]
phospholipase A2, group IVA [Homo sapiens]	PLA2G4A [Homo sapiens]
prohibitin 2 [Homo sapiens]	PHB2 [Homo sapiens]
prohibitin 2 [Homo sapiens]	REA [Homo sapiens]
RAB1A, member RAS oncogene family [Homo sapiens]	RAB1A [Homo sapiens]
RAB1B, member RAS oncogene family [Homo sapiens]	RAB1B [Homo sapiens]
RAB7, member RAS oncogene family [Homo sapiens]	RAB7 [Homo sapiens]
RAN binding protein 5 [Homo sapiens]	RANBP5 [Homo sapiens]
ras-related GTP-binding protein RAB10 [Homo sapiens]	RAB10 [Homo sapiens]
ribophorin I precursor [Homo sapiens]	RPN1 [Homo sapiens]
ribosomal protein S19 [Homo sapiens]	RPS19 [Homo sapiens]

ribosomal protein S3 [Homo sapiens]	RPS3 [Homo sapiens]
ribosomal protein S4, X-linked [Homo sapiens];ribosomal protein S4, X-linked X isoform [Homo sapiens]	RPS4X [Homo sapiens]
RuvB-like 2 [Homo sapiens]	RUVBL2 [Homo sapiens]
splicing factor 3b, subunit 1 isoform 2 [Homo sapiens]	SF3B1 [Homo sapiens]
transferrin receptor [Homo sapiens]	TFRC [Homo sapiens]
tubulin, beta polypeptide [Homo sapiens]	TUBB [Homo sapiens]
tyrosine 3/tryptophan 5 -monooxygenase activation protein, epsilon polypeptide [Homo sapiens]	YWHAE [Homo sapiens]
despite not being identified in control experiments, these proteins are supposed to predominantly represent high aboundant background	
archain [Homo sapiens]	ARCN1 [Homo sapiens]
ATP synthase, H+ transporting, mitochondrial F0 complex, subunit B1 precursor [Homo sapiens]	ATP5F1 [Homo sapiens]
CD9 antigen [Homo sapiens]	CD9 [Homo sapiens]
coatomer protein complex, subunit beta 1 [Homo sapiens]	COPB1 [Homo sapiens]
COPB [Homo sapiens]	COPB [Homo sapiens]
cullin-associated and neddylation-dissociated 1 [Homo sapiens];TIP120 protein [Homo sapiens]	CAND1 [Homo sapiens]
cytochrome P450, family 51 [Homo sapiens]	CYP51A1 [Homo sapiens]
exportin 5 [Homo sapiens]	XPO5 [Homo sapiens]
FGF intracellular binding protein isoform a [Homo sapiens]	FIBP [Homo sapiens]
heat shock 70kDa protein 9B precursor [Homo sapiens]	HSPA9B [Homo sapiens]
hypothetical protein LOC134147 [Homo sapiens]	LOC134147 [Homo sapiens]
hypothetical protein LOC9847 [Homo sapiens]	KIAA0528 [Homo sapiens]
importin 9 [Homo sapiens]	IPO9 [Homo sapiens]
interferon-induced transmembrane protein 3 (1-8U) [Homo sapiens]	IFITM3 [Homo sapiens]
LIM and senescent cell antigen-like domains 1 [Homo sapiens]	LIMS1 [Homo sapiens]
lymphocyte antigen 6 complex G5B [Homo sapiens]	LY6G5B [Homo sapiens]
parvin, alpha [Homo sapiens]	PARVA [Homo sapiens]
proteasome 26S non-ATPase subunit 2 [Homo sapiens]	PSMD2 [Homo sapiens]
RAB2, member RAS oncogene family [Homo sapiens]	RAB2 [Homo sapiens]
ras suppressor protein 1 isoform 1 [Homo sapiens]	RSU1 [Homo sapiens]
ribosomal protein L35a [Homo sapiens]	RPL35A [Homo sapiens]
ribosomal protein P2 [Homo sapiens]	RPLP2 [Homo sapiens]
ribosomal protein S13 [Homo sapiens]	RPS13 [Homo sapiens]
ribosomal protein S6 kinase, 90kDa, polypeptide 1 isoform b [Homo sapiens]	RPS6KA1 [Homo sapiens]
SAR1a gene homolog 1 [Homo sapiens]	SAR1A [Homo sapiens]
signal recognition particle receptor, beta subunit [Homo sapiens]	SRPRB [Homo sapiens]
stratifin [Homo sapiens]	SFN [Homo sapiens]
TATA binding protein interacting protein 49 kDa [Homo sapiens]	RUVBL1 [Homo sapiens]
transmembrane protein 109 [Homo sapiens]	TMEM109 [Homo sapiens]

tubulin, alpha, ubiquitous [Homo sapiens]	K-ALPHA-1 [Homo sapiens]
tyrosine 3/tryptophan 5 -monooxygenase activation protein, theta polypeptide [Homo sapiens]	YWHAQ [Homo sapiens]
tyrosine 3/tryptophan 5 -monooxygenase activation protein, zeta polypeptide [Homo sapiens]	YWHAZ [Homo sapiens]
tyrosine 3-monooxygenase/tryptophan 5-monooxygenase activation protein, beta polypeptide [Homo sapiens]	YWHAB [Homo sapiens]
tyrosine 3-monooxygenase/tryptophan 5-monooxygenase activation protein, gamma polypeptide [Homo sapiens]	YWHAG [Homo sapiens]
[a] Entrez Gene nomenclature	

4.7. Protein kinase selectivity patterns of C1 and the mimic revealed moderate linker effects

During the optimization processes, the compound C1 has been optimized with regard to potent inhibition of CDK2. However, its selectivity was barely improved and is considered to be poor. To analyze the protein kinase selectivity profile of C1, the compound was tested in a panel of 27 recombinant protein kinases, which were identified in the Chemical Proteomics experiments described above. The biochemical determination of the inhibitory potential for the selected kinases was performed by the KinaseProfiler^{TM} Service provided by Upstate/ Millipore. At 1 μM compound concentration, C1 inhibited three other CDKs (CDK1, 5, and 9) and six further kinases (AURKA, CHEK1, MAPK8, MAPK9, STK3, and STK17A) by more than 90 % (Figure 20). In addition, five kinases were inhibited by more than 80 % (CAMK2D, CDK7, PRKD2, STK4, STK10, and ULK3), five kinases by 50-80 % (CAMK2G, CHUK, FER, MAPK1, YES), and six by less than 50 %.

To assess functional effects of the linker, the mimic was tested on the same panel of kinases as C1. A comparison of both selectivity patterns revealed that the mimic had less inhibitory potency against most of the tested kinases. However, a few examples were found where the mimic had more activity against a kinase compared to C1 (CAMK2G, PAK4, PKN2, PRKD2).

Besides the investigation of the protein kinase binding profile of C1 with Chemical Proteomics, another focus of this work was the characterization of non-protein kinase/ compound interactions.

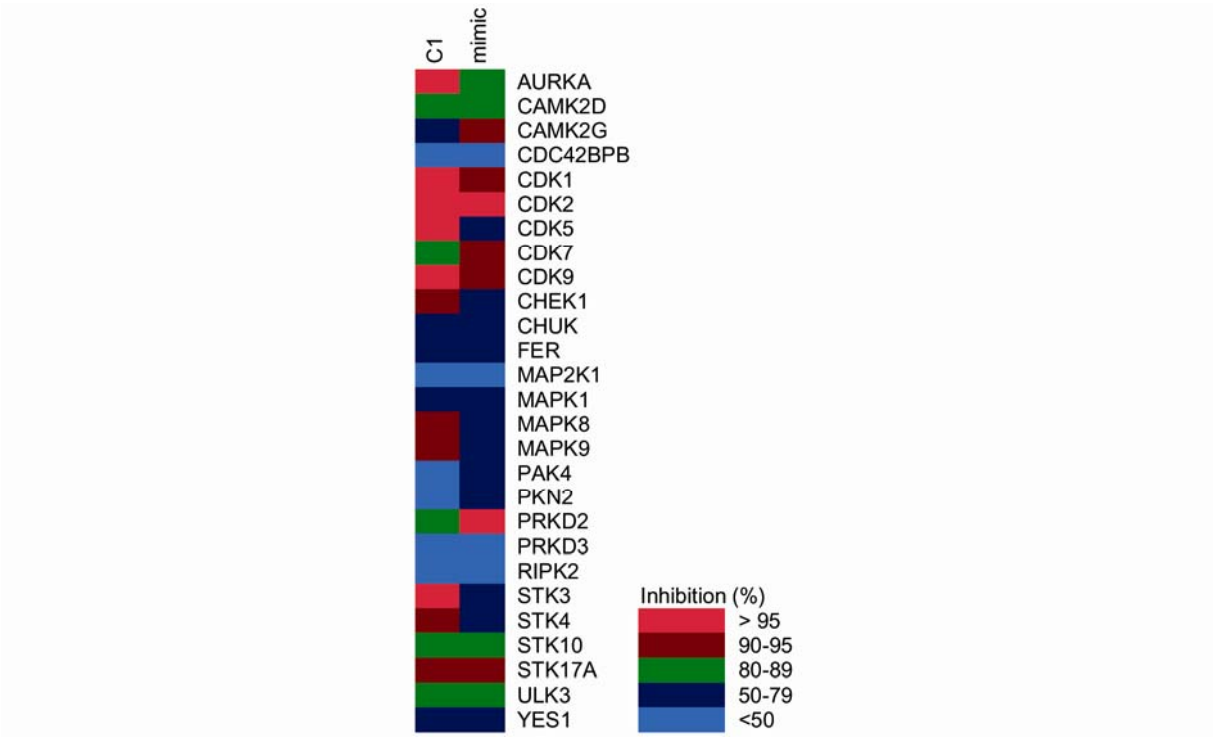

Figure 20. Percentage of inhibition of 27 protein kinases identified by affinity pull-down experiments by C1 and mimic (C1-LL). Inhibitors were tested at 1 µM compound and 10 µM ATP. Only a subset of protein kinases captured by C1-matrix were strongly inhibited by C1. A comparison of the selectivity patterns of C1 and the mimic revealed moderate effects of the linker on the inhibitory potential. Data from the Upstate/ Millipore KinaseProfiler™ Service.

4.8. Characterization of the PDXK/ inhibitor interaction by Chemical Proteomics

Within the Chemical Proteomics approach, the human pyridoxal kinase (PDXK), a non-protein kinase, was identified as being captured by the C1-matrix. PDXK had been found to be targeted by the CDK2 inhibitor *(R)*-roscovitine, as well (Bach, S. et al. 2005). As demonstrated by co-crystallization experiments of PDXK and *(R)*-roscovitine, the ATP-competitive CDK inhibitor was found to selectively target PDXK at the pyridoxal site rather than at the ATP binding site (Tang, L. et al. 2005). Prompted by these findings, the PDXK/ C1 interaction was investigated in more detail for this work.

First, a serial affinity chromatography was performed to confirm a specific binding of PDXK to C1-matrix. For this purpose, HeLa cell extract was incubated with C1-matrix and the flow-through was mixed with fresh C1-matrix. Specific binders are essentially captured by the first affinity matrix, whereas the amounts of non-specifically bound proteins are similar for both matrices. Immunodetection showed that PDXK was mainly retained by the first compound matrix (Figure 21, lane 1), indicating a specific binding to the affinity matrix. No PDXK enrichment resulted from using control matrix (lanes 3 + 4).

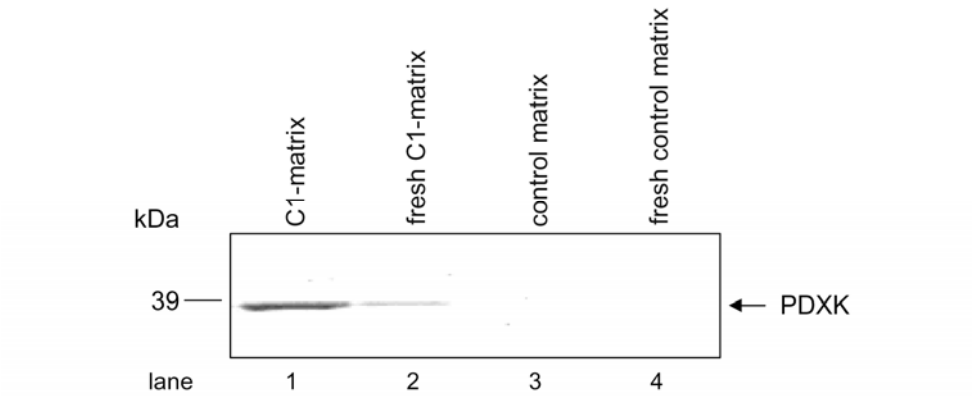

Figure 21. For serial affinity chromatography, HeLa cell extract was incubated with C1-matrix. Subsequently, the flow-through was mixed with fresh C1-matrix. Immunodetection showed that PDXK was essentially captured by the first matrix (lane 1), indicating a specific binding to the affinity matrix. No PDXK enrichment resulted from using control matrix (lane 3 + 4).

After having demonstrated a specific capturing of PDXK, the question was addressed, whether the C1-matrix targets the ATP site or an alternative binding site of PDXK, as shown for *(R)*-roscovitine. For this purpose, HeLa cell extracts were incubated with C1-matrix. After washing procedures, the C1-matrix was sequentially eluted using 10 mM ATP/ 10 mM $MgCl_2$/ low-salt washing buffer, followed by a saturated C1-SL solution in low-salt washing buffer, and finally LDS-SB/ heat to distinguish capturing via the ATP binding site from enrichment via alternative sites. Eluted proteins were loaded on SDS-PAGE, Coomassie stained and analyzed by LC-MS/MS. PDXK was identified only in compound and LDS-SB elution fractions but not in the ATP fraction (Figure 22, lanes 1-3). In parallel, C1-matrix was sequentially eluted using the ATP buffer, a *(R)*-roscovitine buffer and LDS-SB/ heat. *(R)*-roscovitine, which is known to bind PDXK via its pyridoxal binding site, was able to compete with immobilized C1 and released PDXK from the matrix, suggesting a similar binding site for both compounds (Figure 22, lanes 4-6). PDXK was neither enriched nor eluted from control matrix (Figure 22, lanes 7-9).

In order to confirm a binding of C1 to PDXK at the pyridoxal binding site, as suggested by the results with *(R)*-roscovitine, a substrate competition approach was performed (Figure 23). Since pyridoxal has a low solubility at pH 7 in an aqueous buffer, the PDXK substrate pyridoxine was used for the approach. To this end, cell extracts were spiked with several concentrations of pyridoxine and incubated with C1-matrix. Immunodetection revealed that PDXK binding to C1-matrix was nearly completely prevented in the presence of 10 mM spiked pyridoxine, indicating the binding of PDXK to the C1-matrix via the pyridoxal binding site (Figure 23, lane 5).

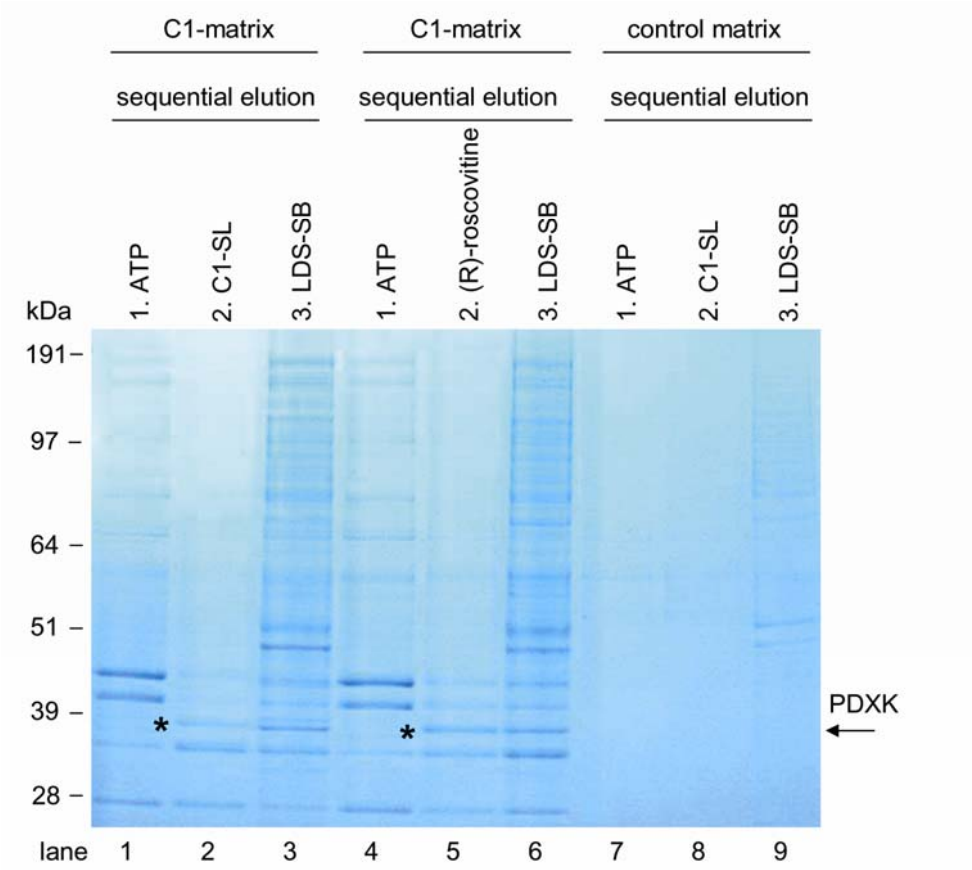

Figure 22. PDXK was found to bind to C1-matrix via an alternative binding site, similar to PDXK/ *(R)*-roscovitine interaction: After incubation with HeLa extracts and washing procedures, a sequential elution of C1-matrix was employed, using 10 mM ATP/ 10 mM $MgCl_2$/ low-salt washing buffer, a saturated C1-SL solution in low-salt washing buffer, LDS-SB/ heat. Eluted proteins were loaded on SDS-PAGE and Coomassie stained. PDXK was only identified by LC-MS/MS in the compound and LDS-SB elution fractions but not in the ATP fraction (asterisk), suggesting an alternative binding site rather than the ATP site (lanes 1-3). The same was observed when C1-SL was replaced by *(R)*-roscovitine, which is known to bind PDXK via its pyridoxal binding site (lanes 4-6). Since *(R)*-roscovitine was able to release PDXK from C1-matrix, a similar PDXK binding site for C1 and *(R)*-roscovitine was assumed. No PDXK enrichment and elution resulted from using control matrix (lanes 7-9).

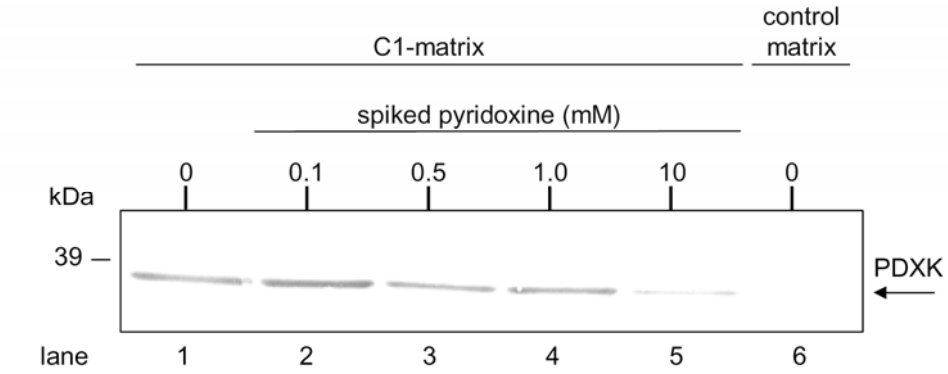

Figure 23. Spiked pyridoxine prevented PDXK from binding to C1-matrix: Cell extracts were spiked with several concentrations of the PDXK substrate pyridoxine. PDXK enrichment by C1-matrix was competed with 10 mM free pyridoxine as shown by immunodetection of PDXK.

In order to perform further interaction analyses, an additional affinity matrix was generated. For this purpose, the substrate of the PDXK, pyridoxal (PL), was coupled to EAH–Sepharose™ beads, resulting in a pyridoxal matrix (Figure 10). Subsequently, C1-matrix, pyridoxal matrix and control matrix were loaded with HeLa extracts, washed and sequentially eluted using 10 mM ATP/ 10 mM $MgCl_2$/ low-salt washing buffer, 10 mM pyridoxine/ low-salt washing buffer, a saturated C1-SL solution in low-salt washing buffer, and finally LDS-SB and heat (Figure 24). Due to better solubility at pH 7, the PDXK substrate pyridoxine was preferred to pyridoxal for this experiment. PDXK was eluted from both affinity matrices by pyridoxine and free C1-SL, as demonstrated by immunodetection (Figure 24, lanes 3+4), but not by ATP (lane 1), indicating that the PDXK/ C1 interaction occurs at the substrate binding site rather than at the ATP site. Again, no PDXK enrichment resulted from using control matrix.

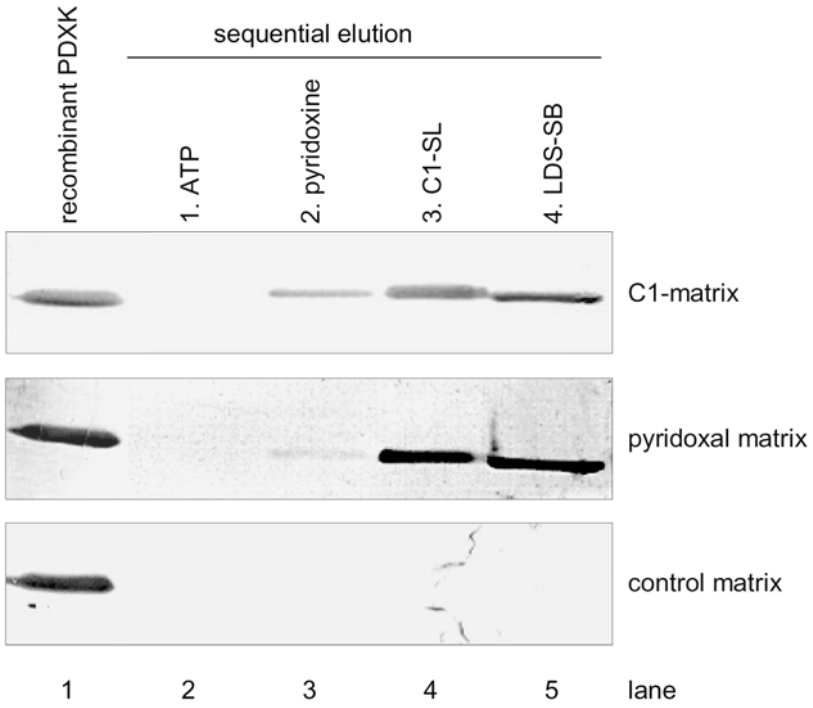

Figure 24. PDXK was targeted by C1-matrix at the pyridoxal binding site rather than the ATP site: C1-matrix, pyridoxal matrix and control matrix were loaded with HeLa extracts, washed and sequentially eluted using 1.) 10 mM ATP/ 10 mM $MgCl_2$/ low-salt washing buffer; 2.) 10 mM pyridoxine/ low-salt washing buffer; 3.) a saturated C1-SL solution in low-salt washing buffer; 4.) 2x LDS-SB/ heat. Since PDXK was eluted from both affinity matrices by pyridoxine and free C1-SL (and LDS-sample buffer, lanes 3-5) as shown by immodetection, but not by ATP (lane 1), it was concluded that the PDXK/ C1 interaction occurs at the substrate binding site rather than at the ATP site.

4.9. Purification of recombinantly expressed PDXK

In order to perform quantitative, biochemical binding studies, a suitable scheme for the recombinant expression and purification for PDXK was planned. The recombinant PDXK had no purification tag and was therefore purified in two steps by affinity chromatography using pyridoxal matrix and size exclusion chromatography. First, *E.coli* cell extract containing recombinant PDXK was loaded onto a preparative pyridoxal matrix column for affinity enrichment. Captured protein was isocratically eluted by 10 mM pyridoxine as shown by Figure 25 A. Since both, pyridoxine and the PDXK, absorb UV-light at 280 nm, capillary electrophoresis (described in the Materials and Methods section) was used to monitor the purification. Figure 25 B shows that all impurities had been removed by the first purification step. The protein containing fractions 1B3 – 2A11 (96 fractions, each 2 mL) were pooled and concentrated.

In order to determine whether the native state of the recombinant PDXK was a monomer or a higher oligomer and to sense the presence of aggregated proteins, an analytical size exclusion chromatography was performed (Figure 26 A). The molecular weight of PDXK was calculated using a molecular weight marker calibration curve (Figure 26 B). A small deviation of 6 kDa was found (41 kDa calculated vs 35 kDa in theory), however, the results indicate, that the PDXK was a monomer and significant amounts of protein aggregates did not occur. Subsequently, a preparative size exclusion chromatography was employed to separate the PDXK substrate pyridoxine, which was used for elution of the pyridoxal matrix, from the protein sample (Figure 27 A + B). Fractions 1F3 - 1G9 were pooled (Figure 27 C) and the protein concentration was determined by the Nanodrop method (c_{final} = 0.17 mg/ mL); the final yield was 4.1 mg of purified PDXK.

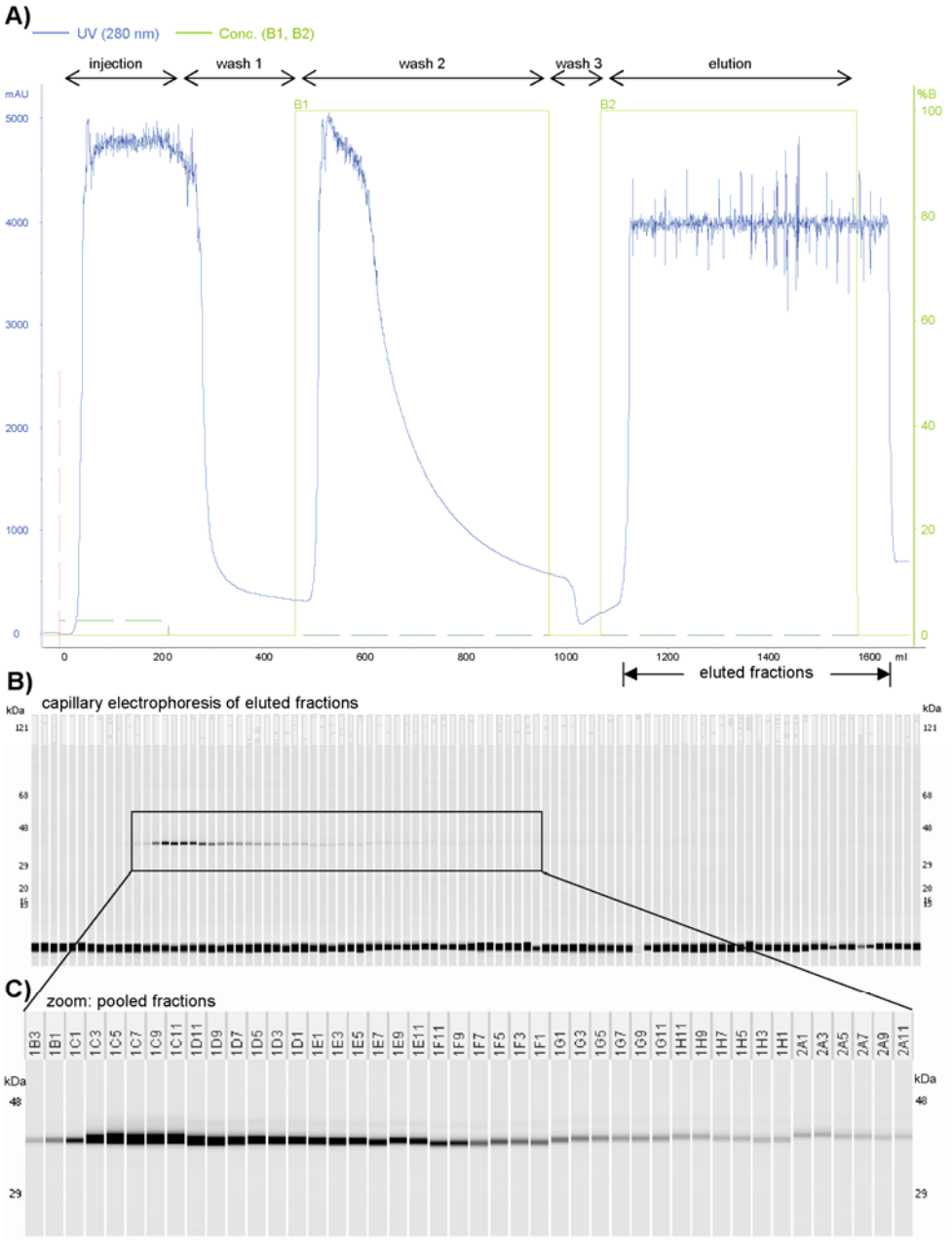

Figure 25. Affinity chromatography (AC) profile of the PDXK purification: After injection, the column was washed three times (B1, A2 (not shown), B1) and the untagged PDXK was isocratically eluted using 10 mM pyridoxine (B2, green curve indicates the B1/B2 buffer). Since both, the protein and pyridoxine, show UV-absorption at 280 nm (blue curve), the protein containing fractions could not be identified by UV detection. B) Capillary electrophoresis was used to monitor the affinity purification of PDXK. The protein containing fractions are framed. C) Capillary electrophoresis shows the pooled protein containing fractions.

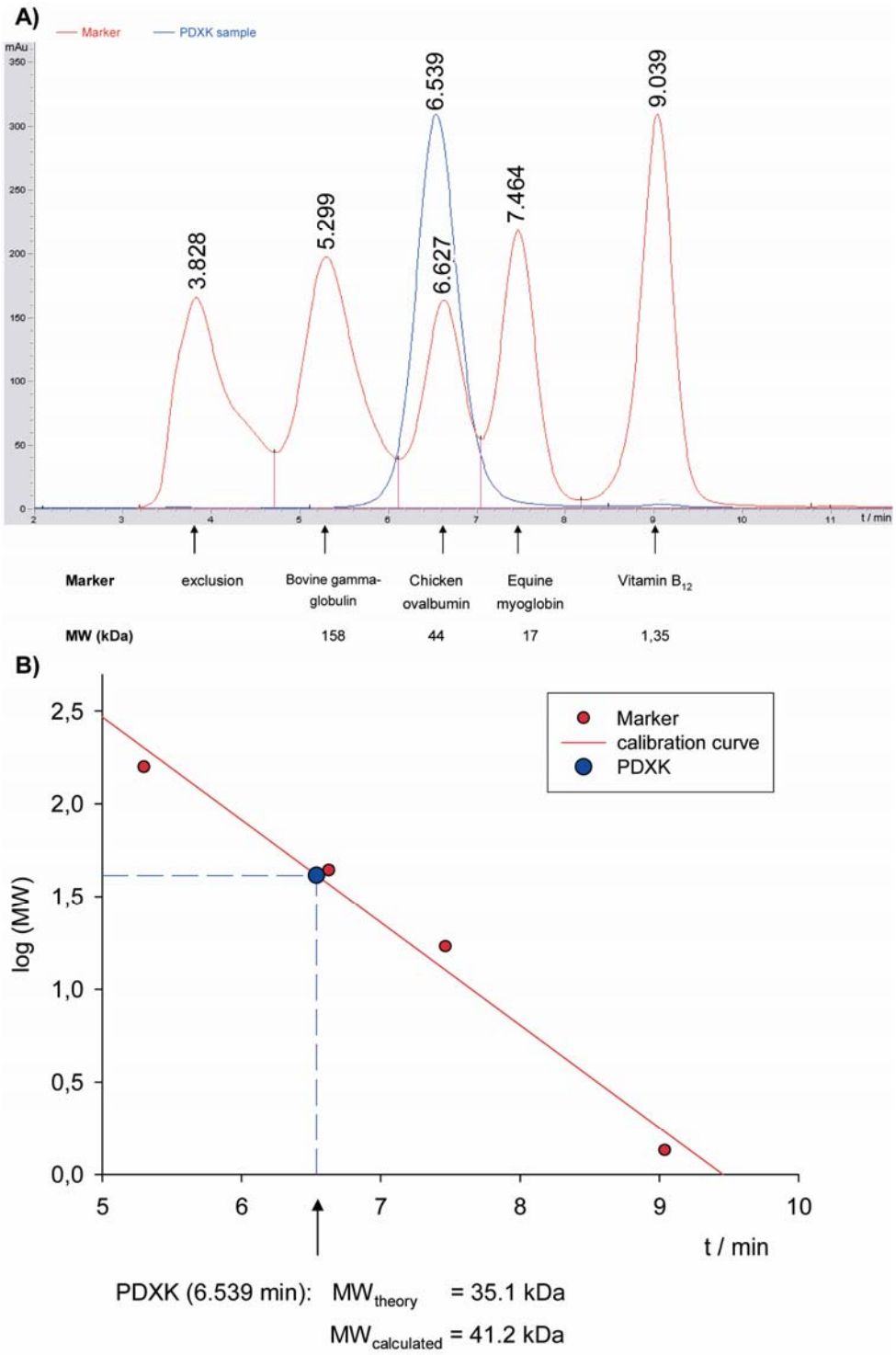

Figure 26. A) Analytical size exclusion chromatography (SEC) profile of PDXK: The blue curve shows the absorption of the PDXK sample at 280 nm, the red curve indicates the absorption of a molecular weight marker. The homogeneity of the PDXK sample was demonstrated and no protein aggregates were found. B) The logarithms of the molecular weights of the marker proteins were plot against the respective retention times. The resulting calibration curve was used to calculate the molecular weight of the PDX.

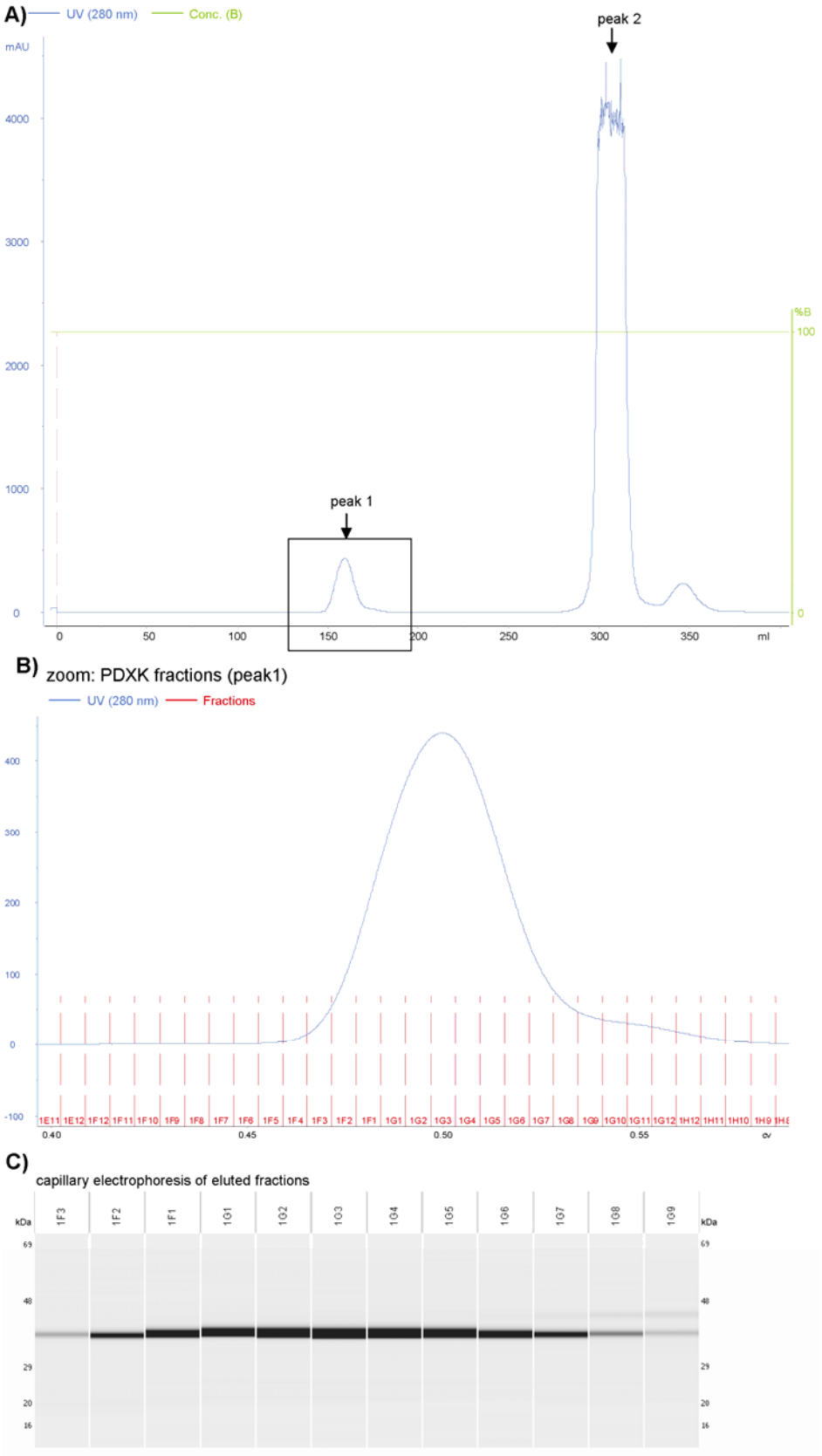

Figure 27. A) Preparative size exclusion chromatography (SEC) profile of the PDXK purification: A preparative SEC was used to separate the PDXK (peak 1, framed) from pyridoxine (peak 2). The blue curve indicates the UV absorption at 280 nm, the green curve shows the B-buffer profile. B) The figure shows the PDXK peak (peak 1, framed in A) of the SEC chromatogram. Fractions (red curves) 1F3 - 1G9 were pooled. C) Capillary electrophoresis was used to confirm the correct molecular weight of the separated PDXK.

The SDS-PAGE in Figure 28 mirrors the complete purification procedure and demonstrates that all impurities were removed (lane 5). The SDS-PAGE band of the purified PDXK was sliced, tryptically in-gel digested and analyzed by LC-coupled MS/MS. Found peptide and fragment ion masses were searched against the human IPI (International Protein Index) database using the parameter settings described in the Materials and Methods section. The isoform one of the human pyridoxal kinase was identified with a sequence coverage of 65.1 % (Figure 29 A). Additionally, the correct mass of the intact protein was confirmed by LC-MS. For this purpose, the cysteine residues of a PDXK sample were reduced and alkylated using dithiothreitol (DTT) and iodoacetamide (IAA). Multiple alkylated protein species with two to four carbamidomethylated cysteine residues and one to two additional non-specific alkylations were detected with the correct masses according to the number of alkylations. (Figure 29 B). The purified PDXK was shock frozen or subjected to biochemical binding studies.

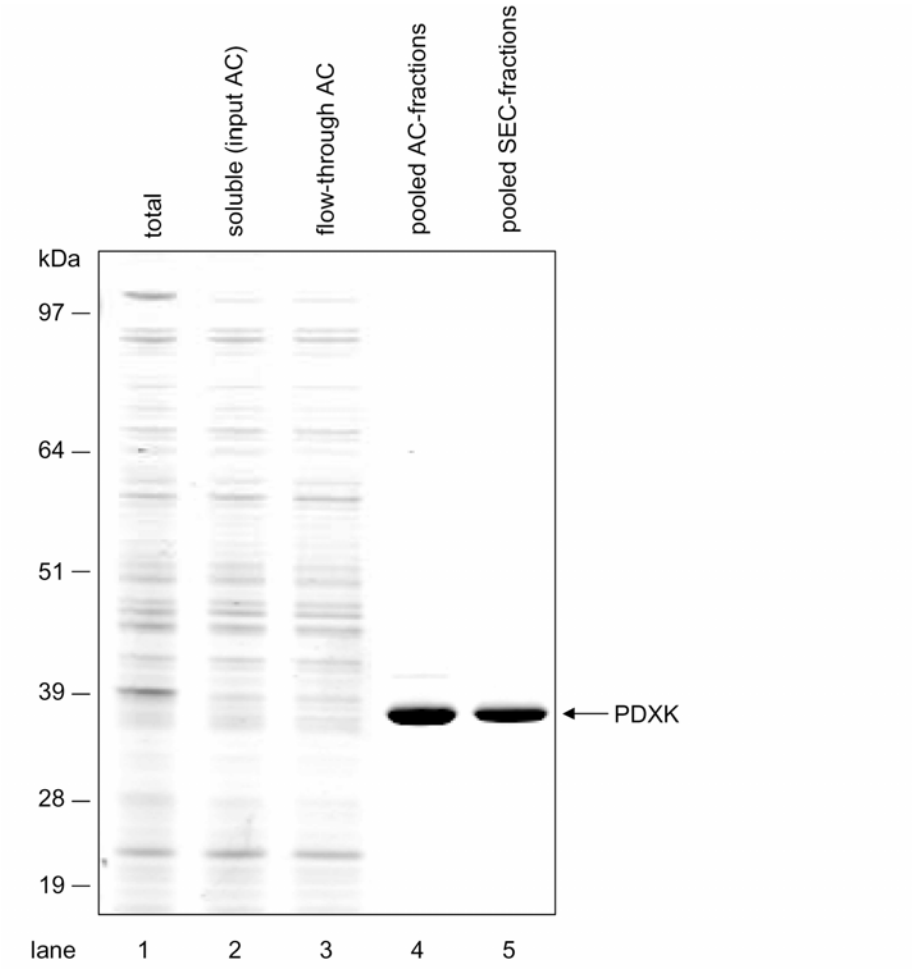

Figure 28. SDS-PAGE of PDXK purification: Subsequent to cell disruption (total), the soluble proteins were loaded onto a pyridoxal matrix column for affinity chromatography (AC). Pyridoxine was used to release enriched PDXK for elution. Nearly all impurities were removed by the first purification step. The second purification step, a size exclusion chromatography, was used to remove remaining impurities and the pyridoxine.

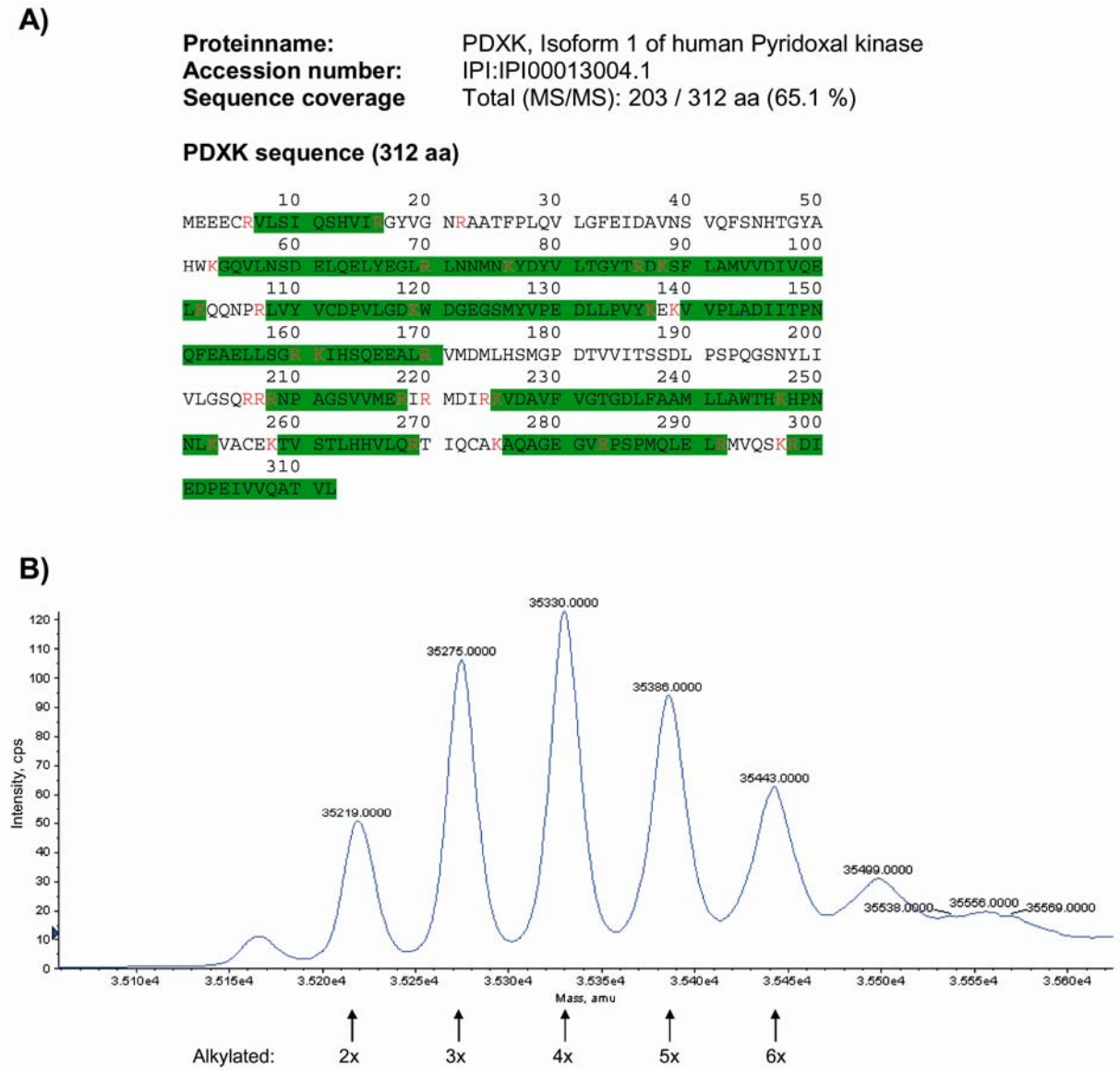

Figure 29. The correct mass and amino acid sequence of the purified PDXK was confirmed by mass spectrometry. A) A tryptically digested PDXK sample was analyzed by LC-MS/MS. Data files were searched against the human IPI database and the isoform 1 of the human pyridoxal kinase (IPI accession number: IPI00013004.1) was identified with a sequence coverage of 65.1 %. B) A reduced and alkylated sample of the intact protein (purified PDXK) was analyzed by LC-MS. The correct masses of double to sixfold alkylated protein spicies were found (2 - 4 alkylated cysteine residues and 1 - 2 additional non-specific alkylations).

4.10. Biochemical characterization of the PDXK/ inhibitor interaction

After having demonstrated the enrichment of PDXK from HeLa cell extracts by C1-matrix via the substrate binding site, a PDXK activity assay was adapted from the literaure (Kastner, U. et al. 2007) in order to quantify the PDXK/ C1 binding affinity. The assay determines the phosphorylation of pyridoxal (PL) by PDXK, by measuring pyridoxal 5'-phosphate (PLP) at its absorbtion maximum at 388 nm (Figure 30 A). A PLP calibration curve, shown in Figure 30 B, was used to calculate the increase of the PLP concentration in subsequent experiments.

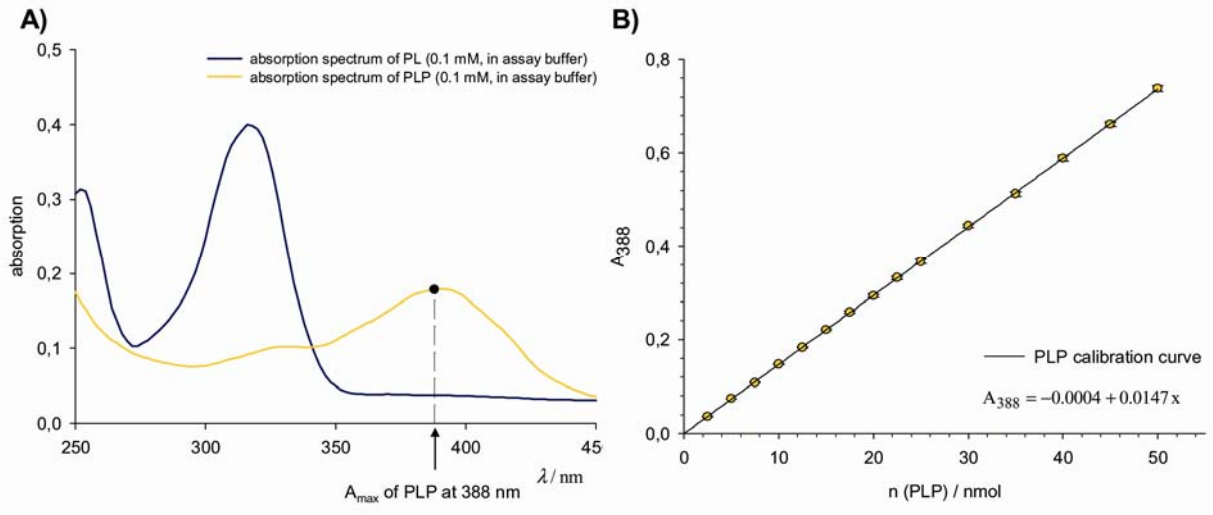

Figure 30. Principle of the PDXK activity assay: A) The figure shows the absorption spectra of pyridoxal (PL, blue) and pyridoxal 5'-phosphate (PLP, yellow). The phosphorylation of PL by PDXK, giving PLP, causes a shift of the absorption maximum to 388 nm. The change in the absorption at 388 nm was used to calculate the PDXK activity. B) A PLP calibration curve was used to calculate the amount of PLP at a certain absorption.

4.10.1. Determination of the Michaelis constant K_m

The Michaelis constant K_m for pyridoxal was determined to confirm that the assay adapted from the literature measures in the described range. The assay was prepared as described in the Materials and Methods section and the absorbtion at 388 nm was determined photometrically in the presence of different starting concentrations of PL in triplicates against a blank. A calibration curve (Figure 30 B) was used to calculate the corresponding PLP concentrations. Subsequently, the initial linear formation rate of PLP was plotted against the substrate concentration (Figure 31). The resulting saturation curve of the PDXK shows the relation between the substrate concentration and the rate, as described by the Michaelis Menten kinetic model. The software Sigma Plot Enzyme Kinetics Module 1.3^{TM} (Systat Software GmbH) was used to determine the maximum velocity, $v_{max} = (2.2 \pm 0.1)$ nmol * µg^{-1} * min^{-1}, and the Michaelis constant, $K_m = (99.4 \pm 12.6)$ µM, of PDXK and its substrate pyridoxal. Since the results of the Michaelis constant determination are in the range described in the literature (summarized in Table 7 in the Discussion), the assay was used for IC_{50}-determinations.

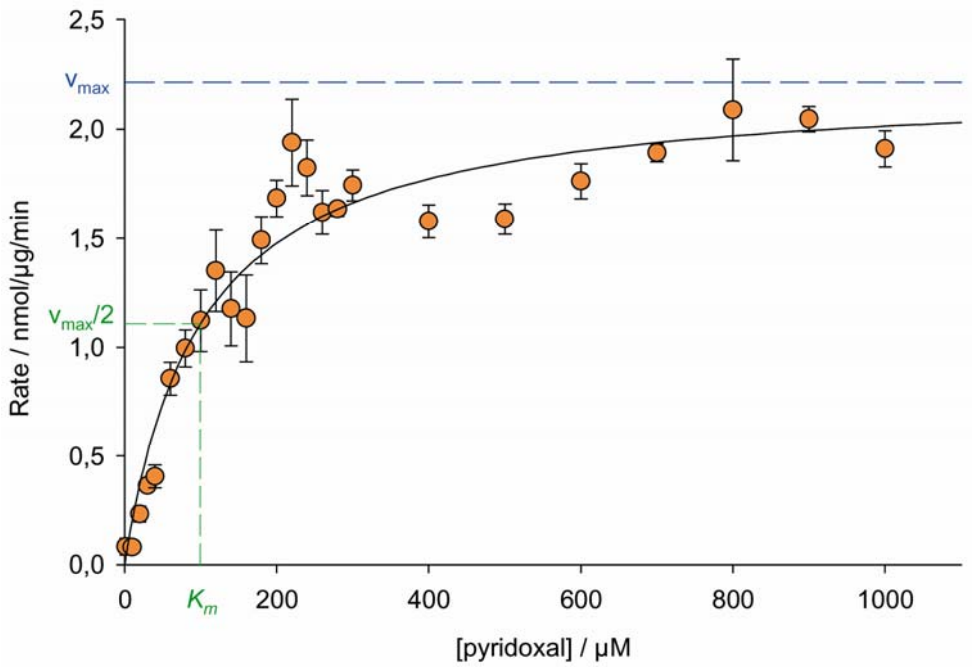

Figure 31. Determination of the Michaelis constant K_m: The PDXK activity was determined photometrically at 388 nm in the presence of different starting concentrations of PL in triplicates against a blank. The Michaelis constant K_m for the binding of pyridoxal to PDXK and the maximum velocity v_{max} were calculated from the saturation curve of enzyme activity versus substrate concentration: K_m = (99.4 ± 12.6) µM; maximum velocity v_{max} = (2.2 ± 0.1) nmol * μg^{-1} * min^{-1}. Curve fitting was carried out using Sigma Plot Enzyme Kinetics Module 1.3™ (Systat Software GmbH).

4.10.2. IC_{50}- & K_D-determination

Motivated by the considerable enrichment of PDXK from HeLa cell extracts by C1-matrix, the activity of recombinant human PDXK was assayed in the presence of different concentrations of C1, C1-SL, mimic, and *(R)*-roscovitine, respectively, covering a range of 1 nM – 50 µM. In agreement with results reported in the literature (Bach, S. et al. 2005), even at the highest concentration tested (50 µM), a very modest inhibition of PDXK was found for *(R)*-roscovitine (Figure 32, PDXK activity = 78 ± 13 % at 50 µM *(R)*-roscovitine). The same inhibition profile was observed for C1 (50 µM, 92 ± 2 %), but, an increasing linker length correlated with a more efficient decrease of PDXK activity (50 µM C1-SL: 81 ± 6 %, 50 µM mimic: 56 ± 7 %). The activity is expressed as percentage of vehicle control (2 % Me_2SO without test compounds), representing maximal activity. 10 mM EDTA served as a negative control; reducing the PDXK activity to 11 ± 1 %.

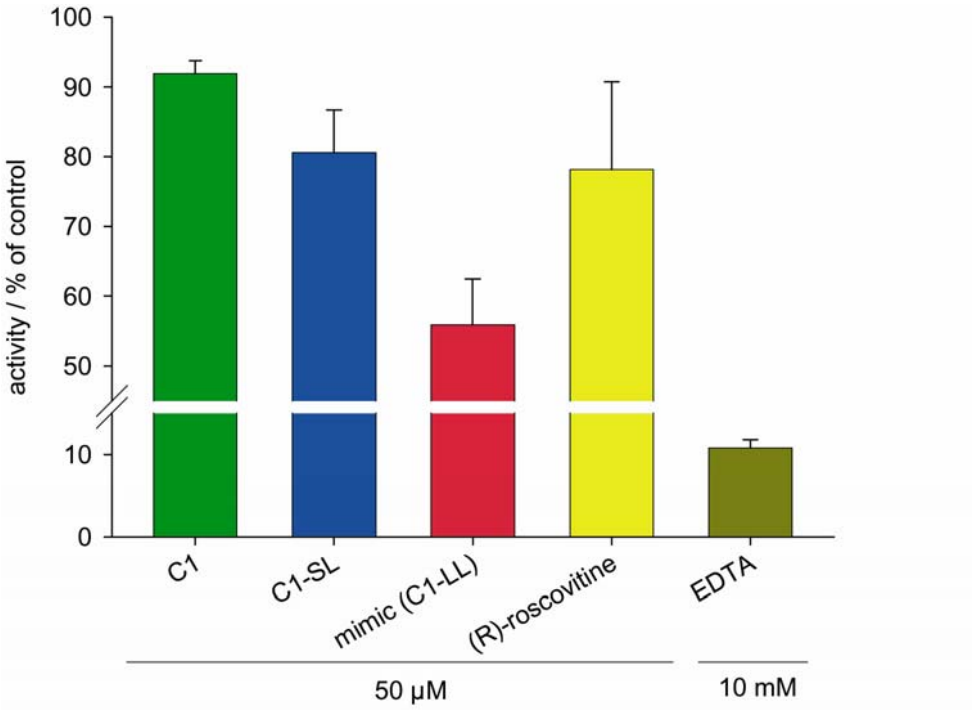

Figure 32. The activity of PDXK was assayed in triplicates in the presence of C1, C1-SL, mimic (C1-LL) and *(R)*-roscovitine. Even at the highest concentration tested (50 µM), C1 as well as *(R)*-roscovitine showed only limited inhibition of PDXK activity; C1: 92 ± 2 %; *(R)*-roscovitine: 78 ± 13 %. However, an increasing linker length caused stronger inhibition; C1-SL: 81 ± 6 %; mimic: 56 ± 7 %. 10 mM EDTA served as a negative control. Activity is expressed as percentage of vehicle control (2 % Me_2SO w/o test compounds). 2 % Me_2SO was shown to have no effect on PDXK activity.

To investigate whether the high ATP concentration in the PDXK activity assay (2.5 mM) might have an influence on the activities measured, an isothermal titration calorimetry (ITC) experiment was carried out and the binding of the compound to PDXK was studied in the absence of ATP and of pyridoxal. For this purpose, C1-SL was titrated into a PDXK sample and the evolved binding heats were measured. To ensure the same buffer conditions, the ligand was dissolved in an aliquot of the SEC buffer, which was used for the PDXK purification. Raw data were collected, corrected for ligand heats of dilution, and integrated using the MicroCal Origin software (MicroCal, LLC). A weak exothermal reaction was measured, but low binding heats, indicated by a linear ITC curve, prevented the exact K_D determination (Figure 33 A + B). However, the data suggest a K_D value > 10 µM, corresponding to the results from the PDXK activity assays.

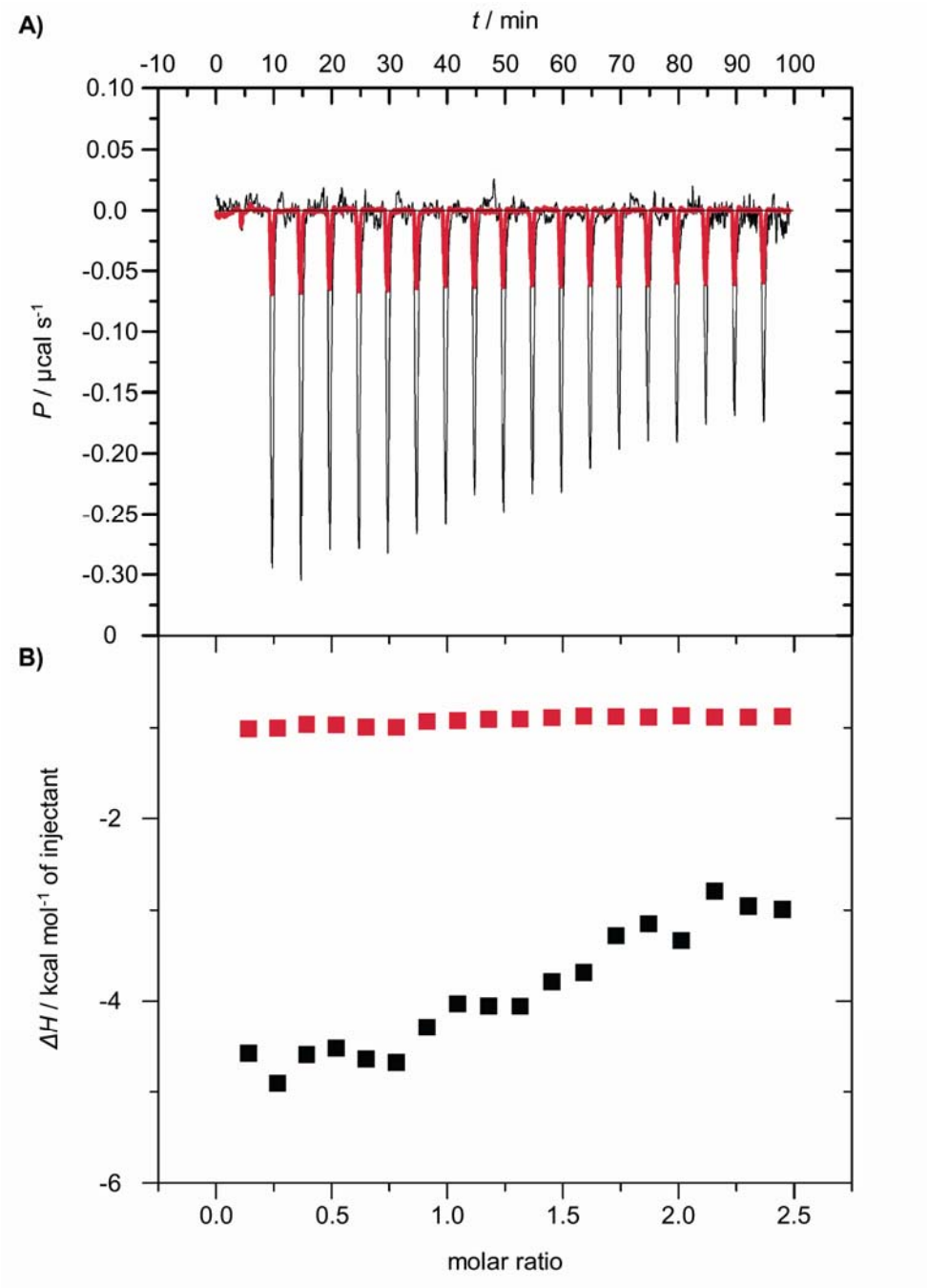

Figure 33. Isothermal titration calorimetry (ITC) for K_D determination: C1-SL (140 µM) was titrated into a PDXK sample (12.6 µM). A weak exothermal reaction was measured, but the shape of the titration curve did not allow the K_D determination. K_D was estimated to be > 10 µM. Figure A) shows the time dependence of the electric power (measured in µcal/ s) necessary to maintain constant the temperature difference between the reaction and reference cells after each injection of C1-SL (black curve). The area under each peak is the heat (µcal) associated with the process. Raw data were corrected for ligand heats of dilution (red curve). B) Analysis of the data using the MicroCal Origin software (MicroCal, LLC) yielded the binding enthalpie ΔH in dependence of the molar ratio of protein and compound. Low binding heats prevented the correct ΔH determination.

4.11. Compound immobilization route 2 - The protein binding profile of C1a-matrix

To profile the C1 interactome more comprehensively, particularly with regard to interactions occurring at the benzenesulfonamide moiety of C1, the analog C1a was coupled to a solid support at the 4-position giving C1a-matrix (Figure 16). C1a was shown to inhibit CDK2 activity at a low nanomolar concentration (Table 4, IC_{50} (CDK2/CycE) = 18 nM) as well.
Benzenesulfonamide moieties are known to inhibit most of the known carbonic anhydrase isozymes (Supuran, C. T. et al. 2007). Especially the ubiquitously expressed cytosolic isoform carbonic anhydrase 2 (CA2) is described to have a very high affinity for sulfonamides (Puccetti, L. et al. 2005). Due to a lack of expression of CA2 in HeLa cells, H460 cells were included into this analysis. CA2 expression in H460 but not in HeLa cells was demonstrated by immunoblotting (Figure 34 A). Subsequently, H460 and HeLa cell extracts were loaded onto C1a-matrix and control matrix, respectively. After the washing procedure, bound proteins were non-specifically as well as specifically eluted by LDS-SB and a saturated solution of C1a in low-salt washing buffer, respectively, precipitated and loaded on SDS-PAGE. A LC-MS/MS analysis was applied on the proteins non-specifically eluted from C1a-matrix by LDS-SB/ heat (Figure 34 B, lane 2). Compared to the number and the intensity of the Coomassie stained protein bands obtained by employing the C1-matrix (Figure 19), a significantly lower amount of total protein was retained by the C1a-matrix as demonstrated by the Coomassie stained SDS-PAGE and the results of the MS-analysis. The overlap of two biological replicates using C1a-matrix resulted in a list of 37 identified proteins fulfilling acceptance criteria (Table 6). Keratins and non-specific binders also identified in control experiments by using control matrix and H460 protein extracts, in total 25 proteins, were not considered for further data interpretation. In addition, some protein kinases (AURKA, CDK1, MAPK9), which were also found by using the C1-matrix, were identified. Eight proteins were exclusively identified by using the C1a-matrix, including CA2 and the previously unknown potential off-target carboxymethylenebutenolidase homolog (CMBL). Both proteins, CA2 and CMBL, were also identified by employing free C1a for a specific elution of the proteins captured by the C1a-matrix (Figure 34 B, lane 3). In addition, CA2 capturing from H460 extracts by C1a-matrix was confirmed by immunodetection of CA2 subsequent to LDS-SB elution of the beads, as shown in Figure 34 C, lane 2. No CA2 enrichment resulted from using control matrix (Figure 34 C, lane 1 and B, lane 1).

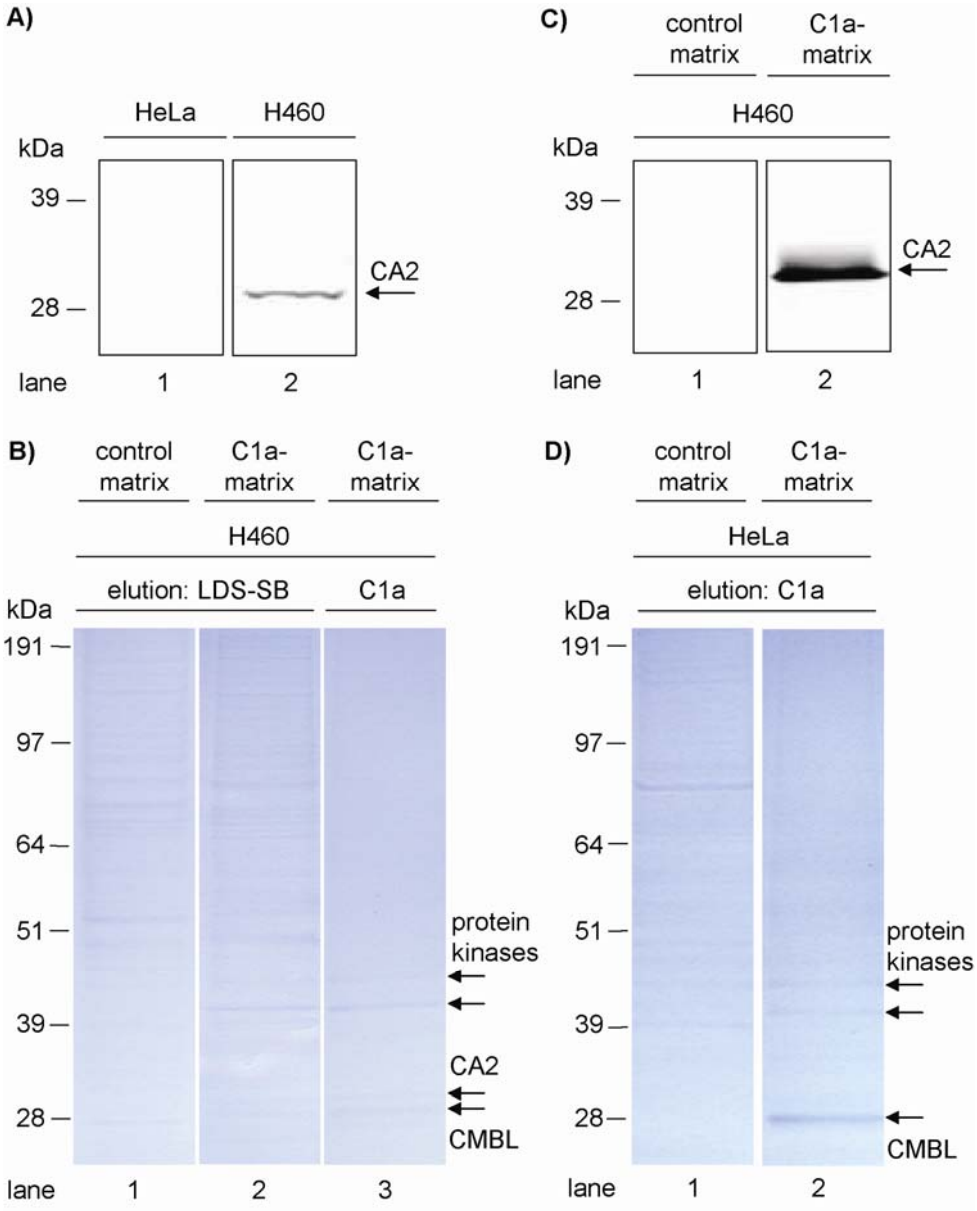

Figure 34. Protein binding profile of C1a-matrix shows capturing of CA2, CMBL and other proteins. A) CA2 expression, which is lacking in HeLa cells (lane 1), was demonstrated for H460 cells by immunodetection (lane 2). B) H460 cell extracts were loaded on C1a-matrix and control matrix, respectively. Beads were extensively washed, bound proteins were non-specifically as well as specifically eluted by LDS-SB and a saturated solution of C1a in low-salt washing buffer, respectively, precipitated and loaded on SDS-PAGE. LC-MS/MS analysis of Coomassie stained gels revealed capturing of CA2 from H460 lysate by C1a-matrix (lane 2 + 3). Moreover, one further potential off-target specifically binding to the sulfonamide moiety, was identified: Carboxymethylenebutenolidase homolog (CMBL). In addtition, some protein kinases (AURKA, CDK1, MAPK9), which also captured by using the C1-matrix, were identified. No CA2, CMBL or kinase capturing resulted from using control matrix (lane 1). C) H460 cell extracts were loaded onto C1a-matrix and control matrix, respectively. Captured proteins were eluted completely by LDS-SB/ heat. Immunodetection of CA2 confirmed its binding to C1a-matrix (lane 2) but not to control matrix (lane 1). D) HeLa cell extracts were loaded on C1a-matrix and control matrix, respectively. Subsequent to washing, the beads were specifically eluted using a saturated solution of C1a in low-salt washing buffer. LC-MS/MS analysis of the most intensive Coomassie stained bands revealed capturing of CMBL by the C1a-matrix (lane 2). In addition, some protein kinases (AURKA, CDK1, MAPK9) were found. Neither CMBL nor kinases were captured by control matrix (lane 1).

The second potential off-target CMBL was found by applying the C1a-matrix and a specific elution on HeLa cell extracts (Figure 34 D, lane 2), as well. Human CMBL is a predicted protein and has not been characterized in the literature yet. However, in Pseudomonas the enzyme is described to have a hydrolase activity and is involved in detoxification pathways (KEGG pathways: 1,4-Dichlorobenzene degradation 00627 and gamma-Hexachloro-cyclohexane degradation 00361). The CMBL/ compound interaction was not characterized in more detail for this study, but might be an object for further investigations regarding C1-profiling.

Table 6 summarizes the results form the LC-MS/MS analysis of the proteins non-specifically eluted from the C1a-matrix:

Table 6. Proteins identified by Chemical Proteomics using C1a-matrix and H460 protein extracts.

Gene Product[a]	Gene[a]
protein identified exclusively by using C1a-matrix	
carbonic anhydrase II [Homo sapiens]	CA2 [Homo sapiens]
epoxide hydrolase 1, microsomal (xenobiotic) [Homo sapiens]	EPHX1 [Homo sapiens]
myoferlin isoform a [Homo sapiens]	FER1L3 [Homo sapiens]
protein disulfide isomerase family A, member 3 [Homo sapiens]	GRP58 [Homo sapiens]
hypothetical protein LOC134147 [Homo sapiens] (carboxymethylenebutenolidase homolog (Pseudomonas))	LOC134147 [Homo sapiens] (CMBL)
protein disulfide isomerase-associated 3 precursor [Homo sapiens]	PDIA3 [Homo sapiens]
Tu translation elongation factor, mitochondrial [Homo sapiens]	TUFM [Homo sapiens]
ubiquitin carboxyl-terminal esterase L1 (ubiquitin thiolesterase) [Homo sapiens]	UCHL1 [Homo sapiens]
protein which were also identified by using C1-matrix and HeLa protein extract	
aurora kinase A [Homo sapiens]; serine/threonine protein kinase 6 [Homo sapiens]	AURKA [Homo sapiens]
cell division cycle 2 protein isoform 1 [Homo sapiens]	CDK1 [Homo sapiens]
lymphocyte antigen 6 complex G5B [Homo sapiens]	LY6G5B [Homo sapiens]
mitogen-activated protein kinase 9 isoform 1 [Homo sapiens]	MAPK9 [Homo sapiens]
keratins and proteins which were also identified in control experiments using blocked Sepharose™ as affinity matrix	
beta actin [Homo sapiens]	ACTB [Homo sapiens]
aldo-keto reductase family 1, member B10 [Homo sapiens]	AKR1B10 [Homo sapiens]
aldolase A [Homo sapiens]	ALDOA [Homo sapiens]
annexin A2 isoform 2 [Homo sapiens]	ANXA2 [Homo sapiens]
ATP synthase, H+ transporting, mitochondrial F1 complex, beta subunit precursor [Homo sapiens]	ATP5B [Homo sapiens]
eukaryotic translation elongation factor 1 alpha 1 [Homo sapiens]	EEF1A1 [Homo sapiens]
enolase 1 [Homo sapiens]	ENO1 [Homo sapiens]

glyceraldehyde-3-phosphate dehydrogenase [Homo sapiens]	GAPD [Homo sapiens]
heat shock protein 90kDa alpha (cytosolic), class A member 1 [Homo sapiens];heat shock protein 90kDa alpha (cytosolic), class A member 1 isoform 1 [Homo sapiens]	HSP90AA1 [Homo sapiens]
heat shock 70kDa protein 8 isoform 1 [Homo sapiens]	HSPA8 [Homo sapiens]
heat shock 60kDa protein 1 (chaperonin) [Homo sapiens];chaperonin [Homo sapiens]	HSPD1 [Homo sapiens]
keratin 1 [Homo sapiens]	KRT1 [Homo sapiens]
keratin 10 [Homo sapiens]	KRT10 [Homo sapiens]
keratin 16 [Homo sapiens]	KRT16 [Homo sapiens]
keratin 19 [Homo sapiens]	KRT19 [Homo sapiens]
keratin 2a [Homo sapiens]	KRT2A [Homo sapiens]
keratin 8 [Homo sapiens]	KRT8 [Homo sapiens]
keratin 9 [Homo sapiens]	KRT9 [Homo sapiens]
keratin 8 [Homo sapiens]	LOC149501 [Homo sapiens]
basic leucine zipper and W2 domains 1 [Homo sapiens]	LOC151579 [Homo sapiens]
ribosomal protein L3 isoform a [Homo sapiens]	RPL3 [Homo sapiens]
ribophorin I precursor [Homo sapiens]	RPN1 [Homo sapiens]
heat shock 60kDa protein 1 (chaperonin) [Homo sapiens]	SPG13 [Homo sapiens]
transketolase [Homo sapiens]	TKT [Homo sapiens]
tubulin, beta polypeptide [Homo sapiens]	TUBB [Homo sapiens]

[a] Entrez Gene nomenclature

4.12. Biochemical characterization of the CA2/ inhibitor interaction – IC_{50}-determination and SAR observations

Having demonstrated the carbonic anhydrase 2 (CA2) capturing by C1a-matrix, the CA2/ compound interaction was quantitatively analyzed in biochemical binding studies. To this end, commercially available human CA2 was assayed in the presence of C1, C1-SL, mimic, and C1a covering a concentration range of 0.01 – 25 µM. IC_{50} values of C1 and C1a were in the submicromolar range (IC_{50} (CA2) = 331 nM (C1), 995 nM (C1a)), whereas C1-SL and the mimic had no inhibitory potential (Figure 35).

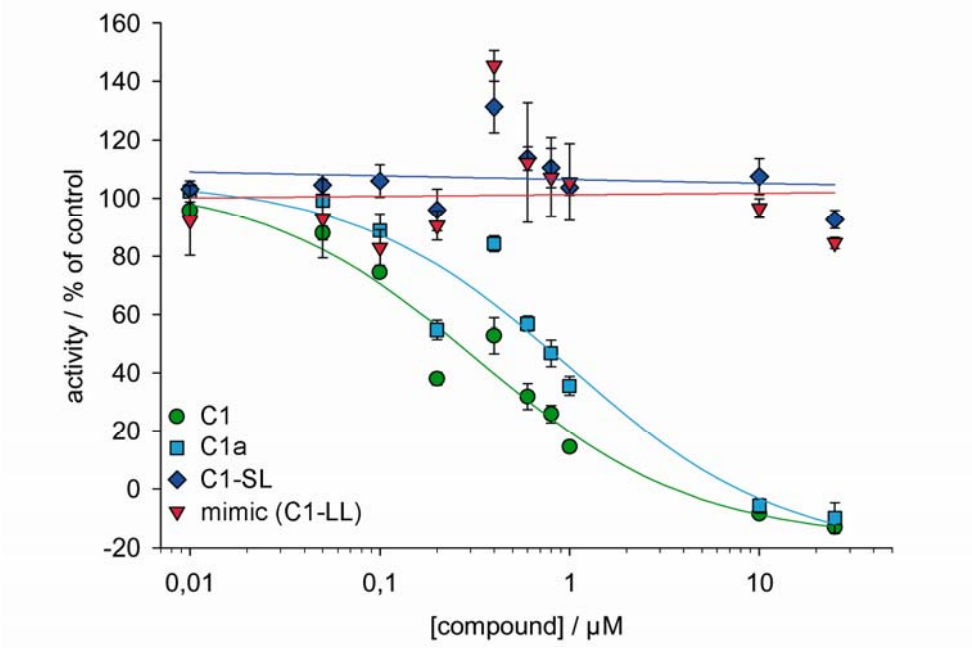

Figure 35. Inhibitory potential of C1, C1-SL, mimic (C1-LL), and C1a on human CA2 activity was determined (IC_{50}). Medium affinity binding was found for C1 (IC_{50} = 331 nM) and C1a (IC_{50} = 995 nM), whereas C1-SL and the mimic had no inhibitory potential. The enzyme activity is expressed as percentage of vehicle control (2 % Me_2SO without test compounds), representing maximal activity.

5. Discussion

5.1. Chemical Proteomics was successfully applied for the capturing of cellular targets

Hits and research compounds found by high-throughput target-centric screens might have additional unknown off-target interactions since counter-screening at this stage is conducted against only a limited number of recombinant proteins available. Thus, additional methods for the identification of cellular targets of research compounds which selectively modulate enzyme activities, can broaden the knowledge of the respective binding profiles and thereby improve the chemical optimization process.

The aim of this work was to profile the research compound and multitarget CDK inhibitor C1 in an unbiased fashion by applying a Chemical Proteomics approach. First, a computational model of a C1/ CDK2 complex was employed for the identification of appropriate sites for different compound immobilization routes (Figure 14 B). Two promising coupling routes for a successful capturing of cellular targets were derived (Figure 15): Due to its solvent accessibility, the sulfonamide group of C1 was found to be suitable for immobilization route one, aimed at capturing protein kinases as well as additional proteins interacting via their ATP or purine binding site. In contrast, immobilization route two via the 4-position of the aminopyrimidine moiety was supposed to hamper the capturing of protein kinases almost entirely. Instead, the second coupling strategy could allow the affinity enrichment of proteins interacting via the benzenesulfonamide moiety of C1.

Indeed, the linkage of C1 at the sulfonamide group did not interfere with the target binding as demonstrated by CDK2 activity assays employing C1 and two analogs provided with a short (C1-SL) and a long linker (C1-LL, mimic) at the sulfonamide mimicking the C1-matrix (Table 4). All analogs showed a CDK2 inhibition in the single digit nanomolar range (IC_{50}). Thus, C1-SL was coupled to epoxy-activated Sepharose^{TM} beads giving C1-matrix. Afterwards, a proof-of-concept experiment was performed, resulting in the successful capturing of CDK2 from HeLa cell extracts as demonstrated by immunodetection (Figure 18, lane 1-3).

In order to identify suitable elution conditions, a sequential elution was performed using 10 mM ATP, a saturated C1-SL solution in an aqueous buffer, and finally the denaturation by LDS-sample buffer and heat. C1-SL was preferred to C1 due to better (but still low) solubility. The elution using 10 mM ATP was used for releasing proteins captured via the

ATP binding site. By using free compound, captured proteins could be specifically eluted, independent from their binding site. In contrast, denaturing conditions would allow a comprehensive but non-specific elution of the bound proteins. Unfortunately, it became apparent, that neither 10 mM ATP in the first elution step, nor free compound in the second elution step were able to quantitatively elute CDK2 from the compound matrix (Figure 18, lane 1-3). Due to the high binding affinity of the immobilized compound (which was supposed to be similar to C1-LL affinity: 3 nM, IC_{50}) and the high local compound density on the beads surface (in the low millimolar range, chapter 4.5.1.), 10 mM ATP was not able to completely release the captured CDK2 from the matrix. The low solubility of free C1-SL in the aqueous buffer (approximately 150 µM at pH 7) prevented CDK2 from being completely and specifically eluted. Similar results were obtained for other protein kinases, as demonstrated by a sequential elution, shown in Figure 22, lanes 1-3. Several of the Coomassie stained protein bands representing different protein kinases appear in the ATP-lane, in the compound lane, and finally in the LDS-SB lane. Thus, the use of C1-SL for elution would result in the specific but incomplete elution of only a subset of captured proteins. In fact, the aim was to obtain a comprehensive binding profile for C1-matrix including all captured protein kinases for further testing them in a biochemical screen. For this reason, denaturing conditions were used in the following experiments for a complete but non-specific elution of the captured proteins. Subsequently, a control matrix, and a biological replicate for the identification of overlaps between two independent experiments were applied to remove non-specific binders from the final protein list.

5.2. The discrimination of specific binders from non-specific interactions is challenging

Having demonstrated the suitability of C1-matrix for the capturing of the cellular target CDK2, LC-MS/MS analysis of the eluted proteins was applied to rapidly and reliably obtain a protein binding profile for the C1-matrix. For this purpose, HeLa cell extracts were incubated with the compound matrix. After a stringent washing procedure, eluted proteins were separated by 1D-SDS-PAGE and Coomassie-stained (Figure 19). By the great number of visible protein bands, it became apparent, that a major challenge was to discriminate the specifically captured proteins, whose binding mediate the biological activities of the compound, from high abundant protein background, non-specifically retained by the compound matrix. A single LC-MS/MS-analysis of the entire separation range resulted in the identification of more than three hundred proteins, illustrating the very high sensitivity of

mass spectrometry. Due to this sensitivity, an immense number of irrelevant proteins and contaminants present at even very low levels in the sample can be identified, explaining the great number of identified hits. Additionally, very weakly but high abundant binding partners such as heat shock proteins (HSPs), kinesins or other ATP-binding enzymes and carrier proteins can hardly be completely removed without losing relevant binders and will therefore be identified by MS. The situation is even more complex since some proteins were co-enriched via their association with captured protein complexes. For instance, several cyclins which are known to tightly bind to CDKs, were captured despite high-salt incubating and washing conditions. In addition, a number of proteins non-specifically associating with captured proteins are very likely to occur. In order to overcome the difficulties in discriminating these non-specific interactions from the primary compound targets, considerable efforts were made in order to optimized the washing procedures. Although several washing conditions were tested, including different amounts of organic solvent (DMSO) or detergent (SDS) in the washing buffers, different temperatures, and several high salt conditions (data not shown), no improvements were found, compared to the conditions described in the literature. However, a major progress was achieved by performing two biological replicates of the Chemical Proteomics approaches. Only proteins, which were identified in both experiments, were added to a final list. MS/MS spectra of proteins with a low Mascot ion score were manually inspected and compared to the lists of identified proteins in similar experiments. Additionally, a control matrix was generated by blocking the functional groups of the epoxy-activated Sepharose^{TM} beads. The resulting inactivated resin was used for negative affinity purification as described by others (Godl, K. et al. 2003). After removing the non-specific and biologically irrelevant protein binders identified by using the control matrix, a final list of approximately 90 proteins was obtained. Besides several proteins assumed to be specific binders (e.g. protein kinases and oxidoreductases), the list still contained more than 30 proteins, the majority of which are presumably non-specific binders since isoforms or other subunits of the same proteins, or other members of the same protein families were found in control experiments, as well.

It was assumed, that a significant number of these non-specific binders was not retained by the beads or the linker, but by non-specifical interactions with the compound itself or with other captured proteins due to hydrophobic effects. First, a significantly lower total number of visible Coomassie bands was found in the control experiment compared to the compound matrix approach (Figure 19). Additionally, the intensities of the bands common in both approaches (control vs. compound matrix), representing high abundant protein background

were much lower in the control approach. Finally, the majority of proteins retained by the compound matrix differed in the two biological replicates of the approach, indicating a random and non-specific binding. It was concluded, that the hydrophobic character of the compound provides additional options for the non-specific binding of high abundant proteins, such as tubulins, actins, etc. which in turn trigger further non-specific association of abundant proteins (snowball effect). Stringent washing helps to reduce these associations but was found not to remove the irrelevant interactions entirely. Thus, the benefit of a blocked resin used as a control matrix is limited. Instead, whenever available, a structural similar but biological inactive compound analog appears to be more favourable compared to a blocked Sepharose™ matrix in order to generate a control matrix. Unfortunately, no inactive compound analog was available for this study due to limited capacities within the synthesis laboratories and time restrictions for this work.

Another possible option to improve the discrimination of specific binders from non-specific interactions might be the inclusion of a cleavable linker between the compound and the resin. Photocleavable linkers are described for the use with activity-based probes (activity-based probe profiling, ABPP) which covalently bind their target proteins (Jeffery, Douglas A. et al. 2003). Here, the cleavage of the linker is essential for the release of the bound proteins. Interestingly, new applications of cleavable linkers for further technology platforms such as reverse chemical proteomics are discussed in the literature (Karuso, P. et al. 2008). However, the findings in this work indicate that a significant portion of the identified proteins seem to non-specifically interact with the compound itself or other specifically and non-specifically captured proteins via hydrophobic interactions but not with the linker or the beads. Thus, the inclusion of a cleavable linker between the compound and the resin would presumably not significantly reduce the amount of non-specific binders in the final elution fraction.

However, several other approaches were suggested, to address this challenge, such as SILAC (Stable isotope labeling with amino acids in cell culture) and other differential isotopic labeling strategies (Ong, S. E. et al. 2002; Oda, Y. et al. 1999). These quantitative proteomic techniques allow the comparison of the amounts of labeled proteins present in two different samples. For this purpose, a protein extract is split into two samples and one sample, which is designated as the reference, is provided with a light isotope label, mixed with the compound matrix and the captured proteins are eluted. A heavy isotope label is added to the other sample before this sample is incubated with a suitable control matrix. After the elution of the binding proteins, both eluted factions are mixed and analyzed by MS. The ratio between the two isotopic labels are given in the mass spectra and can be employed to calculate the relative

protein quantities. A comparative quantitation between compound matrix binders and control matrix binders is then used for the discrimination of specifically captured targets from non-specifically associated proteins (Ishihama, Y. et al. 2005). However, the availability of one (or even more) structural very similar but biological inactive compound analog(s) for the control matrix is mandatory to ensure a stoichiometrically similar distribution of non-specific binders for both, compound and control matrix. This emphasizes the general need for co-ordinated efforts of multiple disciplines, such as medicinal chemistry, biology laboratories, protein analytics, etc. in order to facilitate a comprehensive Chemical Proteomics approach.

Since no inactive compound analog was available for immobilization for this work, a major focus of the thesis was the confirmation of potential targets/ off-targets initially identified by the inhibitor affinity chromatography experiments by conducting several additional methods such as sequential elution schemes, a serial inhibitor affinity chromatography approach, a competition assay, the use of different affinity matrices, biochemical activity assays, and isothermal titration calorimetry (ITC).

5.3. Protein kinase selectivity patterns of compound C1 confirmed its high potency but revealed a limited selectivity of the compound

The high inhibitory potency of compound C1 was known from CDK2 activity assays (IC_{50} determination) described above. Surprisingly, the inhibitor affinity chromatography approach using C1-matrix resulted in the identification of more than 30 additional protein kinases bound to the matrix. Since no protein kinase was captured by the control matrix, the enrichment of these kinases by the compound matrix was assumed to result either from a specific enzyme/ compound interaction or from a co-capturing via the enrichment of protein complexes. In order to analyze the inhibitory potential of the compound toward the kinases retained by the matrix, C1 was tested at a concentration of 1 µM in a panel of 27 recombinant protein kinases (performed by Upstate/ Millipore), which were previously identified in the Chemical Proteomics approach. As expected, CDK2 and three other CDKs (CDK1, 5, and 9) were among the most affected kinases (> 95 % inhibition, Figure 20). CDKs are closely related by sharing a high level of amino acid sequence identity (40 - 70 %) (Chin, K. T. et al. 1999; Morgan, D. O. 1995). Thus, selectivity within the class of CDKs was not expected. In contrast, by inhibiting relating or redundant signaling pathways, the inhibitory potential against multiple CDKs might increase the antitumor and antiproliferative efficacy of the compound and may lead to beneficial synergies. However, eleven further kinases showed a strong inhibition (> 80 %), as well. Although not exclusively, several of these highly affected

kinases belong to or act via the MAP kinase pathway (STK3, MAPK8 MAPK9, STK4, AURKA, PRKD2). Since MAPKs recognize and phosphorylate nuclear proteins, such as transcription factors, co-activators and repressors and chromatin-remodeling molecules (Turjanski, A. G. et al. 2007), their inhibition might have an important impact on the antiprolefirative activity of the compound. However, the eleven highly inhibited kinases originate from diverse kinase families according to the kinase classification introduced by (Manning, G. et al. 2002b). This implicates a low amino acid sequence identity of the catalytic domains of the respective kinases indicating a poor selectivity of the compound C1. Thus, expanding the panel of tested kinases to all human protein kinases available would most likely reveal an increasing number of highly inhibited protein kinases. As a consequence, the biological activity of the compound might result from a multitude of inhibitory effects. In contrast, the biological relevance of the moderate inhibition (50-80 %, 1 µM compound) of five additional kinases (CAMK2G, CHUK, FER, MAPK1, YES) and the low inhibition (< 50 %) of six further kinases (CDC42BPB, MAP2K1, PAK4, PKN2, PRKD3, RIPK2), respectively, is supposed to be small. Moreover, these results indicate, that a capturing in the Chemical Proteomics experiments in the setup used for this study is not necessarily correlated with a high binding affinity but depends on both, affinity and expression level of a protein. For instance, the high local compound density on the bead surface might facilitate an enrichment of moderate binders. Additionally, the protein extract used in this study might not accurately reflect the *in-vivo* situation of intact cells with regard to the physico-chemical behavior of the proteins. Furthermore, it has to be taken into consideration that some of the protein kinases initially identified in the pull-down approach using C1-matrix, do not bind to the inhibitor directly, but instead might be co-captured via their association to a protein complex. Despite the presence of detergent (0.5 % NP-40) during the cell disruption and high salt consitions (1 M NaCl) during the washing procedures (both specified in the Materials and Methods section), some protein complexes might be able to keep their association intact due to tight interactions. Indeed, the identification of several cyclins which are known to tightly interact with several of the identified CDKs, suggests that there are additional associated proteins. In particular, these protein kinases showing only a low inhibition by C1 (CDC42BPB, MAP2K1, PAK4, PKN2, PRKD3, RIPK2) may bind indirectly to the C1-matrix via other target proteins. These findings demonstrate, that there is an essential need for the (de-)validation of the affinity of a compound to any protein captured by inhibitor pull-downs. Moreover, certain linker effects due to the compound immobilization might occur. By providing additional interaction options, a linker might increase the number of captured

proteins compared to the unlinked compound. To address this hypothesis, the mimic (C1-LL), provided with a linker which is structural similar to the linking structure of the Sepharose™ matrix, was screened on the same panel of kinases which was used for the selectivity studies of C1.

5.4. Application of the mimic revealed individual effects of the linker

Testing the mimic on the same panel of 27 kinases revealed differences in the selectivity pattern compared to C1 (Figure 20). Interestingly, the mimic had less inhibitory potency against most of the tested kinases. It was concluded that steric effects of the linker cause a decrease of the inhibitory potential compared to C1. However, a few examples did occur in which the mimic had more inhibitory activity against a kinase compared to C1 (CAMK2G, PAK4, PKN2, PRKD2). In these examples, functional groups of the linker (e.g. the hydroxyl group) might form additional hydrogen bonds and thereby increase the binding affinity. It was concluded, that the effects of the linker depend on the individual structure of the respective binding pocket of a specific target. A mimic is useful to analyze these linker effects on a given target, improving the data interpretation of Chemical Proteomics experiments, but it does not allow a general prediction of linker effects on target binding. However, not only the linker but as well the immobilization itself might affect the binding profile of the test compound. For instance, the coupling chemistry might change the potency of the inhibitor. Additionally, a high local compound concentration on the bead surface might cause an enhanced capturing of moderate binders present in high abundance or cause steric effects that are difficult to predict. Whereas the coupling chemistry is well reflected by the design of the soluble mimic used within this study, the question how the density of the inhibitor on the bead surface influences the binding pattern is barely addressed by testing the soluble mimic and therefore difficult to quantify. Nevertheless, the presented findings on additional linker effects influencing the selectivity pattern of a compound are consistent with those recently reported by Saxena et. al. (Saxena, C. et al. 2008). By employing different kinds of linkers for compound coupling in terms of drug target deconvolution, they found significantly different patterns of captured proteins. Both, their and the results reported herein demonstrate the need for a suitable assay to define the specificity of the interaction of a protein with the ligand under investigation.

Although the reseach compound C1 was shown to potently inhibit its desired on-targets, the CDKs, the results clearly demonstrate the need for further optimization with regard to its protein kinase selectivity profile.

In the following, the characterization of non-protein kinase/ compound interactions identified by inhibitor affinity chromatography, an additional focus of this thesis, is discussed.

5.5. Human pyridoxal kinase was identified as an potential off-target of the C1-matrix

LC-MS/MS analysis of the proteins non-specifically eluted from C1-matrix revealed the human pyridoxal kinase (PDXK) as a potential off-target of the compound C1. PDXK is a non-protein kinase belonging to the salvage pathway. It is responsible for the phosphorylation of pyridoxal (PL), pyridoxine (PN), and pyridoxamine (PM) to the respective 5'-phosphate esters PLP, PNP, and PMP, classified collectively as active forms of vitamin B6. Subsequent to this phosphorylation taking place in the liver, the pyridoxine/ pyridoxamine 5'-phosphate oxidase converts PNP and PMP to PLP (Figure 36).

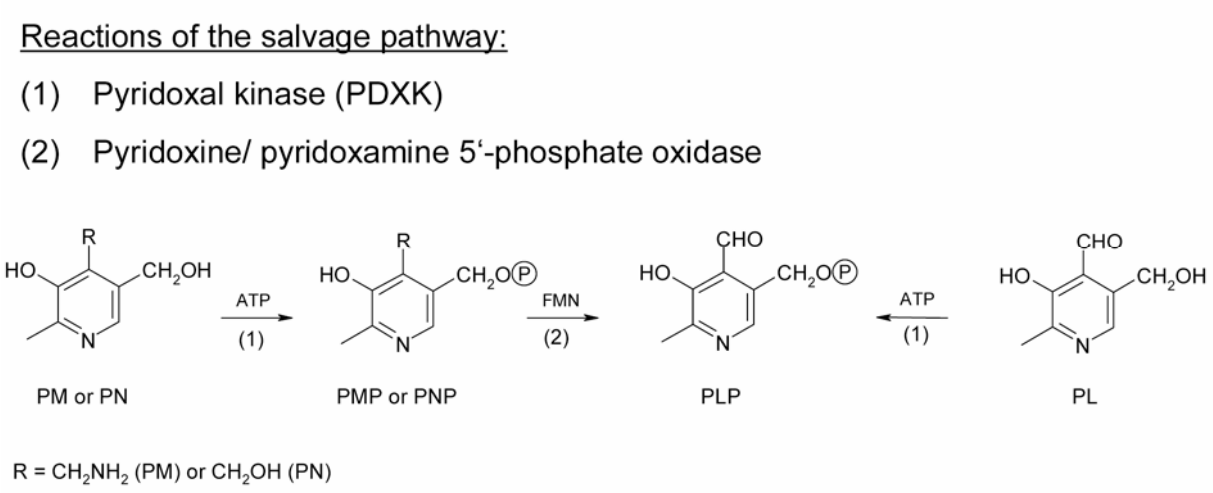

Figure 36. Interconversion of B6-vitamers. The salvage pathway includes the ATP-dependent pyridoxal kinase (PDXK) which is responsible for the phosphorylation of pyridoxal (PL), pyridoxine (PN), and pyridoxamine (PM) to the respective 5'-phosphate esters PLP, PNP, and PMP, classified collectively as active forms of vitamin B6. The pyridoxine/ pyridoxamine 5'-phosphate oxidase converts PNP and PMP to PLP. PLP is an essential cofactor for > 100 enzymes in amino acid, sugar and neurotransmitter metabolisms.

Afterwards, PLP is released to the bloodstream in association with albumin (Brin, M. 1976; Lumeng, L. et al. 1980; Merrill, A. H., Jr. et al. 1984). In order to enter the target cells, circulating PLP becomes dephosphorylated by membrane-associated phosphatases. After crossing the membrane by diffusion, intracellular PDXK converts PL back to the active form PLP. In consequence, PDXK is ubiquitously expressed in mammalian tissues (Hanna, M. C. et al. 1997). PLP is an essential cofactor for > 100 enzymes such as aminotransferases and decarboxylases of which many are involved in amino acid and neurotransmitter metabolisms

(Eliot, A. C. et al. 2004; Kerry, J. A. et al. 1986; Percudani, R. et al. 2003). Low levels of PLP caused by a downregulation of brain PDXK expression or by PL competitors are correlated with epilepsy in animal models (Gachon, F. et al. 2004; Wada, K. et al. 1985). Additionally, a direct inhibition of PDXK activity by different drugs was shown to cause a vitamin B6 deficiency and several side effects related to the central nervous system (Hanna, M. C. et al. 1997; Laine-Cessac, P. et al. 1997).

Interestingly, PDXK is described in the literature as being targeted by the ATP-competitive CDK2 inhibitor *(R)*-roscovitine, as well (Bach, S. et al. 2005). Surprisingly, the binding was shown to occur at the substrate binding site rather than at the ATP binding site, as demonstrated by co-crystallisation experiments (Tang, L. et al. 2005). A contribution of PDXK binding to the biological activity of *(R)*-roscovitine was discussed but found to be unlikely. However, several bioisosteres of roscovitine were generated, showing reduced PDXK binding affinity (Bettayeb, K. et al. 2008; Popowycz, F. et al. 2009).

Motivated by these findings, the PDXK/ C1 interaction was investigate in more detail for this study. As introduced by others (Yamamoto, K. et al. 2006), a serial affinity chromatography was carried out in order to show a specific capturing of PDXK from HeLa cell extracts by C1-matrix. Specific binders are essentially captured by the first affinity matrix whereas the amounts of non-specifically bound proteins are similar for both matrices. Since PDXK was mainly retained by the first matrix, as demonstrated by immunodetection of PDXK, a specific binding of PDXK to the compound matrix was concluded (Figure 21, lane 1 & 2).

In order to identify the targeted binding site of PDXK, a sequential elution was applied on the C1-matrix. To this end, the compound matrix was incubated with HeLa extracts and then sequentially eluted using an ATP buffer, a free C1-SL buffer and finally LDS-sample buffer/ heat to distinguish capturing via the ATP binding site from enrichment via alternative sites. Since PDXK was only identified in the compound and LDS-SB elution fractions but not in the ATP fraction (Figure 22, lanes 1-3), an alternative binding site rather than the ATP binding site was assumed. By replacing the compound C1-SL by *(R)*-roscovitine for a sequential elution in a subsequent experiment, the question was addressed whether both compounds target a similar binding site of PDXK. Whereas ATP again was not able to elute PDXK from the C1-matrix, *(R)*-roscovitine caused a release of PDXK (Figure 22, lanes 4-6). It was concluded, that *(R)*-roscovitine competes with immobilized C1 by targeting a similar binding site. Since *(R)*-roscovitine is known to bind PDXK via its pyridoxal binding site, a similar binding mode was assumed for compound C1.

In order to confirm this assumption, a substrate competition experiment was carried out. Due to better solubility at pH 7 compared to pyridoxal, the alternative PDXK substrate pyridoxine was employed for this approach. Indeed, PDXK enrichment by C1-matrix was nearly entirely prevented by 10 mM free pyridoxine spiked into the cell extract as shown by immunodetection of PDXK (Figure 23, lane 5). In addition, a pyridoxal affinity matrix was generated by immobilizing the PDXK substrate pyridoxal on a suitable resin (Figure 10). Subsequently, a sequential elution scheme using ATP, pyridoxine, free C1-SL, and finally LDS-SB/ heat was applied on C1-matrix, pyridoxal matrix, and control matrix in parallel (Figure 24). Since PDXK was eluted from both affinity matrices by pyridoxine and free C1-SL (and LDS-sample buffer, Figure 24, lanes 3 & 4), but not by ATP (lane 2), as shown by immunodetection, it was concluded that the PDXK/ C1 interaction occurs at the substrate binding site rather than at the ATP site.

5.6. Recombinantly expressed pyridoxal kinase was used for the biochemical characterization of the PDXK/ compound interaction

Prompted by the unexpected binding mode and the considerable enrichment of PDXK from cell extracts using C1-matrix, suggesting a high affinity PDXK/ compound interaction, an appropriate scheme for the expression and purification of PDXK was developed in order to perform quantitative, biochemical binding studies. First, PDXK was recombinantly expressed without a purification tag in *E.coli* and subjected to affinity chromatography using the pyridoxal matrix for the first purification step (Figure 25). Subsequently, an analytical size exclusion chromatography was performed to determine whether the native state of the recombinant PDXK was a monomer or a higher oligomer and to sense the presence of protein aggregates. As a result, the homogeneity of the PDXK sample was demonstrated and no protein aggregates were found. By employing a calibration curve derived from plotting marker proteins against the respective retention times, the molecular weight of the PDX was determined and a monomeric form was calculated (Figure 26) and confirmed by SDS-PAGE (Figure 28). Although PDXK is described to act as a homodimer (Musayev, F. N. et al. 2007), Kwok et al. showed that its catalytic activity is retained upon dissociation into monomers (Kwok, F. et al. 1987). Accordingly, they, as well as other groups (di Salvo, M. L. et al. 2004), employed the monomeric form for biochemical binding studies. In agreement with this, the PDXK monomer generated within this work was kept for subsequent experiments. After having removed all impurities by a preparative size exclusion chromatography (Figure 27), as shown by SDS-PAGE (Figure 28), the identity of the protein was confirmed by MS

and MS/MS analyses (Figure 29). Since the correct mass of the protein and the correct amino acid sequence of several of its tryptic peptides was found, the purified enzyme was employed for the biochemical characterization of the PDXK/ compound interaction.

For this purpose a suitable PDXK activity assay was adapted from the literaure (Kastner, U. et al. 2007). To confirm that the purified PDXK was suitable for quantitative binding studies as well as to show that the assay worked in the range which is described in the literature, the Michaelis constant K_m for pyridoxal was determined and compared to the reported results. Interestingly, as shown in Table 7, the values reported by different groups cover a wide range for the K_m value (3 – 350 µM). Potential reasons for these variations might be the utilization of different expression systems, purification tags, or cations used in the activity assay buffer. By influencing the physico-chemical behavior of the protein, these parameter might have an impact on the enzyme activity and the K_m value. Nevertheless, the recombinant PDXK generated within this study, displayed a K_m value for pyridoxal (99 µM, Figure 31) which is similar to the results reported by Kaestner et al. (59 µM) (Kastner, U. et al. 2007), who used the same expression vector (which was kindly provided by the group for this work) as well as the same parameter regarding the purification tag, the expression host, and the cation used in the activity studies. Thus, the assay was used for subsequent IC_{50}-determination experiments.

Table 7. Kinetic data of PDXK and its substrate pyridoxal.

literature	K_m PL (µM)	organism	purification tag	expression host	cation
This work.	99	[homo sapiens]	w/o	*E.coli*	Zn^{2+}
Kaestner et al., 2007[b]	59	[homo sapiens]	w/o	*E.coli*	Zn^{2+}
Lee et al., 2000[c]	97	[homo sapiens]	MBP[a]	*E.coli*	Zn^{2+}
di Salvo et al., 2004[d]	350 (Zn^{2+}) 30 (Mg^{2+})	[homo sapiens]	w/o	*E.coli*	Zn^{2+}/ Mg^{2+}
Musayev et al., 2007[e]	< 10	[homo sapiens]	w/o	*E.coli*	Mg^{2+}
Hanna et al., 1997[f]	3	[homo sapiens]	w/o	HEK293, transient	Zn^{2+}

[a] maltose binding protein, [b] (Kastner, U. et al. 2007), [c] (Lee, H. S. et al. 2000), [d] (di Salvo, M. L. et al. 2004), [e] (Musayev, F. N. et al. 2007), [f] (Hanna, M. C. et al. 1997)

The activity of the PDXK was assayed in the presence of different concentrations of C1, C1-SL, mimic, and *(R)*-roscovitine, respectively. Confirming previously reported findings (Bach, S. et al. 2005), even at the highest concentration tested (50 µM), a very modest inhibition of PDXK was found for *(R)*-roscovitine (Figure 32). The same was true for the compound C1, but an increasing linker length correlated with a more efficient decrease of PDXK activity. It was assumed that additional interaction options provided by the linker contribute to the binding of the compound to the pyridoxal site, e.g. by hydrogen bonds or hydrophobic interactions. Nevertheless, the low affinity binding of C1 and its analogs to PDXK was surprising. However, as it is suggested for the PDXK/ *(R)*-roscovitine interaction (Bach, S. et al. 2005; Tang, L. et al. 2005), the high ATP concentration in the PDXK activity assay (2.5 mM) might have an impact on the activities measured by either reducing the affinity of PDXK for C1 or enhancing the affinity of PDXK for its substrate pyridoxal. To determine the dissociation constant K_D of the compound to PDXK in the absence of ATP and of pyridoxal, isothermal titration calorimetry (ITC) experiments were performed, using C1-SL. A weak exothermal reaction was measured, but low binding heats prevented the exact K_D determination. However, the data suggested a K_D value > 10 µM, paralleling the results from the PDXK activity assays (Figure 33). It was concluded, that the significant enrichment of PDXK during Chemical Proteomics experiments was not caused by a high binding affinity but instead by a combination of several other reason: a high expression level of the ubiquitous PDXK, additional effects of the linking structure of the Sepharose^{TM} matrix contributing to the compound binding to the pyridoxal site and a high local compound concentration on the bead surface were assumed as potential reasons for the capturing of PDXK. Altogether, it seems unlikely that effects caused by PDXK/ C1 interaction will play a role in pharmacological applications.

5.7. Application of an alternative immobilization route revealed binding of carbonic anhydrase 2 to C1a-matrix

Immobilization of C1 at the sulfonamide group is suitable to identify targets interacting with the aminopyrimidine moiety (e.g. protein kinases). However, due to steric hindrance, interactions occurring at the benzenesulfonamide moiety of C1 are blocked when using the C1-matrix. In fact, benzenesulfonamide moieties are described to have a high inhibitory potential toward most of the known carbonic anhydrase isozymes (Supuran, C. T. et al. 2007). In particular the cytosolic isoform carbonic anhydrase 2 (CA2) has a high binding affinity toward sulfonamides (Puccetti, L. et al. 2005). To profile the C1 interactome more

comprehensively, particularly with regard to CA2 binding, the analog C1a was coupled to a solid support via the side chain at the 4-position giving C1a-matrix (Figure 16). Not being blocked by a linker at the benzenesulfonamide moiety, the C1a-matrix was used for the identification of additional off-targets of the studied compound. Indeed, enrichment of CA2 from H460 cell extracts by C1a-matrix was found by LC-MS/MS-analysis of the proteins non-specifically as well as specifically eluted using LDS-SB and free C1a, respectively, (Figure 34 B) and validated by immunoblotting (Figure 34 C).

For IC_{50}-determinations of C1, C1-SL, mimic, and C1a, commercially available human CA2 was assayed. IC_{50} values of C1 and C1a were in the submicromolar range (IC_{50} (CA2) = 331 nM (C1), 995 nM (C1a)), whereas C1-SL and the mimic had no inhibitory potential (Figure 35), most likely due to steric hindrance caused by the linkers. The ubiquitous CA2 is involved in crucial physiological processes connected with respiration and transport of CO_2/ bicarbonate, electrolyte secretion, bone resorption, calcification etc. (Puccetti, L. et al. 2005; Thiry, A. et al. 2008). Thus, binding of C1 to CA2 at submicromolar concentrations might cause unwanted biological effects of the compound or at least trap the compound and reduce the amount of free inhibitor which is available for on-target interaction. However, the findings presented herein show that the CA2/ C1 interaction specifically occurs at the benzenesulfonamide moiety and that CA2 binding by the compound can easily be prevented by a small modification at the sulfonamide group. This structure-activity relationship information may help to improve the selectivity profile of the research compound in the context of ongoing optimization processes.

5.8. The protein binding profile of C1a-matrix contained some protein kinases and revealed one further potential off-targets

Compared to the C1-matrix, a significantly lower amount of total protein was retained by the C1a-matrix, as demonstrated by a Coomassie-stained SDS-PAGE and a LC-MS/MS analysis applied on proteins non-specifically eluted from C1a-matrix by LDS-SB/ heat (Figure 34 B, lane 2). Whereas approximately 150 proteins were found by using the C1-matrix, only 37 proteins fulfilling acceptance criteria were identified with the C1a-matrix. Two major reasons were assumed for the lower total number of proteins retained by the C1a-matrix compared to the C1-matrix. First, due to steric effects, the ATP-pocket of protein kinases and other purine binding proteins is much less accessible by the C1a-matrix. Thus, fewer specific interactions are supposed to occur. Secondly, due to a lower number of direct interacting proteins, much

less indirect capturing of proteins via association to other target proteins and protein complexes or via unspecific hydrophobic interaction may occur.

Surprisingly, some protein kinases (AURKA, CDK1, MAPK9) were identified by employing C1a-matrix which were also captured by using the C1-matrix. This indicates, that binding into the ATP binding pocket is not completely hampered by using C1a matrix. It was assumed, that the entrance to the ATP binding site is less size restricted within this group of kinases compared to the kinases found only with the C1-matrix. Since the linker arm of the matrix is flexible and can fold into the direction of the sulfonamide group, the immobilized compound might still be able to bind to the hinge region of the respective kinases. A very high inhibitory potency was found for C1 in the biochemical selectivity screen for these kinases (> 90 for MAPK9 and even > 95 % for CDK1 and AURKA, Figure 3), therefore the possibility that some of these kinases are co-captured by binding to protein complexes appears very unlikely. However, since the C1a-matrix was not optimized for the capturing of protein kinases, these findings were not investigated in more detail.

Among others, carbonic anhydrase 2 and the carboxymethylenebutenolidase homolog (CMBL) were exclusively identified by using the C1a-matrix. Since CMBL was not found by using the C1-matrix, it was concluded that it binds to the sulfonamide moiety of the compound. Whereas carbonic anhydrases are well described in the literature, only little information is available regarding CMBL, indicating a major limitation of Proteomics approaches.

5.9. Limitations and chances of Chemical Proteomics

The lack of comprehensive information available regarding the function of CMBL in eukaryotic cells demonstrates one of the most significant limitations of the inhibitor affinity chromatography approach which is common to all Proteomics approaches. Since the knowledge of the function and the biochemical activities of individuals proteins is often very limited, the consequence of an identified compound/ protein interaction remains unclear in many cases. Thus, a considerable effort is necessary to follow up the initially observed interactions with additional investigations regarding the effects on intracellular signaling pathways by employing recombinant proteins and/ or appropriate functional readouts in phenotypic cell assays. However, by advancing the functional mapping of the human proteins, a deeper understanding of the data generated by Chemical Proteomics will become accessible.

In recent years, impressive progress in LC-MS-based quantitative Proteomics has been achieved (Kruse, U. et al. 2008). By combining these quantitative mass spectrometry

methods with the affinity capturing methods in Chemical Proteomics approaches, not only the protein binding profile of a compound can be assessed, but also quantitative binding data for numerous of the captured proteins can be determined in parallel.

By taking into account these advances, Chemical Proteomics in combination with different compound immobilization routes as described within this work may become a valuable tool for future off-target and target identification strategies.

6. References

Bach, S., Knockaert, M., Reinhardt, J., Lozach, O., Schmitt, S., Baratte, B., Koken, M., Coburn, S. P., Tang, L., Jiang, T., Liang, D. C., Galons, H., Dierick, J. F., Pinna, L. A., Meggio, F., Totzke, F., Schachtele, C., Lerman, A. S., Carnero, A., Wan, Y., Gray, N., and Meijer, L. 2005. Roscovitine Targets, Protein Kinases and Pyridoxal Kinase. *Journal of Biological Chemistry.* **280:** 31208-31219

Bantscheff, M., Eberhard, D., Abraham, Y., Bastuck, S., Boesche, M., Hobson, S., Mathieson, T., Perrin, J., Raida, M., Rau, C., Reader, V., Sweetman, G., Bauer, A., Bouwmeester, T., Hopf, C., Kruse, U., Neubauer, G., Ramsden, N., Rick, J., Kuster, B., and Drewes G. 2007. Quantitative chemical proteomics reveals mechanisms of action of clinical ABL kinase inhibitors. *Nat Biotech.* **25:** 1035-1044

Baselga, J. 2006. Targeting tyrosine kinases in cancer: the second wave. *Science.* **312:** 1175-1178

Benson, J. D., Chen, Y. N., Cornell-Kennon, S. A., Dorsch, M., Kim, S., Leszczyniecka, M., Sellers, W. R., and Lengauer, C. 2006. Validating cancer drug targets. *Nature.* **441:** 451-456

Bettayeb, K., Sallam, H., Ferandin, Y., Popowycz, F., Fournet, G., Hassan, M., Echalier, A., Bernard, P., Endicott, J., Joseph, B., and Meijer, L. 2008. N-&-N, a new class of cell death-inducing kinase inhibitors derived from the purine roscovitine. *Molecular Cancer Therapeutics.* **7:** 2713-2724

Bluggel, M., Bailey, S., Korting, G., Stephan, C., Reidegeld, K. A., Thiele, H., Apweiler, R., Hamacher, M., and Meyer, H. E. 2004. Towards data management of the HUPO Human Brain Proteome Project pilot phase. *Proteomics.* **4:** 2361-2362

Boehm, J. S., Zhao, J. J., Yao, J., Kim, S. Y., Firestein, R., Dunn, I. F., Sjostrom, S. K., Garraway, L. A., Weremowicz, S., Richardson, A. L., Greulich, H., Stewart, C. J., Mulvey, L. A., Shen, R. R., Ambrogio, L., Hirozane-Kishikawa, T., Hill, D. E., Vidal, M., Meyerson, M., Grenier, J. K., Hinkle, G., Root, D. E., Roberts, T. M., Lander, E. S., Polyak, K., and Hahn, W. C. 2007. Integrative genomic approaches identify IKBKE as a breast cancer oncogene. *Cell.* **129:** 1065-1079

Booher, R. N., Holman, P. S., and Fattaey, A. 1997. Human Myt1 is a cell cycle-regulated kinase that inhibits Cdc2 but not Cdk2 activity. *J Biol Chem.* **272:** 22300-22306

Boozer, C., Kim, G., Cong, S., Guan, H., and Londergan, T. 2006. Looking towards label-free biomolecular interaction analysis in a high-throughput format: a review of new surface plasmon resonance technologies. *Curr.Opin.Biotechnol.* **17:** 400-405

Bradford, M. M. 1976. A rapid and sensitive method for the quantitation of microgram quantities of protein utilizing the principle of protein-dye binding. *Anal.Biochem.* **72:** 248-254

Brehmer, D., Godl, K., Zech, B., Wissing, J., and Daub, H. 2004. Proteome-wide Identification of Cellular Targets Affected by Bisindolylmaleimide-type Protein Kinase C Inhibitors. *Molecular Cellular Proteomics.* **3:** 490-500

Brehmer, D., Greff, Z., Godl, K., Blencke, S., Kurtenbach, A., Weber, M., Muller, S., Klebl, B., Cotten, M., Keri, G., Wissing, J., and Daub, H. 2005. Cellular Targets of Gefitinib. *Cancer Research.* **65:** 379-382

Brin, M. 1976. Human Vitamin B6 Requirements. *National Academyof Sciences, Washington, D.C.* 1-20

Buckbinder, L., Crawford, D. T., Qi, H., Ke, H. Z., Olson, L. M., Long, K. R., Bonnette, P. C., Baumann, A. P., Hambor, J. E., Grasser, W. A., III, Pan, L. C., Owen, T. A., Luzzio, M. J., Hulford, C. A., Gebhard, D. F., Paralkar, V. M., Simmons, H. A., Kath, J. C., Roberts, W. G., Smock, S. L., Guzman-Perez, A., Brown, T. A., and Li, M. 2007. Proline-rich tyrosine kinase 2 regulates osteoprogenitor cells and bone formation, and offers an anabolic treatment approach for osteoporosis. *Proc Natl Acad Sci U S A.* **104:** 10619-10624

Budillon, A., Bruzzese, F., Di Gennaro, E., and Caraglia, M. 2005. Multiple-target drugs: inhibitors of heat shock protein 90 and of histone deacetylase. *Curr.Drug Targets.* **6:** 337-351

Capdeville, R., Buchdunger, E., Zimmermann, J., and Matter, A. 2002. Glivec (STI571, imatinib), a rationally developed, targeted anticancer drug. *Nat Rev Drug Discov.* **1:** 493-502

Carpten, J. D., Faber, A. L., Horn, C., Donoho, G. P., Briggs, S. L., Robbins, C. M., Hostetter, G., Boguslawski, S., Moses, T. Y., Savage, S., Uhlik, M., Lin, A., Du, J., Qian, Y. W., Zeckner, D. J., Tucker-Kellogg, G., Touchman, J., Patel, K., Mousses, S., Bittner, M., Schevitz, R., Lai, M. H., Blanchard, K. L., and Thomas, J. E. 2007. A transforming mutation in the pleckstrin homology domain of AKT1 in cancer. *Nature.* **448:** 439-444

Carr, S., Aebersold, R., Baldwin, M., Burlingame, A., Clauser, K., and Nesvizhskii, A. 2004. The need for guidelines in publication of peptide and protein identification data: Working Group on Publication Guidelines for Peptide and Protein Identification Data. *Mol.Cell Proteomics.* **3:** 531-533

Cash, C. D., Maitre, M., Rumigny, J. F., and Mandel, P. 1980. Rapid purification by affinity chromatography of rat brain pyridoxal kinase and pyridoxamine-5-phosphate oxidase. *Biochemical and Biophysical Research Communications.* **96:** 1755-1760

Changelian, P. S., Flanagan, M. E., Ball, D. J., Kent, C. R., Magnuson, K. S., Martin, W. H., Rizzuti, B. J., Sawyer, P. S., Perry, B. D., Brissette, W. H., McCurdy, S. P., Kudlacz, E. M., Conklyn, M. J., Elliott, E. A., Koslov, E. R., Fisher, M. B., Strelevitz, T. J., Yoon, K., Whipple, D. A., Sun, J., Munchhof, M. J., Doty, J. L., Casavant, J. M., Blumenkopf, T. A., Hines, M., Brown, M. F., Lillie, B. M., Subramanyam, C., Shang-Poa, C., Milici, A. J., Beckius, G. E., Moyer, J. D., Su, C., Woodworth, T. G., Gaweco, A. S., Beals, C. R., Littman, B. H., Fisher, D. A., Smith, J. F., Zagouras, P., Magna, H. A., Saltarelli, M. J., Johnson, K. S., Nelms, L. F., Des Etages, S. G., Hayes, L. S., Kawabata, T. T., Finco-Kent, D., Baker, D. L., Larson, M., Si, M. S., Paniagua, R., Higgins, J., Holm, B., Reitz, B., Zhou, Y. J., Morris, R. E., O'Shea, J. J., and Borie, D. C. 2003. Prevention of organ allograft rejection by a specific Janus kinase 3 inhibitor. *Science.* **302:** 875-878

Chene, P. 2003. The ATPases: a new family for a family-based drug design approach. *Expert.Opin.Ther.Targets.* **7:** 453-461

Cherry, M. and Williams, D. H. 2004. Recent kinase and kinase inhibitor X-ray structures: mechanisms of inhibition and selectivity insights. *Curr.Med.Chem.* **11:** 663-673

Chin, K. T., Ohki, S. Y., Tang, D., Cheng, H. C., Wang, J. H., and Zhang, M. 1999. Identification and Structure Characterization of a Cdk Inhibitory Peptide Derived from Neuronal-specific Cdk5 Activator. *Journal of Biological Chemistry.* **274:** 7120-7127

Cohen, P. 2002. Protein kinases--the major drug targets of the twenty-first century? *Nat Rev Drug Discov.* **1:** 309-315

Cohen, P. and Frame, S. 2001. The renaissance of GSK3. *Nat Rev Mol Cell Biol.* **2:** 769-776

Collins, I. and Workman, P. 2006. New approaches to molecular cancer therapeutics. *Nat Chem Biol.* **2:** 689-700

Cravatt, B. F., Wright, A. T., and Kozarich, J. W. 2008. Activity-based protein profiling: from enzyme chemistry to proteomic chemistry. *Annu.Rev Biochem.* **77:** 383-414

Daub, H. 2005. Characterisation of kinase-selective inhibitors by chemical proteomics. *Biochimica et Biophysica Acta (BBA) - Proteins & Proteomics.* **1754:** 183-190

Davies, H., Bignell, G. R., Cox, C., Stephens, P., Edkins, S., Clegg, S., Teague, J., Woffendin, H., Garnett, M. J., Bottomley, W., Davis, N., Dicks, E., Ewing, R., Floyd, Y., Gray, K., Hall, S., Hawes, R., Hughes, J., Kosmidou, V., Menzies, A., Mould, C., Parker, A., Stevens, C., Watt, S., Hooper, S., Wilson, R., Jayatilake, H., Gusterson, B. A., Cooper, C., Shipley, J., Hargrave, D., Pritchard-Jones, K., Maitland, N., Chenevix-Trench, G., Riggins, G. J., Bigner, D. D., Palmieri, G., Cossu, A., Flanagan, A., Nicholson, A., Ho, J. W., Leung, S. Y., Yuen, S. T., Weber, B. L., Seigler, H. F., Darrow, T. L., Paterson, H., Marais, R., Marshall, C. J., Wooster, R., Stratton, M. R., and Futreal, P. A. 2002. Mutations of the BRAF gene in human cancer. *Nature.* **417:** 949-954

de la, Motte S. and Gianella-Borradori, A. 2004. Pharmacokinetic model of R-roscovitine and its metabolite in healthy male subjects. *Int.J Clin Pharmacol.Ther.* **42:** 232-239

di Salvo, M. L., Hunt, S., and Schirch, V. 2004. Expression, purification, and kinetic constants for human and Escherichia coli pyridoxal kinases. *Protein Expr.Purif.* **36:** 300-306

Drewes G., Hopf C., and Bantscheff M. 2007. Pathway proteomics and chemical proteomics team up in drug discovery. *Neurodegener Dis.* **4:** 270-280

Elias, J. E., Haas, W., Faherty, B. K., and Gygi, S. P. 2005. Comparative evaluation of mass spectrometry platforms used in large-scale proteomics investigations. *Nat Methods.* **2:** 667-675

Eliot, A. C. and Kirsch, J. F. 2004. Pyridoxal phosphate enzymes: mechanistic, structural, and evolutionary considerations. *Annu.Rev Biochem.* **73:** 383-415

Engelman, J. A., Zejnullahu, K., Mitsudomi, T., Song, Y., Hyland, C., Park, J. O., Lindeman, N., Gale, C. M., Zhao, X., Christensen, J., Kosaka, T., Holmes, A. J., Rogers, A. M.,

Cappuzzo, F., Mok, T., Lee, C., Johnson, B. E., Cantley, L. C., and Janne, P. A. 2007. MET amplification leads to gefitinib resistance in lung cancer by activating ERBB3 signaling. *Science.* **316:** 1039-1043

Fattaey, A. and Booher, R. N. 1997. Myt1: a Wee1-type kinase that phosphorylates Cdc2 on residue Thr14. *Prog.Cell Cycle Res.* **3:** 233-240

Fischer, P. M. 2004. The design of drug candidate molecules as selective inhibitors of therapeutically relevant protein kinases. *Curr.Med.Chem.* **11:** 1563-1583

Fukuda, M., Asano, S., Nakamura, T., Adachi, M., Yoshida, M., Yanagida, M., and Nishida, E. 1997. CRM1 is responsible for intracellular transport mediated by the nuclear export signal. *Nature.* **390:** 308-311

Gachon, F., Fonjallaz, P., Damiola, F., Gos, P., Kodama, T., Zakany, J., Duboule, D., Petit, B., Tafti, M., and Schibler, U. 2004. The loss of circadian PAR bZip transcription factors results in epilepsy. *Genes and Development.* **18:** 1397-1412

Godl, K., Gruss, O. J., Eickhoff, J., Wissing, J., Blencke, S., Weber, M., Degen, H., Brehmer, D., Orfi, L., Horvath, Z., Keri, G., Muller, S., Cotten, M., Ullrich, A., and Daub, H. 2005. Proteomic Characterization of the Angiogenesis Inhibitor SU6668 Reveals Multiple Impacts on Cellular Kinase Signaling. *Cancer Research.* **65:** 6919-6926

Godl, K., Wissing, J., Kurtenbach, A., Habenberger, P., Blencke, S., Gutbrod, H., Salassidis, K., Stein-Gerlach, M., Missio, A., Cotten, M., and Daub, H. 2003. An efficient proteomics method to identify the cellular targets of protein kinase inhibitors. *Proceedings of the National Academy of Sciences.* **100:** 15434-15439

Goldstein, D. M., Gray, N. S., and Zarrinkar, P. P. 2008. High-throughput kinase profiling as a platform for drug discovery. *Nat Rev Drug Discov.* **advanced online publication:**

Hall, S. E. 2006. Chemoproteomics-driven drug discovery: addressing high attrition rates. *Drug Discov Today.* **11:** 495-502

Hanna, M. C., Turner, A. J., and Kirkness, E. F. 1997. Human pyridoxal kinase. cDNA cloning, expression, and modulation by ligands of the benzodiazepine receptor. *J Biol Chem.* **272:** 10756-10760

Hantschel, O. and Superti-Furga, G. 2004. Regulation of the c-Abl and Bcr-Abl tyrosine kinases. *Nat Rev Mol Cell Biol.* **5:** 33-44

Harding, M. W., Galat, A., Uehling, D. E., and Schreiber, S. L. 1989. A receptor for the immunosuppressant FK506 is a cis-trans peptidyl-prolyl isomerase. *Nature.* **341:** 758-760

Harper, J. W. and Elledge, S. J. 1996. Cdk inhibitors in development and cancer. *Curr.Opin.Genet.Dev.* **6:** 56-64

Hayashi, M. L., Rao, B. S., Seo, J. S., Choi, H. S., Dolan, B. M., Choi, S. Y., Chattarji, S., and Tonegawa, S. 2007. Inhibition of p21-activated kinase rescues symptoms of fragile X syndrome in mice. *Proc Natl Acad Sci U S A.* **104:** 11489-11494

Hitomi, M., Yang, K., Guo, Y., Fretthold, J., Harwalkar, J., and Stacey, D. W. 2006. p27Kip1 and cyclin dependent kinase 2 regulate passage through the restriction point. *Cell Cycle.* **5:** 2281-2289

Ishihama, Y., Sato, T., Tabata, T., Miyamoto, N., Sagane, K., Nagasu, T., and Oda, Y. 2005. Quantitative mouse brain proteomics using culture-derived isotope tags as internal standards. *Nat.Biotechnol.* **23:** 617-621

Jeffery, Douglas A. and Bogyo, Matthew. 2003. Chemical proteomics and its application to drug discovery. *Current Opinion in Biotechnology.* **14:** 87-95

Kaldis, P. 1999. The cdk-activating kinase (CAK): from yeast to mammals. *Cell Mol Life Sci.* **55:** 284-296

Karuso, P. and Piggott, A. M. 2008. Rapid Identification of a Protein Binding Partner for the Marine Natural Product Kahalalide F by Using Reverse Chemical Proteomics. *Chembiochem.*

Kastner, U., Hallmen, C., Wiese, M., Leistner, E., and Drewke, C. 2007. The human pyridoxal kinase, a plausible target for ginkgotoxin from Ginkgo biloba. *FEBS Journal.* **274:** 1036-1045

Katayama, H. and Oda, Y. 2007. Chemical proteomics for drug discovery based on compound-immobilized affinity chromatography. *Journal of Chromatography B.* **855:** 21-27

Kerry, J. A., Rohde, M., and Kwok, F. 1986. Brain pyridoxal kinase. Purification and characterization. *Eur.J Biochem.* **158:** 581-585

King, R. W., Glotzer, M., and Kirschner, M. W. 1996. Mutagenic analysis of the destruction signal of mitotic cyclins and structural characterization of ubiquitinated intermediates. *Mol Biol Cell.* **7:** 1343-1357

Knockaert M, Gray N, Damiens E, Chang YT, Grellier P, Grant K, Fergusson D, Mottram J, Soete M, Dubremetz JF, Le Roch K, Doerig C, Schultz P, and Meijer L. 2000. Intracellular targets of cyclin-dependent kinase inhibitors: identification by affinity chromatography using immobilised inhibitors. *Chem Biol.* **7:** 411-422

Knockaert, M. and Meijer, L. 2002. Identifying in vivo targets of cyclin-dependent kinase inhibitors by affinity chromatography. *Biochemical Pharmacology.* **64:** 819-825

Kruse, U., Bantscheff, M., Drewes, G., and Hopf, C. 2008. Chemical and pathway proteomics: Powerful tools for oncology drug discovery and personalized health care. *Molecular Cellular Proteomics.*

Kwok, F., Scholz, G., and Churchich, J. E. 1987. Brain pyridoxal kinase dissociation of the dimeric structure and catalytic activity of the monomeric species. *Eur.J Biochem.* **168:** 577-583

Laemmli, U. K. 1970. Cleavage of structural proteins during the assembly of the head of bacteriophage T4. *Nature.* **227:** 680-685

Laine-Cessac, P., Cailleux, A., and Allain, P. 1997. Mechanisms of the inhibition of human erythrocyte pyridoxal kinase by drugs. *Biochem.Pharmacol.* **54:** 863-870

Lawrence, D. S. and Niu, J. 1998. Protein kinase inhibitors: the tyrosine-specific protein kinases. *Pharmacol.Ther.* **77:** 81-114

Lee, H. S., Moon, B. J., Choi, S. Y., and Kwon, O. S. 2000. Human pyridoxal kinase: overexpression and properties of the recombinant enzyme. *Mol Cells.* **10:** 452-459

Lin, S., Fischl, A. S., Bi, X., and Parce, W. 2003. Separation of phospholipids in microfluidic chip device: application to high-throughput screening assays for lipid-modifying enzymes. *Anal.Biochem.* **314:** 97-107

Lipinski, M. M. and Jacks, T. 1999. The retinoblastoma gene family in differentiation and development. *Oncogene.* **18:** 7873-7882

Liu, Y., Shreder, K. R., Gai, W., Corral, S., Ferris, D. K., and Rosenblum, J. S. 2005. Wortmannin, a Widely Used Phosphoinositide 3-Kinase Inhibitor, also Potently Inhibits Mammalian Polo-like Kinase. *Chemistry & Biology.* **12:** 99-107

Lolli, G., Thaler, F., Valsasina, B., Roletto, F., Knapp, S., Uggeri, M., Bachi, A., Matafora, V., Storici, P., Stewart, A., Kalisz, H. M., and Isacchi, A. 2003. Inhibitor affinity chromatography: profiling the specific reactivity of the proteome with immobilized molecules. *Proteomics.* **3:** 1287-1298

Luecking, U., Siemeister, G., Schaefer, M., Briem, H., Krueger, M., Lienau, P., and Jautelat, R. 2007. Macrocyclic Aminopyrimidines as Multitarget CDK and VEGF-R Inhibitors with Potent Antiproliferative Activities. *ChemMedChem.* **2:** 63-77

Lumeng, L. and Li, T.-K. 1980. Vitamin B6, Metabolism and Role in Growth. -2751.

Lundgren, K., Walworth, N., Booher, R., Dembski, M., Kirschner, M., and Beach, D. 1991. mik1 and wee1 cooperate in the inhibitory tyrosine phosphorylation of cdc2. *Cell.* **64:** 1111-1122

Malumbres, M., Pevarello, P., Barbacid, M., and Bischoff, J. R. 2008. CDK inhibitors in cancer therapy: what is next? *Trends Pharmacol.Sci.* **29:** 16-21

Manning, G., Plowman, G. D., Hunter, T., and Sudarsanam, S. 2002a. Evolution of protein kinase signaling from yeast to man. *Trends in Biochemical Sciences.* **27:** 514-520

Manning, G., Whyte, D. B., Martinez, R., Hunter, T., and Sudarsanam, S. 2002b. The protein kinase complement of the human genome. *Science.* **298:** 1912-1934

Massague, J. 2004. G1 cell-cycle control and cancer. *Nature.* **432:** 298-306

McClue, S. J., Blake, D., Clarke, R., Cowan, A., Cummings, L., Fischer, P. M., MacKenzie, M., Melville, J., Stewart, K., Wang, S., Zhelev, N., Zheleva, D., and Lane, D. P. 2002. In vitro and in vivo antitumor properties of the cyclin dependent kinase inhibitor CYC202 (R-roscovitine). *Int.J Cancer.* **102:** 463-468

Meijer, L., Leclerc, S., and Leost, M. 1999. Properties and potential-applications of chemical inhibitors of cyclin-dependent kinases. *Pharmacol.Ther.* **82:** 279-284

Merrill, A. H., Jr., Henderson, J. M., Wang, E., McDonald, B. W., and Millikan, W. J. 1984. Metabolism of vitamin B-6 by human liver. *J.Nutr.* **114:** 1664-1674

Morgan, D. O. 1995. Principles of CDK regulation. *Nature.* **374:** 131-134

Morgan, D. O. 1997. Cyclin-dependent kinases: engines, clocks, and microprocessors. *Annu.Rev Cell Dev.Biol.* **13:** 261-291

Morin, M. J. 2000. From oncogene to drug: development of small molecule tyrosine kinase inhibitors as anti-tumor and anti-angiogenic agents. *Oncogene.* **19:** 6574-6583

Morphy, R., Kay, C., and Rankovic, Z. 2004. From magic bullets to designed multiple ligands. *Drug Discov Today.* **9:** 641-651

Morwick, T., Berry, A., Brickwood, J., Cardozo, M., Catron, K., DeTuri, M., Emeigh, J., Homon, C., Hrapchak, M., Jacober, S., Jakes, S., Kaplita, P., Kelly, T. A., Ksiazek, J., Liuzzi, M., Magolda, R., Mao, C., Marshall, D., McNeil, D., Prokopowicz, A., III, Sarko, C., Scouten, E., Sledziona, C., Sun, S., Watrous, J., Wu, J. P., and Cywin, C. L. 2006. Evolution of the thienopyridine class of inhibitors of IkappaB kinase-beta: part I: hit-to-lead strategies. *J Med.Chem.* **49:** 2898-2908

Musayev, F. N., di Salvo, M. L., Ko, T. P., Gandhi, A. K., Goswami, A., Schirch, V., and Safo, M. K. 2007. Crystal Structure of human pyridoxal kinase: structural basis of M(+) and M(2+) activation. *Protein Science.* **16:** 2184-2194

Nilsson, I. and Hoffmann, I. 2000. Cell cycle regulation by the Cdc25 phosphatase family. *Prog.Cell Cycle Res.* **4:** 107-114

Oda, Y., Huang, K., Cross, F. R., Cowburn, D., and Chait, B. T. 1999. Accurate quantitation of protein expression and site-specific phosphorylation. *Proc.Natl.Acad.Sci.U.S.A.* **96:** 6591-6596

Ong, S. E., Blagoev, B., Kratchmarova, I., Kristensen, D. B., Steen, H., Pandey, A., and Mann, M. 2002. Stable isotope labeling by amino acids in cell culture, SILAC, as a simple and accurate approach to expression proteomics. *Mol.Cell Proteomics.* **1:** 376-386

Pavletich, N. P. 1999. Mechanisms of cyclin-dependent kinase regulation: structures of Cdks, their cyclin activators, and Cip and INK4 inhibitors. *J Mol Biol.* **287:** 821-828

Percudani, R. and Peracchi, A. 2003. A genomic overview of pyridoxal-phosphate-dependent enzymes. *EMBO Rep.* **4:** 850-854

Pevarello, P., Brasca, M. G., Amici, R., Orsini, P., Traquandi, G., Corti, L., Piutti, C., Sansonna, P., Villa, M., Pierce, B. S., Pulici, M., Giordano, P., Martina, K., Fritzen, E. L., Nugent, R. A., Casale, E., Cameron, A., Ciomei, M., Roletto, F., Isacchi, A., Fogliatto, G., Pesenti, E., Pastori, W., Marsiglio, A., Leach, K. L., Clare, P. M., Fiorentini, F., Varasi, M., Vulpetti, A., and Warpehoski, M. A. 2004. 3-Aminopyrazole inhibitors of CDK2/cyclin A as antitumor agents. 1. Lead finding. *J Med.Chem.* **47:** 3367-3380

Pocker, Y. and Stone, J. T. 1967. The catalytic versatility of erythrocyte carbonic anhydrase. 3. Kinetic studies of the enzyme-catalyzed hydrolysis of p-nitrophenyl acetate. *Biochemistry.* **6:** 668-678

Popowycz, F., Fournet, G., Schneider, C., Bettayeb, K., Ferandin, Y., Lamigeon, C., Tirado, O. M., Mateo-Lozano, S., Notario, V., Colas, P., Bernard, P., Meijer, L., and Joseph, B. 2009. Pyrazolo[1,5-a]-1,3,5-triazine as a purine bioisostere: access to potent cyclin-dependent kinase inhibitor (R)-roscovitine analogue. *Journal of Medicinal Chemistry.* **52:** 655-663

Puccetti, L., Fasolis, G., Cecchi, A., Winum, J. Y., Gamberi, A., Montero, J. L., Scozzafava, A., and Supuran, C. T. 2005. Carbonic anhydrase inhibitors: synthesis and inhibition of cytosolic/tumor-associated carbonic anhydrase isozymes I, II, and IX with sulfonamides incorporating thioureido-sulfanilyl scaffolds. *Bioorganic & Medicinal Chemistry Letters.* **15:** 2359-2364

Sadaghiani, A. M., Verhelst, S. H., and Bogyo, M. 2007. Tagging and detection strategies for activity-based proteomics. *Curr.Opin.Chem.Biol.* **11:** 20-28

Saxena, C., Zhen, E., Higgs, R. E., and Hale, J. E. 2008. An Immuno-Chemo-Proteomics Method for Drug Target Deconvolution. *Journal of Proteome Research.*

Senderowicz, A. M. and Sausville, E. A. 2000. Preclinical and clinical development of cyclin-dependent kinase modulators. *J Natl Cancer Inst.* **92:** 376-387

Sharma, P. S., Sharma, R., and Tyagi, R. 2008. Inhibitors of cyclin dependent kinases: useful targets for cancer treatment. *Curr.Cancer Drug Targets.* **8:** 53-75

Shevchenko, A., Tomas, H., Havlis, J., Olsen, J. V., and Mann, M. 2006. In-gel digestion for mass spectrometric characterization of proteins and proteomes. *Nat Protoc.* **1:** 2856-2860

Smith, W. W., Pei, Z., Jiang, H., Dawson, V. L., Dawson, T. M., and Ross, C. A. 2006. Kinase activity of mutant LRRK2 mediates neuronal toxicity. *Nat Neurosci.* **9:** 1231-1233

Smits, V. A. and Medema, R. H. 2001. Checking out the G(2)/M transition. *Biochim.Biophys.Acta.* **1519:** 1-12

Soda, M., Choi, Y. L., Enomoto, M., Takada, S., Yamashita, Y., Ishikawa, S., Fujiwara, S., Watanabe, H., Kurashina, K., Hatanaka, H., Bando, M., Ohno, S., Ishikawa, Y., Aburatani, H., Niki, T., Sohara, Y., Sugiyama, Y., and Mano, H. 2007. Identification of the transforming EML4-ALK fusion gene in non-small-cell lung cancer. *Nature.* **448:** 561-566

Solinas, G., Vilcu, C., Neels, J. G., Bandyopadhyay, G. K., Luo, J. L., Naugler, W., Grivennikov, S., Wynshaw-Boris, A., Scadeng, M., Olefsky, J. M., and Karin, M. 2007. JNK1 in hematopoietically derived cells contributes to diet-induced inflammation and insulin resistance without affecting obesity. *Cell Metab.* **6:** 386-397

Strebhardt, K. and Ullrich, A. 2006. Targeting polo-like kinase 1 for cancer therapy. *Nat Rev Cancer.* **6:** 321-330

Supuran, C. T. and Scozzafava, A. 2007. Carbonic anhydrases as targets for medicinal chemistry. *Bioorganic & Medicinal Chemistry.* **15:** 4336-4350

Tang, L., Li, M. H., Cao, P., Wang, F., Chang, W. R., Bach, S., Reinhardt, J., Ferandin, Y., Galons, H., Wan, Y., Gray, N., Meijer, L., Jiang, T., and Liang, D. C. 2005. Crystal structure of pyridoxal kinase in complex with roscovitine and derivatives. *J Biol Chem.* **280:** 31220-31229

Taunton, J., Hassig, C. A., and Schreiber, S. L. 1996. A mammalian histone deacetylase related to the yeast transcriptional regulator Rpd3p. *Science.* **272:** 408-411

Thiry, A., Supuran, C. T., Masereel, B., and Jean, M. 2008. Recent Developments of Carbonic Anhydrase Inhibitors as Potential Anticancer Drugs. *Journal of Medicinal Chemistry.* **51:** 3051-3056

Toledo, L. M., Lydon, N. B., and Elbaum, D. 1999. The structure-based design of ATP-site directed protein kinase inhibitors. *Curr.Med.Chem.* **6:** 775-805

Tse, A. N., Carvajal, R., and Schwartz, G. K. 2007. Targeting checkpoint kinase 1 in cancer therapeutics. *Clin Cancer Res.* **13:** 1955-1960

Tsihlias, J., Kapusta, L., and Slingerland, J. 1999. The prognostic significance of altered cyclin-dependent kinase inhibitors in human cancer. *Annu.Rev Med.* **50:** 401-423

Turjanski, A. G., Vaque, J. P., and Gutkind, J. S. 2007. MAP kinases and the control of nuclear events. *Oncogene.* **26:** 3240-3253

Uttamchandani, M., Walsh, D. P., Yao, S. Q., and Chang, Y. T. 2005. Small molecule microarrays: recent advances and applications. *Curr.Opin.Chem.Biol.* **9:** 4-13

Valsasina, B., Kalisz, H. M., and Isacchi, A. 2004. Kinase selectivity profiling by inhibitor affinity chromatography. *Expert Review of Proteomics.* **1:** 303-315

Verweij, J. and de Jonge, M. 2007. Multitarget tyrosine kinase inhibition: [and the winner is...]. *Journal of Clinical Oncology.* **25:** 2340-2342

Wada, K., Ishigaki, S., Ueda, K., Sakata, M., and Haga, M. 1985. An antivitamin B6, 4'-methoxypyridoxine, from the seed of Ginkgo biloba L. *Chem.Pharm.Bull.(Tokyo).* **33:** 3555-3557

Weinmann, H. and Metternich, R. 2005. Drug discovery process for kinase inhibitors. *Chembiochem.* **6:** 455-459

Weisberg, E., Manley, P. W., Cowan-Jacob, S. W., Hochhaus, A., and Griffin, J. D. 2007. Second generation inhibitors of BCR-ABL for the treatment of imatinib-resistant chronic myeloid leukaemia. *Nat Rev Cancer.* **7:** 345-356

Whartenby, K. A., Calabresi, P. A., McCadden, E., Nguyen, B., Kardian, D., Wang, T., Mosse, C., Pardoll, D. M., and Small, D. 2005. Inhibition of FLT3 signaling targets DCs to ameliorate autoimmune disease. *Proc Natl Acad Sci U S A.* **102:** 16741-16746

Wissing, J., Godl, K., Brehmer, D., Blencke, S., Weber, M., Habenberger, P., Stein-Gerlach, M., Missio, A., Cotten, M., Muller, S., and Daub, H. 2004. Chemical Proteomic

Analysis Reveals Alternative Modes of Action for Pyrido[2,3-d]pyrimidine Kinase Inhibitors. *Molecular Cellular Proteomics.* **3:** 1181-1193

Wittman, M., Carboni, J., Attar, R., Balasubramanian, B., Balimane, P., Brassil, P., Beaulieu, F., Chang, C., Clarke, W., Dell, J., Eummer, J., Frennesson, D., Gottardis, M., Greer, A., Hansel, S., Hurlburt, W., Jacobson, B., Krishnananthan, S., Lee, F. Y., Li, A., Lin, T. A., Liu, P., Ouellet, C., Sang, X., Saulnier, M. G., Stoffan, K., Sun, Y., Velaparthi, U., Wong, H., Yang, Z., Zimmermann, K., Zoeckler, M., and Vyas, D. 2005. Discovery of a (1H-benzoimidazol-2-yl)-1H-pyridin-2-one (BMS-536924) inhibitor of insulin-like growth factor I receptor kinase with in vivo antitumor activity. *J Med.Chem.* **48:** 5639-5643

Woo, R. A. and Poon, R. Y. 2003. Cyclin-dependent kinases and S phase control in mammalian cells. *Cell Cycle.* **2:** 316-324

Yamamoto, K., Yamazaki, A., Takeuchi, M., and Tanaka, A. 2006. A versatile method of identifying specific binding proteins on affinity resins. *Analytical Biochemistry.* **352:** 15-23

Zhang, H. S., Gavin, M., Dahiya, A., Postigo, A. A., Ma, D., Luo, R. X., Harbour, J. W., and Dean, D. C. 2000. Exit from G1 and S phase of the cell cycle is regulated by repressor complexes containing HDAC-Rb-hSWI/SNF and Rb-hSWI/SNF. *Cell.* **101:** 79-89

Zhu, L. 2005. Tumour suppressor retinoblastoma protein Rb: a transcriptional regulator. *Eur.J Cancer.* **41:** 2415-2427

7. Abbreviations

°C	Degree celcius
µ	Micro
1D/2D	One-/Two-dimensional
aa	Amino acid
Abl	Abelson tyrosine kinase
ABPP	Activity-based probe profiling
AC	Affinity chromatrography
A_{max}	Peak absorption
Asp	Aspartate
ATP	Adenosine triphosphate
Brc	Breakpoint cluster region
Brc-Abl	Brc-Abl tyrosine kinase
BSA	Bovine serum albumin
C1	Compound C1
C1a	Compound C1 analog
C1-LL	C1-long linker
C1-SL	C1-short linker
CA2	Carbonic anhydrase 2
CAKs	CDK activating kinases
cal	Calorie
CDK	Cyclin-dependent protein kinase
CID	Collision-induced dissociation
CKIs	Natural CDK inhibitor proteins
CMBL	Carboxymethylenebutenolidase homolog
CML	Chronic myelogenous leukemia
conc.	Concentration
ctr	Control
Cyc	Cyclins
Da	Dalton
D-box	N-terminal destruction-box
DMF	N,N-Dimethylformamide
DMSO	Dimethyl sulfoxide
DNA	Desoxyribonucleic acid
DTT	Dithiothreitol
E. coli	Escherichia coli
e.g.	exempli gratia ('for the sake of example')
EDTA	Ethylenediamine tetraacetic acid
EGTA	Ethylene glycol tetraacetic acid

ESI	Electrospray ionization
FBS	Fetal bovine serum
FDA	U.S. Food and Drug Administration
FDR	False discovery rate
g	Gram
G0-phase	Quiescence
G1/G2-phase	Growth phase 1/2
gene ID	Gene identity
GISTs	Gastrointestinal stromal tumors
GTP	Guanosine triphosphate
h	Hours
H460	Human large cell lung carcinoma cell line
HDAC	Histone deacetylase
HeLa	Human cervix carcinoma cell line
HPLC	High pressure liquid chromatography
HSP	Heat shock protein
IAA	Iodoacetamide
IAC	Inhibitor affinity chromatography
IC50	Half maximal inhibitory concentration
ID	Inner diameter
Ile	Isoleucine
IPI human DB	International Protein Index protein database
IPTG	Isopropyl beta-D-thiogalactopyranoside
ITC	Isothermal titration calorimetry
K_D	Dissociation constant
K_m	Michaelis constant
L	Liter
LC	Liquid chromatography
LDS	Lithium dodecyl sulfate
M	Molar
m	Meter
m/z	Mass-to-charge ratio
MALDI	Matrix-assisted laser desorption/ionization
MAPK	Mitogen-activated protein (MAP) kinases
min	Minutes
mol	Mol
M-phase	Mitosis
MS	Mass spectrometry
MS/MS	Tandem mass spectrometry
MW	Molecular weight
NMR	Nuclear Magnetic Resonance

PAGE	Polyacrylamide Gel Electrophoresis
PBS	Phosphate buffered saline
PCR	Polymerase Chain Reaction
PDGF-R	Platelet-derived growth factor receptor
PDXK	Pyridoxal kinase
pH	Minus the decimal logarithm of the hydrogen ion activity in an aqueous solution
PL	Pyridoxal
PLP	Pyridoxal 5'-phosphate
PM	Pyridoxamine
PMP	Pyridoxamine 5'-phosphate
PN	Pyridoxine
PNP	Pyridoxine5'-phosphate
ppm	Parts-per-million
Rb	Retino blastoma
RNA	Ribonucleic acid
RNAi	RNA interference
rpm	Revolutions per minute
RT	Room temperature
s	Seconds
SB	Sample buffer
SDS	Sodium Dodecyl Sulfate
SEC	Size exclusion chromatography
SILAC	Stable isotope labeling with amino acids in cell culture
S-phase	Synthesis phase
SPR	Surface plasmon resonance
t	Time
TAE buffer	Tris-acetate-EDTA buffer
TFA	Trifluoroacetic acid
Thr	Threonine
Tyr	Tyrosine
UV-Vis	Ultraviolet-visible
V	Volt
v/v	Volume/volume
VEGF-R	Vascular endothelial growth factor receptor
v_{max}	Maximum velocity
w/o	Without
w/v	Weight/volume
WB	Washing buffer
x-ray	X-radiation
ΔH	Binding enthalpie
λ	Wavelength

8. Acknowledgement

First of all, I thank Prof. Dr. Peter Donner very much for being an excellent supervisor, who was always willing to take the time for excellent scientific discussions and suggestions. In particular, I appreciate his continuous support and dedication even in personally challenging times.

I also would like to thank Prof. Dr. P. Knaus for co-reviewing my work and for giving me the opportunity to present the results of this work in one of the symposia that she organizes for PhD students at the Free University Berlin.

I am deeply grateful to Inke Bahr and Volker Badock, I truely learned and benefited a lot from their broad knowledge in protein analytics. To do my PhD as well as my diploma thesis in their labs was a great fortune. I appreciate a lot the friendly and very open atmosphere there. I had a brilliant time!

I am very thankful to Dr. Ulrich Lücking for his excellent support with the compound synthesis, for his willingness to provide additional compound analogues and for a lot of helpful discussions. I also would like to thank Dr. Gerhard Siemeister for providing resources the support with regard to the cell culture and the activity assays in his lab as well as for his valuable scientific advices. Moreover, I would like to thank Klaus Burmeister and Karl Sauvageot for their excellent technical help and support.

I greatly thank Dr. Vera Pütter for her invaluable help and advice regarding the expression and purification of the pyridoxal kinase and Petra Rothhaupt for supporting me during the purification approach of this kinase.

I also greatly thank Dr. Jörg Fanghänel for innumerable discussions about enzyme activity assays and his great support with the isothermal titration calorimetry experiments.

I am very grateful to Norbert Otto and all other colleagues from the Protein Technology department for sharing their tremendous knowledge on protein chemistry with me whenever I was looking for help and advice. Thanks a lot!

I thank Dr. Andreas Becker for funding and supporting my research and for giving me the opportunity to gain experience on international meetings. I thank Dr. Anke Müller-Fahrnow for reviewing my thesis and giving helpful comments.

I am thankful to Dr. Martina Schäfer for preparing the computational model of the CDK2-compound complex and I would like to thank Marina Drawert for helping me with the organization of my scientific trips.

I thank Dr. Annette Sommer for carefully reading the manuscript of the publication and giving valuable comments.

Special thanks are extended to E. Leistner (Institute for Pharmaceutical Biology, University Bonn) for providing me with a recombinant vector of human PDXK and to E. Kirkness (Institute for Genomic Research, Rockville, MS) for his agreement to use the vector.

And last but not least I would like to thank my parents for their care and support during my entire study and of course Sabine; she exercised infinite patience during exhausting times and I appreciate a lot her tireless encouragement, especially at the end of my PhD thesis.

Best regards, Enrico!